Thermal diffusion behavior of complex fluid mixture

Hui Ning

Ning, Hui
Thermal diffusion behavior of
complex fluid mixture
Thesis, University of Twente, Enschede
ISBN: ???????
Printed by ???????
????????

Copyright©2007 by H. Ning, Weiche Materie,Institut fü Festkörperforschung
,Forschungszentrum Jülich, Germany

Front cover: *??????*
Back cover: *??????*

Typeset in LaTeX, by the author

Thermal diffusion behavior of complex fluid mixture

DISSERTATION

to obtain
the doctor's degree at the University of Twente,
on the authority of the rector magnificus,
prof. dr. H.W.M. Zijm,
on account of the decision of the graduation committee,
to be publicly defended
on Wednesday, 28.02.2007 at 15:00

by

Hui Ning

born on 28 February 1978
in Zhuozhou, P. R. China

This dissertation has been approved by:

the promoter

Prof. Dr. Jan K. G. Dhont

Prof. Dr. W. J. Briels

Contents

1 Introduction **1**

1.1 Thermal diffusion 1

1.2 Experimental methods for measuring the Soret coefficient 3

1.3 TDFRS setup 6

1.3.1 Setup 6

1.3.2 Count rate linearization of photomultiplier 7

1.3.3 Contrast factors 9

1.3.4 Data analysis 11

1.3.5 Influence from the dye 16

1.4 Experimentally studied systems 18

1.4.1 Simple liquid mixtures 18

1.4.2 Complex fluid mixtures 19

1.4.3 Close to the critical point and other scaling laws 22

1.5 Theoretical descriptions and simulations 23

1.5.1 Selected theories 23

1.5.2 MD Simulations and Lattice model calculations 27

1.6 Outline of the thesis 29

2 Experimental investigation of the Soret effect in acetone/water and dimethylsulfoxide/water mixture **31**

2.1 Introduction 31

2.2 Experiment 32

2.2.1 Sample preparation 32

2.2.2 Data analysis and set-up 33

2.2.3 Refractive index increments 33

2.3 Results and discussion 33

2.4 Conclusion 38

3 Thermal diffusion behavior of hard sphere suspensions 40

3.1 Introduction 41

3.2 Theory 43

3.2.1 The interaction potential between colloids 43

3.2.2 Thermal diffusion of interacting colloids 44

3.3 Experiment 46

3.3.1 Synthesis 46

3.3.2 Sample preparation 46

3.3.3 Thermal diffusion forced Rayleigh scattering (TDFRS) 48

3.3.4 Dynamic light scattering (DLS) 50

3.3.5 Static light scattering (SLS) 51

3.4 Results 51

3.4.1 Characterization and phase behaviour of the colloidal dispersion 51

3.4.2 Thermal diffusion measurements 55

3.4.3 Thermal diffusion of free octadecane in toluene 57

3.5 Discussion 59

3.6 Conclusion 63

3.7 Appendix: Conversion of D_T^{theo} to D_T 64

4 Soret effect in a nonionic surfactant system with a simple phase behavior 66

4.1 Introduction 66

4.2 Experiment and data analysis 70

4.2.1 Sample Preparation and contrast factors 70

4.2.2 TDFRS and DLS 70

4.2.3 Data analysis 71

4.3 Results and Discussion 71

4.4 Conclusions 77

5 Soret effect in a nonionic surfactant system with a complex phase behavior 78

5.1 Introduction 80

5.2 Working equations 82
5.2.1 TDFRS 82
5.2.2 DLS 84
5.3 Experiment 84
5.3.1 Sample Preparation. 84
5.3.2 Refractive index increments 87
5.3.3 Dynamic light scattering 87
5.3.4 TDFRS 87
5.3.5 Dye influence on the TDFRS signal 88
5.4 Results 91
5.4.1 Characteristics of $C_{12}E_6$ in water 91
5.4.2 Characteristics of some additional non-ionic surfactant systems 97
5.4.3 Characteristics of the surfactant solutions in the presence of salt 100
5.5 Discussion 100

Bibliography **111**

1 Introduction

1.1 Thermal diffusion

Ludwig-Soret effect [55, 101] describes the occurrence of a mass flux caused by a temperature gradient in a multi-component system. One early application of the effect was the separation of isotopes [37, 12, 13]. Understanding of the Soret effect is helpful for exploring the mechanics of crude oil extraction and its reservoir characterization [15], and also benefits the research of the global circulation of see water. The Soret effect is utilized for the polymer characterization by thermal field flow fractionation (TFFF). The recent studies on the Soret effect of the bio-systems, like protein and DNA solutions, might reveal the mechanism of mysterious life phenomenon [8, 73].

In a binary fluid mixture with non-uniform temperature profile, the thermal diffusion behavior can be described by the mass flow J_m of component 1 containing both contributions stemming from the concentration and from the temperature gradient [18]:

$$J_{\mathrm{m}} = -\rho D \nabla c - \rho c(1-c) D_{\mathrm{T}} \nabla T \tag{1.1}$$

where D denotes the collective diffusion coefficient, D_{T} the thermal diffusion coefficient, ρ the mass density, and c the concentration of component 1 in weight fractions. In a stationary state where the diffusion flow J_{m} vanishes, the Soret coefficient S_T is given by

$$S_{\mathrm{T}} \equiv \frac{D_{\mathrm{T}}}{D} = -\frac{1}{c(1-c)} \frac{\nabla c}{\nabla T}. \tag{1.2}$$

Typically the Soret coefficient S_{T} in simple liquid mixtures lies in the range $10^{-5} < S_{\mathrm{T}} < 10^{-3}$ K^{-1} [114, 64], while in polymer, micellar solutions and colloidal dispersions $10^{2} < S_{\mathrm{T}} < 10^{-2}\mathrm{K}^{-1}$ [47, 44, 66, 42, 24, 65]. The larger value for S_{T} in the macromolecular solutions is mainly caused by the slower diffusion of the systems.

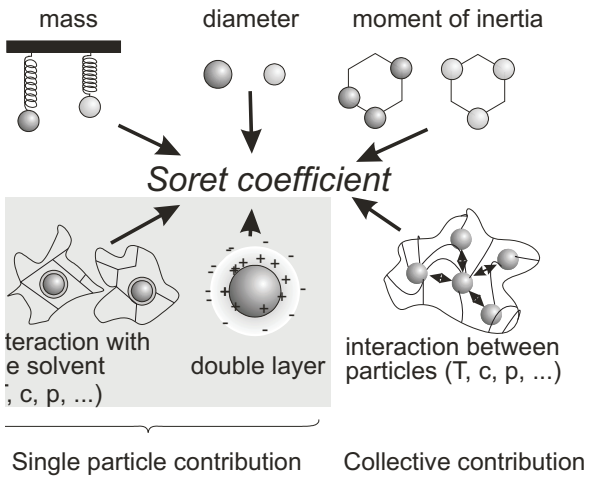

Figure 1.1: The main contributions for the thermal diffusion behavior

Despite the discovery of the effect by Ludwig [55] and the first systematic investigations by Soret [101, 102] dated back roughly 150 and 130 years, respectively, there is so far no fully microscopic understanding for this effect in liquids, which makes it difficult to predict the Soret effect even for simple fluid mixtures. in the beginning and in middle of the 20th century the research was mainly concentrated on gases and simple fluids mixtures [107]. From last decade, with the improvement of experimental technique, especially the application of modern optical methods, studies on complex systems such as polymers [93], micelles [66, 71], colloidal dispersion [71, 65], magnetic fluids [59] and bio-macromolecule [24] became possible and attracted more and more interest. More recently, with the development of new simulation techniques and microscopic theories, reasonable predictions of Soret coefficients for low molecular weight mixtures became possible [38, 62, 70, 121, 77].

As can be seen in Fig.1.1, thermal diffusion in fluid mixtures can be differentiated into several contributions. The above features, known as physical parameters, like mass, size, density of the component and moment of inertia are easily accessed and explicit, and rules of thumb was obtained for these contributions. While contributions from chemical interactions, including the short-range (solute-solvent and solute-solute) interactions and long-range (such as the interaction between the charged particles), are for most case implicit, and rarely can be

assumed to be additive. There are as well other physical parameters like thermal expansion, surface tension, surface charge density, thermal conductivity correlate to thermophoresis. Thermal diffusion in fluid mixtures can also be distinguished by highly dilute solution and concentrated solution. In dilute solution, the specific interaction between the solute particle and solvent molecules at surface dominates thermal diffusion behavior. The changing of the surrounding environment (temperature, pressure, ionic strength, pH) may dramatically influence the Soret effect. While for concentrated solution, solute-solute interaction play an important role. Experiments, theories and computational simulations has been performed to probe the contributions from these features.

1.2 Experimental methods for measuring the Soret coefficient

According to the purpose, the instruments for measuring the Soret coefficient can be separated into two class. One kind of instrument is to achieve the goal of large separation. An example is thermogravitational columns. While another kind of instruments is developed mainly for the analysis purpose. In the following discussion, we will discuss only analytical methods.

Diffusion cells: Diffusion cell is a traditional experimental method for measuring the Soret coefficient [28, 113, 57, 61, 35]. The cell is heated from above and cooled from below to avoid convection. In the earlier work compositions was analyzed layer by layer, nowadays an optical beam deflection technique is used to determine the concentration gradient [52, 118]. The time to reach diffusion equilibrium is determined by the gap between the two plates. For a typical gap distance of 2 mm, it takes for simple low molecular mixtures several minutes to reach the steady state, while for macromolecular systems such as polymer solutions and colloidal dispersions, the required time can be 10 hours or more. Haugen utilized the diffusion cell with deflection beams of two different wavelength [41]. This allows using the dispersion of the light the investigation of ternary systems. Putnam and Cahill [79] built a beam defection setup with micrometre-scale gap, which speeds up the measurement time by a factor around 300, and the measurement on the mixture of dodecane and 1,2,3,4-tetrahydronaphthalene compared well with benchmark values obtianed for the system [75].

Thermal diffusion cells have been used to investigate low molecular mixtures [119, 52,

54] and polymer solutions [36]. Recently, this technique was also used by Piazza *et al.* for charged micelle and some colloidal systems [71, 42].

Thermal field flow fractionation: Thermal field flow fractionation (TFFF or thFFF) is used for separation or analysis for polymer solutions and colloidal suspensions. For the low molecular weight mixtures the TFFF method is less suitable due to the required high temperature gradient. It is built on the basic principle of field-flow fractionation techniques, for which an external field is applied on a laminar flow of the investigated solution within a relatively narrow channel. In the case of TFFF, a temperature gradient is applied perpendicular to the flow channel and causes a concentration gradient versus the flow profile due to the Soret effect. A so called micro-thermal field-flow fractionation (μ-TFFF) has been developed, which needs only 1 μL sample and can shorten the measurement time to 10 minutes for colloidal systems [43]. The Soret coefficient for polymers [34, 90, 91], cross linked microgels [3], and most recently colloids [2] in solution have been reported by TFFF. So far the TFFF has not been validated in a benchmark test.

Thermal lens method: In a thermal lens experiment the laser beam itself is used for heating and detection simultaneously. The local heating of the laser beam on a partially absorbing medium creates a concave lens, if the refractive index decreases with increasing temperature. An exception is the thermal lens in water which changes a converging lens to a diverging lens with temperature around -0.01 °C [31]. Due to the Soret effect in binary or multi-component mixtures a concentration lens will be created additionally that changes the profile of the transmitting laser beam. Under the assumption of a gaussian laser profile the changing of the profile can be probed by measuring the change in the central-beam intensity.

An advantage of the thermal lens method compared to the diffusion cell is the short equilibration time due to small distances in the order of the focal beam width, which makes it possible to investigate slow diffusing systems, such as polymer blends and colloidal dispersions. For polymeric systems with typical diffusion constants of the order $D = 10^{-7}$ cm^2 s^{-1} this leads to an equilibrium time of $\tau < 100$ ns for a focal beam width of 100 nm. The main disadvantage of the method is its sensitivity to convection, astigmatism of the beam and the fact that no single scattering vector q can be selected, as in the case of the grating experiments.

So far the thermal lens method has not been validated in a benchmark. The thermal lens

method has been used to study the thermal diffusion behavior of ferrofluids [1] and ionic surfactant systems [88]. These studies showed agreement with forced Rayleigh scattering and beam deflection measurements, respectively. In contrast, Voit did not find agreement with other methods. For one of the benchmark mixtures n-dodecane/1,2,3,4 tetrahydronaphthalene, Voit found a 40% too small value [112], which was probably influenced by convection. In order to minimized the influence of convection, fairly thin cells have to be used, which leads on the other hand to a very low signal to noise ratio.

Microfluidic fluorescence: Microfluidic fluorescence is a recently developed optical technique to measure the thermophoresis of large bio-molecule and colloids [25, 23]. The temperature difference is created by a focused infrared laser with a wavelength 1480 nm, which is strongly absorbed by water in a 10 μm thickness water chamber. The temperature profile is detected by measuring the fluorescence of a temperature dependent dye, and the concentration of the solute particles is calculated from an average of the image stack. This method allows the direct observation of the temperature driven diffusion process. The chamber thickness is so small that the thermal convection can be avoided. The disadvantage is that the method is limited to fairly large molecules or fluorescence labeled system, which dissolve in water. Thermal diffusion behavior of colloidal dispersions such as polystyrene bead (40 nm-2 μm) [24] and DNA [23] was investigated using this technique.

Holographic grating technique: A holographic grating technique named Thermal Diffusion Forced Rayleigh Scattering (TDFRS) has been developed and extensively applied on the studies of thermal diffusion behavior of simple fluid mixtures [19, 70, 49, 64], polymer solutions [17, 44, 81], micellar solutions [66] and colloidal dispersions [16]. The principle and experimental detail for this technique will be described in the next section. The advantages of the method are the small temperature difference ($\sim$20 μK) and the small fringe spacing ($\sim$20 μm) which keeps the system close to the thermal equilibrium and allow also the investigation of slow system such as polymer and colloids. On the other hand it works also for low molecule weight mixtures. one limitation is that it works generally only for binary systems. Only for special ternary mixture where one of the components diffuses much slower, an investigation is possible. For aqueous systems the addition of a small amount of inert dye, which converts the optical grating in a temperature grating, can sometimes influence the thermal diffusion behavior [16, 66].

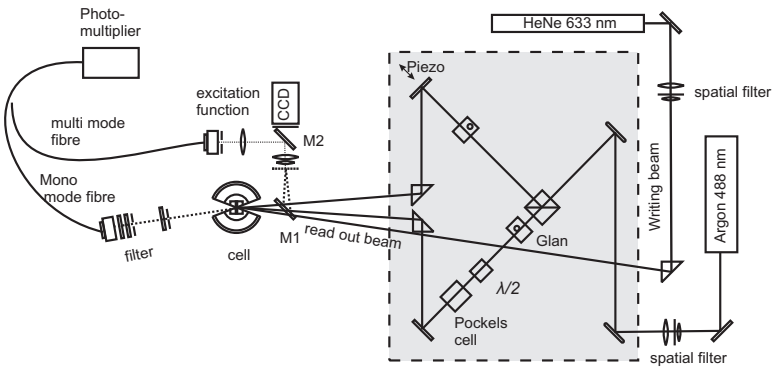

Figure 1.2: Schematic drawing of a thermal diffusion forced Rayleigh scattering (TDFRS) setup

1.3 TDFRS setup

Since 1978, the first time Thyagarajan and Lallemand observed a signal contribution due to the thermal diffusion in a forced Rayleigh scattering experiment, the optical holographic grating technique had been improved [50, 115, 84] and applied to study thermal diffusion behavior in simple and complex fluids.

1.3.1 Setup

The main components of a TDFRS setup are similar to a standard forced Rayleigh scattering (FRS) experiment as described in many publications [76, 49, 48]. The setup used in this work is sketched in Fig. 1.2. The experiment is mounted on a optical table with tuned damping. An argon-ion laser operating at 488 nm is used as writing beam. Its beam is spatially filtered and expanded to a diameter of 5-10 mm. The polarization is perpendicular to the optical table. The beam is split into two beams of equal intensity . The glued polarizing prism are used to refine the polarization for better contrast. A mirror is mounted on piezo ceramics, which is used for phase stabilization and phase modulation of the grating. The half wave plate and the Pockels cell are for shifting the grating by 180 °. For a better mechanical stability all optical components in the dotted frame are mounted on a separate breadboard which is placed on passive isolators. The writing beams are reflected by two prisms. The optical path length of

two separated beam is equal with in 0.5 cm. By changing the distance of the two prism on the angle it is possible to vary the grating vector q.

The angle θ between the two writing beams is typically in the order of 2-4 °. Such a small angle is difficult to measure, therefore we image the interference grating directly on a CCD camera by using the flip mirror M1. The created fringe spacing is compared to a reticle with a 25 μm scale. This procedure allows the determination of the grating vector $q = 4\pi\ sin(\theta/2)/\lambda$ with a accuracy of 0.5 %. The mirror M2 in front of the CCD camera reflects the grating of the writing beams directly on the photomultiplier. By selecting one of the interference stripes the real excitation function can be measured directly. This function is used for iterative correction.

The sample cell is mounted inside a brass holder and can be adjusted in z-directions orthogonal to the optical axis. The quartz cell (Hellma) for TDFRS measurement have a layer thickness 0.2 mm, and the cell can be sealed tightly by Teflon stoppers. The temperature of the brass holder is controlled by a circulating water from a thermostat (Lauda) with an uncertainty of 0.02 °C. By using an external temperature sensor mechanism, the thermostat controls the temperature in the cell.

The diffraction efficiency of the grating created in the sample cell is read by a He-Ne laser with a wavelength 632.8 nm at the Bragg-angle condition. A pinhole and bandpass filter in front of the detector separate the diffracted beam from unwanted stray light. As shown in Fig.1.2, a single mode fiber is directly connect to the photomultiplier tube operating in photon counting mode. For the first experiment we used a home-made counter card, later we used a commercial one from National instruments. At high count rates above 10^6 s^{-1}, the respond of the photomultiplier is not linear any more, therefore a calibration of the non-linearity efficiency of the photomultiplier is necessary [48].

1.3.2 Count rate linearization of photomultiplier

As already mentioned in Sec.1.3.1, at high intensity the counting system does not respond linearly. We applied a linearization procedure according to Köhler [48]. We measured intensity once by the photomultiplier $\nu_m(\nu_r)$ a second time by attenuating the intensity by a neutral density filter $\nu_m(\nu_r/\alpha_0)$. α_0 is the true attenuation factor. We calculate the ratio of

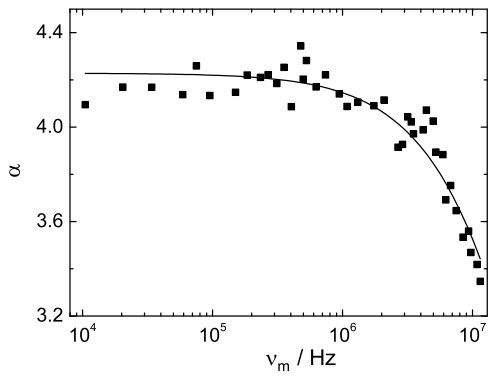

Figure 1.3: The apparent attenuation factor α as a function of count rate. The measurement was done with a neutral density filter with nominal optical density 0.6. Solid line is the fit of α to Eq.1.6

the count rate $\alpha(\nu_m)$ by

$$\alpha(\nu_m) = \frac{\nu_m(\nu_r)}{\nu_m(\nu_r/\alpha_0)}. \tag{1.3}$$

The measured counter rate ν_m relates to the real counter rate ν_r as

$$\nu_m = \nu_t \int_{\tau_{min}}^{\infty} \nu_r e^{-\nu_r \tau} d\tau = \nu_t e^{-\nu_t \tau_{min}} \tag{1.4}$$

where τ_{min} is the minimum time, at which two pulses can be distinguished as two events. In our case $\nu_r \tau_{min} \ll 1$, thus Eq.1.4 can be inverted to be

$$\nu_r = \nu_m(1 + \nu_m \tau_{min}). \tag{1.5}$$

We can take place Eq.1.5 into Eq.1.3 and thus it yields

$$\alpha(\nu_m) = \frac{\nu_m(\nu_r)}{\nu_m(\nu_r/\alpha_0)} \approx \frac{\alpha_0}{1 + \nu_m \tau_{min}}. \tag{1.6}$$

τ_{min} and α_0 can be obtained by fitting the Eq.1.6 to experimental data.

In the calibration process, we use He-Ne laser with a power of 5 mW or 25 mW as light source. To control the power of the laser, a grey wheel filter or a combination of neutral

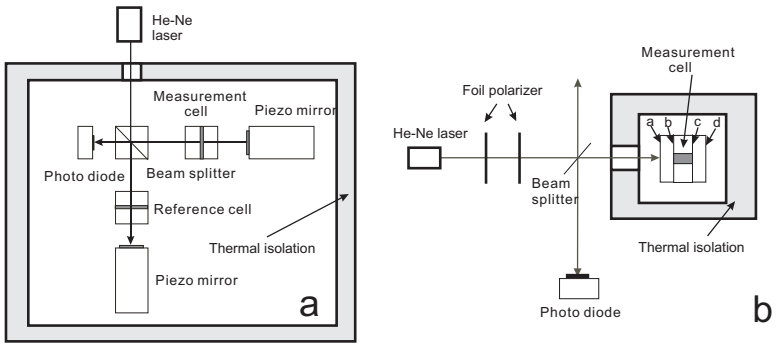

Figure 1.4: Sketch of the dn/dc interferometer

density filters were used to adjust the primary laser intensity. The filters with an optical density of 0.3 or 0.6 was used for attenuation. A typical measurement using an attenuate filter with an optical density 0.6 is shown in Fig.1.3. Obvious α deviates from its nominal value at count rate above 1E6 Hz. We repeated the procedure 6 times and obtained an average value for τ_{min}=(2.10±0.14) E-8 Hz.

1.3.3 Contrast factors

The contrast factors $(\partial\ n/\partial\ T)_{c,p}$ and $(\partial\ n/\partial\ c)_{T,p}$ taken at the wavelength of the readout laser need to be measured in separate experiments. For this purpose, we use two different interferometers.

Refractive index increment with concentration

A sketch of $(\partial\ n/\partial\ c)$-interferometer is shown in Fig. 1.4(a). The laser beam is split into two beams by beam splitter. One beam passes the measurement cell and the other one passes the reference cell. Both of them are reflected by the mirrors and interfere at the photo diode. Ideally the phase of the reference beam stays always constant. This is not always the case due to unavoidable temperature fluctuations. Typically the phase changes by 0.0198 in 2 hours which is a typical time for one measurement. To determine the phase difference between the two beams, the voltage across the piezo is linearly periodically ramped with an amplitude of $U_{2\pi}$, which corresponds to a mirror displacement of $\lambda/2$ and a 2π phase shift. During

the periodic mirror scan, the intensity at the photo diode is obtained. The phase angle is determined by

$$I_{\text{diode}} = A(1 + cos(\frac{U}{U_{2\pi}} - \phi)) + B, \tag{1.7}$$

where A and B are constants.

The phase difference ϕ between two beams is determined by the wave-vector of the laser light, $k = 2\pi/\lambda$, and the optical path difference between the two interferometer arms s:

$$\phi = 2ks. \tag{1.8}$$

The change of ϕ can be stemmed from changes of both k and s:

$$d(\phi) = 2s{\cdot}dk + 2k{\cdot}ds. \tag{1.9}$$

Since the laser is very stable, the first term of Eq.1.9 is ignored . For differential interferometer the path difference $ds = l \cdot dn$, l is the thickness of the measurement cell. Thus

$$d(\phi) = 2k{\cdot}ds = 2kl{\cdot}dn, \tag{1.10}$$

and

$$(\frac{\partial n}{\partial c}) = (2kl)^{-1}(\frac{\partial \phi}{\partial c}) = (2kl)^{-1}(\frac{\partial \Delta\phi}{\partial c}). \tag{1.11}$$

The precise thickness l needs to be determined in a separate calibration run.

Refractive index increment with temperature

Figure 1.4(b) shows a sketch of the $\partial\ n/\partial\ T$-setup. Two foil polarizers are used to adjust the intensity. The laser beam is split into two beams. One beam goes through the beam splitter to the measurement cell and is reflected at the back window of the measurement cell. The reflected beam at the front window (**a** ,**b**) and at the back window (**c**, **d**) are superposed at the photodiode. The main contribution of the reflections stem from **a** and **d** due to the large refractive index difference (~ 0.5) to air compared to the smaller refractive index difference at **b** and **c** (~ 0.01) at the inner window, which is in contact with the liquid.

The main difference to the $(\partial\ n/\partial\ c)$-setup is that the $(\partial\ n/\partial\ T)$-instrument does not contain any moving parts. The optical path difference depends on the change of the refractive

index n and n_{w} and the length l and l_{w} of the sample and the window, respectively

$$ds = d(nl) + d(2n_w l_w). \tag{1.12}$$

The temperature derivative of refractive index is obtained by,

$$\frac{\partial n}{\partial T} = \frac{1}{2kl} \cdot \frac{\partial \phi}{\partial T} - 2 \cdot \frac{n_w}{l} \cdot \frac{\partial l_w}{\partial T} - 2 \cdot \frac{l_w}{l} \cdot \frac{\partial n_w}{\partial T} - \frac{n}{l} \cdot \frac{\partial l}{\partial T}. \tag{1.13}$$

For this setup, n_w=1.457. Thermal expansion coefficients $\partial l_w/\partial T$ and $\partial l/\partial T$ are 5.1E-7 and 7.5E-7, respectively. $2 \cdot (l_w/l) \cdot (\partial n_w/\partial T)$ is measured to be 2.45E-6 K^{-1}.

1.3.4 Data analysis

Heterodyne signal

The measured intensity I in the TDFRS experiment contains contributions from the electric field amplitude of diffracted beam E_{s}, the coherent electric field amplitude E_{c} and incoherent electric field amplitude E_{inc}, and can be writen as:

$$I = \mid E_{\mathrm{c}} + E_{\mathrm{s}} e^{i\phi} \mid^2 + E_{\mathrm{inc}}^2 = E_s^2 + 2E_{\mathrm{s}}E_{\mathrm{c}} \cos\phi + E_c^2 + E_{\mathrm{inc}}^2, \tag{1.14}$$

where ϕ is the phase shift between the signal and the coherent background. The homodyne (S_{hom}) and heterodyne (S_{het}) signal can be expressed as follows

$$S_{hom} = \frac{1}{2}(I_\phi + I_{\phi+\pi}) = E_{\mathrm{s}}^2 + E_{\mathrm{c}}^2 + E_{\mathrm{inc}}^2 \tag{1.15}$$

$$S_{het} = \frac{1}{2}(I_\phi - I_{\phi+\pi}) = 2E_{\mathrm{c}}E_{\mathrm{s}} \cos\phi \tag{1.16}$$

The background from incoherent scattering can be completely suppressed by heterodyne signal detection. Due to the signal and background level in actual TDFRS experiment, the heterodyne detection is always superior to the homodyne [84].

Working equations

Temperature grating: First of all, an optical grating is excited by the interference of two writing beams operating at the wavelength λ=488 nm. The dye with strong adsorption at

this wavelength converts the optical grating into a temperature grating. The evolution of the temperature grating can be described as

$$\frac{\partial T(x,t)}{\partial t} = D_{\text{th}} \frac{\partial^2}{x^2} T(x,t) + S(x,t) \tag{1.17}$$

where D_{th} is thermal diffusivity and the source term $S(x,t)$ is given by

$$S(x,t) = \frac{\alpha}{\rho c_p} I(x,t) = S_0 + S_q(t) e^{iqx}. \tag{1.18}$$

Here α is an optical absorption coefficient, C_{p} the specific heat at constant pressure, $I(x,t)$ intensity of the writing beam. Eq. (1.17) is solved by

$$T(x,t) = T_0 + T_m(t) + T_q(t) e^{iqx}, \tag{1.19}$$

where T_0 is the initial sample temperature and $T_m(t) = \alpha I_0 t / \rho c_p$ is the mean sample temperature. The amplitude $T_q(t)$ of the temperature grating is expressed as a linear response for arbitrary excitations $S_q(t) = \alpha(\rho c_p)^{-1} I_q(t)$:

$$T_q(t) = \int_{-\infty}^{t} dt' S_q(t') e^{-(t-t')/\tau_{\text{th}}} \tag{1.20}$$

$\tau_{\text{th}} = (D_{\text{th}} q^2)^{-1}$ is the decay time for the heat diffusion, after which a stable temperature grating is reached.

Concentration grating: In TDFRS setup, the build-up of the concentration grading driven by a temperature grating due to the Ludwig-Soret effect in a fluid mixture can be evaluated from a one-dimensional diffusion equation

$$\frac{\partial c(x,t)}{\partial t} = D \frac{\partial^2}{x^2} c(x,t) + D_{\text{T}} c_0 (1 - c_0) \frac{\partial^2}{x^2} T(t,x) \tag{1.21}$$

with the solution

$$c(x,t) = c_0 + c_q(t) e^{iqx} \tag{1.22}$$

where

$$c_q(t) = -q^2 D_{\text{T}} c_0 (1 - c_0) \int_{-\infty}^{t} dt' T_q(t') e^{-(t-t')/\tau}. \tag{1.23}$$

τ is the decay time for the collective diffusion.

In analogy to the concentration grating, the refractive index grating can be expressed as

$$n(x,t) - n_0 = n_q(t)e^{iqx} = [(\frac{\partial n}{\partial T})_{c,p}T_q(t) + (\frac{\partial n}{\partial c})_{T,p}c_q(t)]e^{iqx}, \tag{1.24}$$

where n is the refractive index at the readout wavelength (633 nm).

TDFRS analysis equation: The heterodyne diffraction signal $\zeta_{\text{het}}(t)$ is proportional to the refractive index modulation depth:

$$\zeta_{\text{het}} \propto E_{\text{c}}E_{\text{s}}\cos\phi \propto n_q(t) \tag{1.25}$$

Combining Eq.1.19, 1.20, 1.23, 1.24, 1.25, the heterodyne signal can be evaluate

$$\zeta_{\text{het}} = 1 - e^{-t/\tau_{\text{th}}} - A(\tau - \tau_{\text{th}})^{-1}[\tau(1 - e^{-t/\tau}) - \tau_{\text{th}}(1 - e^{-t/\tau_{\text{th}}})] \tag{1.26}$$

A is the ratio of the steady-state amplitudes of the concentration grating $\zeta_{\text{c}}(t \to \infty)$ to the thermal contribution $\zeta_{\text{th}}(t \to \infty)$:

$$A = \frac{\zeta_c(t \to \infty)}{\zeta_{\text{th}}(t \to \infty)} = (\frac{\partial n}{\partial c})_{p,T}(\frac{\partial n}{\partial T})^{-1}_{p,c}S_{\text{T}}c_0(1 - c_0) \tag{1.27}$$

Due to the fact $\tau_{th} \ll \tau$, Eq.1.26 can be simplified as

$$\zeta_{\text{het}} = 1 - e^{-t/\tau_{\text{th}}} - (\frac{\partial\ n}{\partial\ c})_{p,T}(\frac{\partial\ n}{\partial\ T})^{-1}_{p,c}S_{\text{T}}c_0(1 - c_0)(1 - e^{-t/\tau}) \tag{1.28}$$

Eq.1.28 is used to fit the experimental heterodyne diffraction signal. The two contrast factors $(\partial\ n/\partial\ T)_{c,p}$ and $(\partial\ n/\partial\ c)_{T,p}$ are obtained separately (cf. Sec.1.3.1) and the transport coefficients D_{th}, D, D_{T}, and Soret coefficient S_{T} can be determined.

Excitation function and iterative correction

The derivation of Eq.1.28 assumes an ideal excitation function of the thermal grating, however in practice it is not realized due to the finite switching time of the Pocket cell. In Fig.1.5 one can see the actual excitation function measured for different sample time. Generally, the excitation takes 10 μs to rise up to almost 1 and the plateau is reached after 160 ms.

Fig.1.6(a) shows the data of a measurement (solid curve) and the least-squares fit according to Eq.1.28. In Fig.1.6(b) the residuals are plotted. Systematic deviations are found. The large residuals arise from a non-ideal excitation function and can be correct for an iterative method developed by Wittko and Köhler [115].

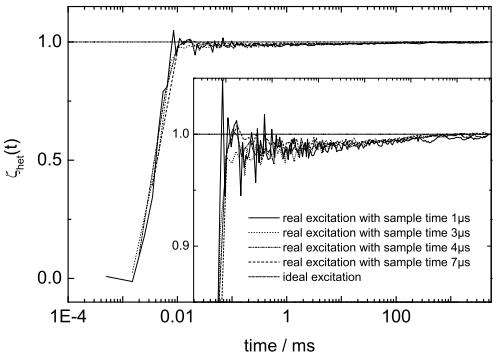

Figure 1.5: Measurements of the real excitation with various sample time

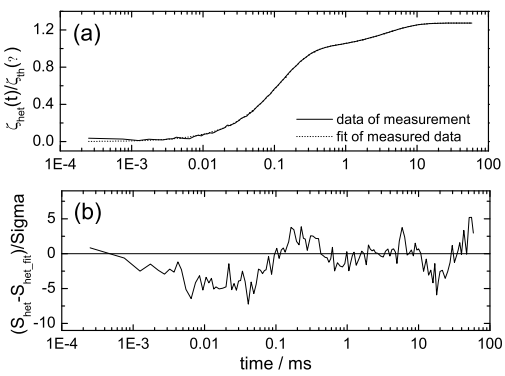

Figure 1.6: (a) Least-squares fit (solid curve) of the measured data (dot curve) with equation (1.26). (b) The residuals for the Toluene and n-hexane ($c = 0.517; T = 23°C$))

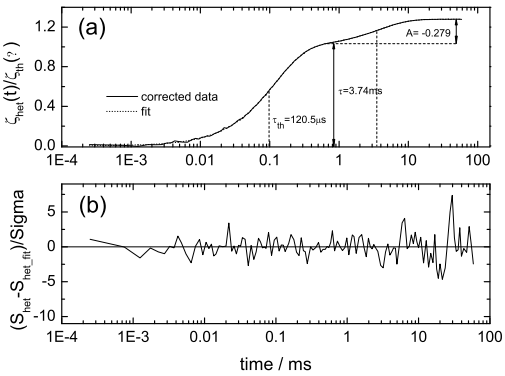

Figure 1.7: Corrected data of Fig.1.6.

In brief, we measured the TDFRS signal $\zeta_{\text{het}}^{exp}(t)$ and excitation function s_q. s_q can be separated into a contribution from the ideal excitation s_q^i and its deviation δs_q. If the deviations are small, $\zeta_{\text{het}}^{exp}(t)$ is a function depends linearly on the parameters s_q and t

$$\zeta_{het}^{exp} \equiv F_x[s_q,t] = F_x[s_q^i,t] + F_x[\delta s_q,t], \tag{1.29}$$

where x indicates the parameters A, τ, and τ_{th}.

The iterative loop start like this: First, $F_{x0}[s_q^i,t] \approx \zeta_{\text{het}}^{exp}(t)$ is fitted to Eq.1.28 without considering the deviation. The parameters x_0 are obtain for $F_{x0}[s_q^i,t]$, therefore we can calculate $F_{x0}[\delta s_q,t]$ according to Eq.1.29.

In the second step, a better function $F_{x1}[s_q^i,t]$ is obtained by considering the term $F_{x0}[\delta s_q,t]$, which accounts for deviations

$$F_{x1}[s_q^i,t] = \zeta_{het}^{exp} - F_{x0}[\delta s_q,t]. \tag{1.30}$$

x_1 is obtained by fitting $F_{x1}[s_q^i,t]$ to Eq.1.28, and is used to calculated $F_{x1}[\delta s_q,t]$ in the next loop. After sufficient iterations, we can get a function $F_{xk}[s_q^i,t]$, which agrees with the fitting curve without systematic deviations (in Fig.1.7), and the corresponding parameters $x_k = A, \tau$ and τ_{th} are used to calculate the thermal diffusion coefficient D_{T}, translation diffusion coefficient D and thermal diffusivity D_{th}, respectively.

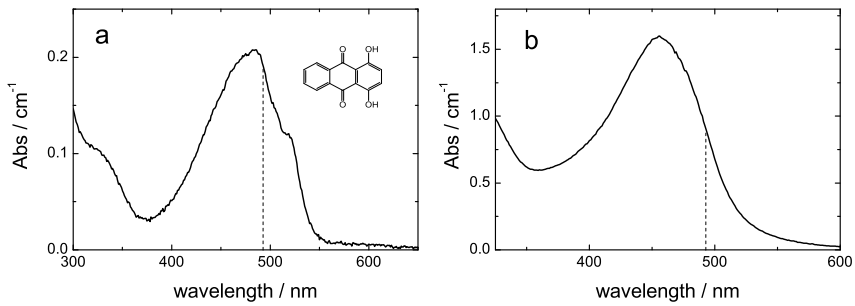

Figure 1.8: The adsorption spectrometry for qunizarin (a) and Basantol yellow (b)

1.3.5 Influence from the dye

As it has been mentioned in Sec.1.3.1, small amount of inert dye should be added into the solution mixture to convert the optical intensity gradient into a temperature gradient. The requirement for the dye is, that it should have a strong adsorption at the wavelength of the writing beam (λ=488 nm), while at the same time it is transparent at the wavelength of reading beam (λ=633 nm). The qualified dye candidates should also be physical and chemical inert for the measured mixtures, and should not show photo bleaching. After an extensive examinations over 30 kind of possible dyes, two organic compounds was selected out and proven to be suitable for the TDFRS measurements. They are quinizarin (in Fig.1.8 (a)) applied for non-polar or organic mixtures and basantol yellow (in Fig.1.8 (b)) working in polar or aqueous solutions.

It is worth to notice that basantol yellow is a kind of organic salt and its adsorption band is very sensitive to the pH value of the surrounding environment. In Fig.1.9, we can observe that at low pH conditions, the peak shifts to the low wavelength region and the requirement for the TDFRS measurement can not be fulfilled.

Although the amount of the dye (generally less than 10^{-4} wt) in the solution can be neglected. Wittko and Köhler studied the influence of quizarin and found that the average values are not changed by the addition of the dye []. We studied the contribution of basantol

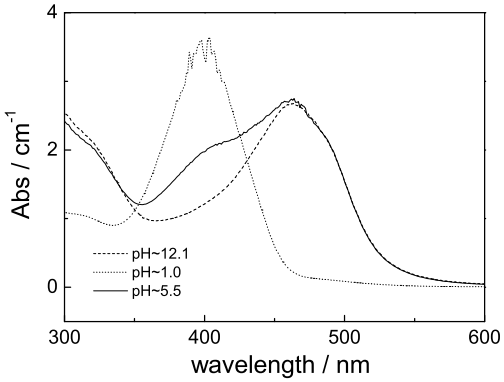

Figure 1.9: The pH dependence of the adsorption spectrometry for basantol yellow.

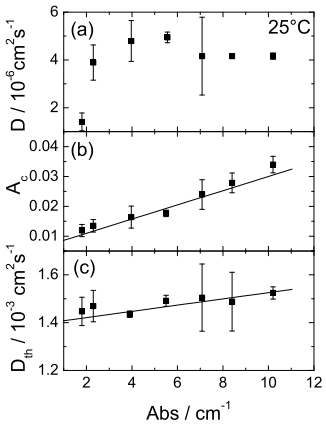

Figure 1.10: Diffusion coefficient (a), concentration amplitude (b) and thermal diffusivity (c) of Basantol yellow in water as a function of the optical density at λ=488 nm. Solid lines are linear fit to the data.

yellow to the concentration signal, by determining the amplitude of the concentration signal A_c, the diffusion coefficient D, and the thermal diffusivity D_{th} as function of the dye content (see Fig. 1.10). At an optical density of 2 cm^{-1}, where the TDFRS measurement was carried out, A_c is around 0.01. For strong TDFRS concentration signal the dye contribution is in the orders of 1%, but at low concentration the influence of the dye needs to be considered.

1.4 Experimentally studied systems

1.4.1 Simple liquid mixtures

Since the discovery of the Ludwig-Soret effect around 150 years ago, the thermal diffusion behavior for simple fluid mixtures especially for binary liquid mixtures had been extensively studied. Here we call them 'simple' fluid mixtures in contrast to the micellar systems and colloidal dispersions discussed later, which often show a complex phase behavior.

For the studies of thermal diffusion behavior, the simple fluid mixtures can be classified into associated and non-associated fluid mixtures. For non-associated mixtures, most of them belonging to organic compounds, the interactions and its orientation between the molecules are weak, so that they can be used to study the contribution from chemical parameters. Based on the data base on the studied non-polar system, some rules of the thumb were obtained [114]. Typically, the components with larger mass and density prefer moving to the cold side, and Soret effect becomes stronger with decreasing solubility. By studying the isotope effect on the mixture of benzene and cyclohexane, Debuschewitz [19] *et al.* proposed that the Soret coefficient can be split into the additive contributions stemming from the difference in mass δM and moment of inertia δI

$$S_T = S_T^0 + \alpha_M \delta M + b_I \delta I. \tag{1.31}$$

$\delta\, M$ and $\delta\, I$ were initially defined as relative difference [19]

$$\delta\, M = \frac{M_1 - M_2}{M_1 + M_2}, \quad \delta\, I = \frac{I_1 - I_2}{I_1 + I_2}, \tag{1.32}$$

and later $\delta\, M$ and $\delta\, I$ denoted the absolute differences [116]

$$\delta\, M = M_1 - M_2, \quad \delta\, I = I_1 - I_2. \tag{1.33}$$

The architecture effect was also investigated by Polyakov *et al.* for heptane and its isomeric compound in benzene. They found that the alkane with highest degree of branching tends to move to the cold side, while all other heptane isomers move to the warm side. Typically, the Soret coefficient of non-associated mixtures has not strong dependence on the compositions and the temperature.

For associated fluid mixtures, including aqueous solution and mixtures with specific interactions such as hydrogen bond formation, the thermal diffusion behavior depends strongly on the temperature and the concentration.

1.4.2 Complex fluid mixtures

Complex fluid mixtures refer to these systems with large molecules, such as micellar solutions, polymer solutions and colloidal dispersions. Often those systems show a complex phase behavior. Those particles perform Brownian motion and hydrodynamic interactions become important. Due to their large structure length scale compared to the surrounding solvent, the number density of their translational degrees of freedom is many orders of magnitude smaller than that for an ordinary, molecular material.

Polymer solutions Polymers are macromolecules with a number of repeated unit segments. In several cases, polymers in solution exhibits random chain conformation. The flexibility of the chain makes not only inter-polymer but also intra-polymer interaction very important. The thermal diffusion behavior of polymer in organic solvents were first systematically studied by Schimpf *et al.* with TFFF [90, 89]. The studies on 17 polymer-solvent systems show that the thermal diffusion behavior of polymer is dominated by the nature of the monomer and solvent. D_{T} for a infinite diluted solution becomes independent of the degree of polymerization. This rule was confirmed later by Rossmanith *et al.* with TDFRS for the system polystyrene in ethyl acetate [84]. Recently, Rauch and Köhler showed that the molar mass independence of the thermal diffusion coefficient at infinite dilution break down for polymers with less than 10 repeating units [82]. Non-equilibrium simulations predict that D_{T} should become independent of the molar mass, when the chain length is around two to three times of the persistence length [121]. For most case, polymers in organic solvents tend to enrich in the cold side and correspond to positive Soret coefficient. Studies also show that thermal diffusion of a polymer might be related to thermal conductivity, density and

activation energy [].

Thermophoresis of polymer chains in aqueous/associated solutions is complex due to the strong interaction (such as hydrogen bond) existing between the solvent, and the polymer show a complex thermal diffusion behavior. Chan *et al.* studied polyethylene Glycol (PEG) in water [11] with TFFF. The independence rule of D_T on the mass of the polymer was extended to this aqueous system for the PEG polymer and oligomers with molecular weight larger than trimer. Poly(ethylene oxide)(PEO) in the mixture solvents water/ethanol was investigated by Kita *et al.* with TDFRS [17, 47]. Water is a good solvent for PEO, while ethanol is a poor solvent. Dilute polymer solution (5 g/L) was prepared to avoid the interaction between the polymers. It was found that the Soret coefficient of PEO changes the sign from negative to positive with increasing water content, which has also been proven later by a simple lattice model with statistical mechanics method. The sign change composition consists with the composition where the hydrogen bond network breaks, which indicates the strong influence from the environment on a single polymer chain. This was the first time that a sign change of S_T for polymer was observed experimentally. Later, a sign change of the Soret coefficient of PEO water/ethanol mixture (water mass fraction 0.8-0.85) was also observed with temperature [47]. Poly(N-isopropylacrylamide)(PNiPAM) in water shows coil-globule transition with increasing temperature. Experimentally it was shown that the Soret coefficient of PNiPAM is enhanced at the θ temperature, where the coil-globule transition occurs [46]. S_T for PNiPAM in ethanol shows a sign change with increasing temperature at 34 °C from positive to negative, and the sign change is independent of the concentration in the investigated concentration range from 0.2 g/L-5 g/L [44]. The study for PNiPAM resolved in various alcohols reveals the correlation between the Soret coefficient and the Hildebrand solubility parameter (also known as cohesive energy density) [45].

Micelle solutions Amphiphilic molecule, which have both hydrophobic part and hydrophilic part, in the solution, will form micelles with a variety of structures and properties depending on temperature and concentration. Ionic surfactant sodium dodecyl sulphate (SDS) in water has been studied by Piazza *et al.* with a thermal lens and a beam deflection setup (a kind of diffusion cell) [71]. The inverse $1/S_T$ of SDS displays a linear function with the SDS concentration, and the slope decrease with the addition of salt. This indicates the strong influence from the electrostatic interactions. SDS and a non-ionic surfactant β-dodecyl

maltoside (MD) and a mixture of both were investigated in water in a temperature range 5-35 °C [42]. The Soret coefficient for all three systems increases with increasing temperature. However in the studied temperature range, DM micelles show a positive Soret coefficients, and SDS micelles show a negative Soret coefficient, while for the 1:1 molar mixture of DM and SDS, a sign change of S_T is observed with increasing temperature. It is found that the Soret coefficient S_T and thermal diffusion coefficient D_T of the micelles follow a exponential law and a linear increase with increasing temperature, respectively,

$$S_\mathrm{T} = S_\mathrm{T}^\infty[1 - exp(\frac{T^\pm - T}{T_0})], \tag{1.34}$$

where S_T^∞ the high-T thermophobic limit, $T^\pm$ the sign change temperature and T_0 indicating the strength of the temperature effect; linear dependence on temperature was found for thermal diffusion coefficient

$$D_\mathrm{T} = A(T - T^\pm), \tag{1.35}$$

where A is a system-dependent amplitude. As a quite universal rule, this was confirmed later by other complex systems like polymers, colloids and bio-molecular suspensions.

Rigid colloidal dispersions and bio-molecules dispersions As a model system, a magnetic colloidal dispersions made of Fe_3O_4 were extensively studied with different experimental methods [110, 111, 6, 1]. The magnetic colloids can either be charged stabilized or be sterically stabilized by a surfactant layer. In the most cases the magnetic particles in water showed a negative Soret coefficient, while a positive Soret coefficient was obtained in organic solvent. Putnam and Cahill studied a charged polystryrene (PS) particles with diameter 26±5 nm in water using a micro-scale beam deflection setup. A negative Soret coefficient was found for the PS particles [79]. Charged silica particles with radius 11 nm was investigated by Rusconi *et al.* by thermal lens setup. A negative Soret coefficient was detected and found to decrease with increasing salt content [88]. Duhr and Braun studied a charged polystyrene sphere in water with various particle diameters by microfluidic fluorescence [24]. They found that the Soret coefficient is proportional to the surface area $S_\mathrm{T} \propto a^2$, while the thermal diffusion coefficient is proportional to the diameter $D_\mathrm{T} \propto a$. The dimension dependence is explained qualitatively by a relationship between S_T and the Gibbs free enthalpy of the particle. Besides spherical colloids, rod-like boehmite colloids (γ-AlOOH) in ethanol/water mixtures were studied [16].

There have been numerous studies of the thermal diffusion behavior for bio-molecules. For instance the influence of temperature, ionic strength, salt species and pH on the thermal diffusion behavior of lysozyme solutions has been studied by thermal lens method [73]. The Soret coefficient of lysozyme decreases with increasing ionic strength, and increases with increasing temperature. A sign change of S_T occurs from negative to positive with increasing temperature. The pH and the salt species influence the temperature dependence of S_T only slightly. A microfluidic fluorescence study on DNA in water shows that DNA molecules tend to migrate to the cold side[23, 8].

1.4.3 Close to the critical point and other scaling laws

Close to the critical point the dynamics of the system is slowed down and large concentration fluctuation exist.

In 1956 Thomaes showed that the Soret coefficient of nitrobenzene/n-hexane close to the critical point [104]. Roughly 20 years later Giglio and Vendramini [35] found experimentally for the mixture aniline/cyclohexane that the Soret coefficient diverges with a scaling low $S_\mathrm{T} \propto (T - T_\mathrm{c})^{-\varphi}$ when the critical temperature is approached. The critical exponent was determined as φ=0.73. Later Wiegand found φ=0.68$\pm$0.03 by TDFRS measurement [114].

Lately, Enge *et al.* [29] studied the thermal diffusion behavior of a polymer blend poly(dimethyl siloxane) (PDMS) and poly(ethyl-methyl siloxane) (PEMS) close to the critical point. Approaching the critical temperature T_c the polymer blend performs a crossover from mean field to Ising behavior. The Soret coefficient of PDMS follows the mean field scaling law with $S_\mathrm{T} \propto \varepsilon^{-1.0}$, while in Ising regime as $S_\mathrm{T} \propto \varepsilon^{-0.67}$ holds, with the reduced temperature $\varepsilon = (T - T_\mathrm{c})/T_\mathrm{c}$.

Rauch *et al.* demonstrated for the system polystyrene/toluene that the thermal diffusion coefficient D_T decays sharply when the glass transition is approached [81]. S_T decreases with the concentration of polystyrene as

$$S_\mathrm{T} \propto C^{-0.77} \tag{1.36}$$

In the diluted regime the Soret coefficient S_T increases with the molecular weight M as,

$$S_\mathrm{T} \propto M^{0.53} \tag{1.37}$$

and above the overlap concentration C^* S_T becomes mass independent.

1.5 Theoretical descriptions and simulations

1.5.1 Selected theories

The simplest way to look at the thermophoretic motion is to treat the system as an ideal gas. For more complex systems, as already explained in Sec.1.1 the thermophoretic motion can be conceptually be separated into two contributions: one stemming from the *single particle contribution* and one stemming from the *interaction contribution* between the interacting particles. In the following we will briefly sketch the present theories according to this line: ideal gas approach, single particle contribution and interacting particle contributions.

Ideal gas approach: Generally, one can describe the thermophoretic motion of a highly diluted colloidal suspension analog to an ideal gas. Thus the mass flow of the dilute solution of particles is driven by the number density gradient (∇n) and the temperature gradient (∇T),

$$J = -D(\nabla n + nS_{\mathrm{T}}\nabla T). \tag{1.38}$$

In the stationary state $J = 0$, a temperature modulation $\triangle T(r)$ induces a relative change in density $\triangle n/n = -S_{\mathrm{T}}\nabla T$. In the absence of interactions, the particles form an ideal gas with an osmotic pressure $p = nkT$, and the stationary state p=const. This relation leads to an explicit expression for the current,

$$J_0 = -D_0(\nabla n + \frac{n}{T}\nabla T), \tag{1.39}$$

where $D_0 = kT/(6\pi\eta a)$ is the Stokes-Einstein's diffusion coefficient for a particle with radius a in a solvent with viscosity η. Thus one finds

$$S_{\mathrm{T}}^{o} = \frac{1}{T}. \tag{1.40}$$

However due to the absence of interaction in the derivation, this ideal-gas theory rarely agrees with experimental results.

A similar approach was used by Brenner [9] to describe the thermophoretic motion of highly diluted, inert Brownian particles. He found that the thermal diffusion coefficient D_{T} only depends on solvent properties as

$$D_{\mathrm{T}} = \alpha\beta, \tag{1.41}$$

with the solventexpansion coefficient $\beta = (1/\rho)(\partial(1/\rho)/\partial T)$ and thermometric diffusivity $\alpha = k/\rho c_{\mathrm{p}}$, where k, ρ, c_p are the thermal conductivity, density, specific heat and specific volume. This simple approach only predicts qualitative features of the thermal diffusion.

Single particle behavior: Würger [117] showed for solid nano-particles using a mechanical force balance concept that S_{T} is determined by the difference of the heat capacity of the solute particle c_{p} and the solvent c_{s}

$$S_{\mathrm{T}} = \alpha + n\kappa V_{\mathrm{p}}(c_{\mathrm{p}} - c_{\mathrm{s}}). \tag{1.42}$$

with the thermal expansion coefficient $\alpha = -(1/n)(\partial n/\partial T)$ and the osmotic compressibility $\kappa = (1/n)(\partial n/\partial P)$. This expression is in general larger than the ideal gas value $S_{\mathrm{T}} = 1/T$. Using Eq. 1.42 it is possible to explain the positive Soret coefficients of magnetic particles in organic solvents and the negative Soret coefficient in aqueous suspensions [110, 111, 6, 1].

Many publications, which focus on the single particle behavior analyze the thermal diffusion behavior of ionic colloids. For instance Morozov [59, 60] derives an expression for the Soret coefficient considering the force balance of electrical and viscous force acting on the particle. He introduces two characteristic dimensionless parameters: the surface potential of the particle ψ_{s} and the ratio of the double layer d_{dl} thickness to the particle radius a $\lambda = d_{\mathrm{dl}}/a$. Finally, he calculates the velocity of the thermophoretic motion $u = u(\lambda, \psi_{\mathrm{s}})$ as function of those characteristic parameters and expresses the Soret coefficient as

$$S_{\mathrm{T}} = -\frac{3R\phi}{4l_{\mathrm{B}}T} u(\lambda, \psi_{\mathrm{s}}), \tag{1.43}$$

where ϕ is the volume fraction of the colloids and l_{B} is the Bjerrum length. Probably due to the approximations made in the derivation experimental data are under estimated by a factor of two.

Ruckenstein [87] expressed the thermophoretic velocity for this double layers on the basis of Navier-Stokes equations and thermodynamic relations. Piazza and Guarino [72] used the thermoporetic velocity to calculate the Soret coefficient

$$TS_{\mathrm{T}}^{\mathrm{dl}} = 1 + \frac{3\pi}{4}\left(\frac{4\pi l_{\mathrm{B}}^2 \sigma}{e}\right)^2 \frac{R}{l_{\mathrm{B}}^3 \kappa^2} \tag{1.44}$$

with κ the inverse Debye length, σ the surface charge. They explained their experimental data for SDS micelles, but in general the quadratic dependence of S_{T} on the Debye screening length could not be confirmed by experiments [22].

Later, Parola and Piazza [67, 68] used a similar microscopic approach to derive a microscopic expression for the Soret coefficient of neutral and charged colloids in dilute suspension. In the Debye-Hückel approximation they found

$$TS_{\mathrm{T}} = 1 + \frac{Z^2 q^2}{k_{\mathrm{B}} T} \frac{1}{\varepsilon a (1+\kappa a)^2}, \tag{1.45}$$

where the "ideal-gas contribution" has been added and with the colloidal charge Zq and the permittivity ε. For infinitely thin double layers, this expression agrees with Morozov [59], but this expression has the same κ^{-2} found before, which could not be comfirmed by experiments. Also the a^{-3} dependence was not found experimentally.

Lately, Dhont *et al.* [22] derived an expression for the thermal diffusion coefficient of charged colloids in water. The theory is based on the force balance on the Brownian time scale and thermal dynamics in terms of reversible work for the formation of a solvation layer and electrical double layer. This approach covers thin as well thick double layers, and the Soret coefficient is given by

$$\begin{aligned} T S_T^{(dl)} &= 1 + \frac{1}{4}\left(\frac{4\pi l_B^2 \sigma}{e}\right)^2 \frac{1}{(1+\kappa a)^2} \frac{\kappa a^4}{l_B^3} \left\{ 1 - \frac{d\ln\varepsilon}{d\ln T}\left(1+\frac{2}{\kappa a}\right)\right\} \\ &\quad + \left(\frac{4\pi l_B^2 \sigma}{e}\right)^2 \frac{1}{1+\kappa a}\left(\frac{a}{l_B}\right)^3 \frac{d\ln Q}{d\ln T}, \end{aligned} \tag{1.46}$$

where Q is the total charge on the surface. Thus the dependence of the Soret coefficient on the Debye-Hückel screening length $\lambda_{\mathrm{DH}} = \kappa^{-1}$ is obtained, and confirmed by experimental studies of polystyrene beads and SDS micelles as well.

Further, it is worth to point out that S_{T} depends on a^2, which was also found experimentally. The a^2 dependence has also been found by Duhr and Braun by an heuristic argument [24].

Semenov and coworkers [93, 97, 95, 96, 92, 94], derived expression for the thermal diffusion coefficient of molecules, polymers and colloids. Basically, they supposed that a temperature-dependent pressure gradient is the driving force for thermal diffusion process. The derivation of the thermophoretic mobility (thermal diffusion coefficient) follows three steps: 1. calculate the temperature around the component; 2. derive the excess pressure distribution around the component; 3. derive the expression for solvent velocity profile around the component, the component thermophoretic velocity and the thermal diffusion coefficient

by the Navier-Stokes equation $\eta \Delta u = -\nabla \Pi$, where η is the viscosity, u is the velocity of the liquid and $-\nabla \Pi$ is the local pressure gradient around the solute particle.

By neglecting the difference between thermal conductivity of the solute particle and the solvent, the thermal diffusion of polymer has been derived as [92]

$$D_{\mathrm{T}} = -\frac{8}{27}\frac{\alpha_{\mathrm{T}} r_{\mathrm{m}}^2 (A_m A_s)^{0.5}}{\eta v_0}, \tag{1.47}$$

where $\alpha_{\mathrm{T}} = \partial(ln v_0)/\partial T$ is the cubic thermal expansion coefficient, A_m and A_s are the the monomer-monomer and solvent-solvent Hamaker constants, r_{m} is the radius of a monomer, v_0 is the specific volume occupied by a solvent molecule. The thermal diffusion of a particle is derived as [97]

$$D_{\mathrm{T}} = -\frac{ln3}{4}\frac{\alpha_{\mathrm{T}} r_0^2 (A_{\mathrm{p}} A_{\mathrm{s}})^{0.5}}{\eta v_0 (n+2)}, \tag{1.48}$$

where A_{p} is the Hamaker constant for the particle, and r_0 is the radius of the a solvent molecule.

A practical problem with this approach is that the Hamaker constants calculated from the experimental D_{T} values are several times smaller than the tabulated ones, which is equivalent to overestimate the thermal diffusion coefficient. Further more, D_{T} is very sensitive to the choice of the radius, because the dependence is quadratic. Often it is not clear which radius such as the van der Waals radius, the radius determined from the molar volume, the hydrodynamic radius or the radius of gyration should be used.

Interacting colloidal dispersions: Bringuier and Bourdon [10] propose an expression for the thermal diffusion coefficient in terms of the temperature derivative of the total internal energy U (see their eq.(13)), based on similar arguments put forward by van Kampen [108]. In the case of concentrated dispersions U contains the interactions from all particles, while in the case of a highly diluted suspension U reduces to a single-particle contribution. So for instance in the case of a highly diluted suspension of charged colloids the Soret coefficient S_{T} is given by [22]

$$T S_T^{(dl)} \;=\; 1 + \frac{1}{4}\left(\frac{4\pi l_B^2 \sigma}{e}\right)^2 \frac{1}{(1+\kappa R)^2}\frac{\kappa R^4}{l_B^3} \;\; . \tag{1.49}$$

This result agrees with Eq.**??** for thin and thick double layers [22].

Dhont developed a theory for the thermal diffusion behavior of interacting colloidal particles [20, 21]. He integrated the Smoluchowski equation for systems with spatially varying temperature and determined microscopic expressions for the collective part of the thermal diffusion coefficient. If the interaction potential between the colloidal particles are known, the concentration dependence of the thermal diffusion coefficient can be be calculated. The temperature dependence of the potential of mean-force is shown to give rise to sign changes of the Soret coefficient on changing the temperature and/or concentration under appropriate conditions. Detailed expression of S_{T} and D_{T} are given in chapter **??**.Hui please, give the chapter with the colloidal paper the label Chap:colloids

Fayolle *et al.* [30] derive an expression for charged particles in an electrolyte solution. There derivation uses a similar argumentation as van Kampen [108]. They apply their theory to a charged micellar system, and reproduce quantitatively the data [71] as functions of salinity and micelle concentration.

1.5.2 MD Simulations and Lattice model calculations

MD simulations: In last decade non-equilibrium simulation methods have been developed and applied to study the thermal diffusion of simple fluid mixtures. Molecular dynamics (MD) simulations have been proved to be a powerful tool in studies of transport properties in liquid, and several MD algorithms have been developed [40]. To perform the MD simulations, the cross-interaction potential parameters, indicating the interaction between components of different species, were needed and play an important role. In many MD studies, Lorentz-Berthelot rule[62, 63, 69] $\varepsilon_{ij} = \sqrt{\varepsilon_i \varepsilon_j}$ and $\sigma_{ij} = (\sigma_i + \sigma_j)/2$ or its modified version[33, 32] $\varepsilon_{ij} = (1 - k_{ij})\sqrt{\varepsilon_i \varepsilon_j}$ and $\sigma_{ij} = (1 - l_{ij})(\sigma_i + \sigma_j)/2$ were used, where ε and σ are Lennard-Jones parameters for potential depth and diameter, k_{ij} and l_{ij} are cross-interaction parameters. Lorentz-Berthelot rule usually results in a cross-interaction, which is weaker than the average value of the pure-component interaction.

Hafskjold *et al.* performed non-equilibrium molecular dynamic (NEMD) simulations on isotope mixtures with various density and mass ratios [39]. The simulation results showed that the lighter component tends to migrate to the warm side, which agrees with the general rule obtained from the experiment. Additionally, the study shows that the flux of kinetic energy is dominated by lighter components, while the energy transfer by interactions

is dominated by heaver components. This explains from the view of energy the mass effect on the Soret coefficient. Reith *et al.* [83] and later Galliéro [33] investigated the thermal diffusion sensitivity on a large range of molecular parameters like mass, inertia, interaction strength ratios, diameter ratios, cohesive energy density (Hildebrand solubility parameter) and cross interaction parameters. EMD and NEMD simulation (dynamical and stationary) were performed by many groups on realistic mixtures. The studies were initially carried on non-associated fluid mixtures argon/kryton [69], methane/n-decane [100] , n-pentane/n-decane [70, 32] and benzene/cyclohexane [120], and lately on the associated fluid mixtures methanol, ethanol, acetone and dimethylsulfoxide (DMSO) in water [62]. Compared to the experimentally obtained Soret coefficient, the results from MD simulation for associated and non-associated mixtures show not only comparable amplitude but also consistent sign change composition. Simulations were also performed on dilute polymer solutions. Zhang *et al.* [121] used reversed non-equilibrium molecular dynamics (RNEMD) simulation method to investigate the influence of chain length, chain stiffness and solvent quality. A bead-spring model was used for describing the polymers, and the solvent qualities were represented by solvent-monomer interactions. They found that polymers tend to move to the cold side in good solvent. The experimentally known chain-length independence of D_{T} was reproduced, and it was found that flexible chains achieve constant D_{T} at shorter chain lengths than rigid chains.

Luettmer-Srathmann used a two-chamber Lattice model approach to determine the Soret coefficient of ethanol in water [56], PEO in water/ethanol [47] and lately also for alkanes in benzene [77]. The interaction parameters used in the model are adjusted by comparing with other properties of the mixture such as density, thermal expansion coefficient *etc*. In the case of ethanol/water and PEO/ethanol/water the sign change could be predicted. For the alkane mixtures quantitative agreement was found.

In a simple two-dimensional Ising kinetic model calculation [85] it was shown that a strong cross-interaction ($\varepsilon_{ij} > \varepsilon_{ii}$ and $\varepsilon_{ij} > \varepsilon_{jj}$) can lead to a sign change of the thermal diffusion. By increasing the cross-interaction parameter from $\min(\varepsilon_{ii}, \varepsilon_{jj})$ to $1.25 \cdot \max(\varepsilon_{ii}, \varepsilon_{jj})$ the slope of the concentration dependence of S_{T} change from possible to negative. The lattice calculation [56, 62] could only reproduce the sign change if the cross-interaction were stronger than the pure-components interactions, while the full MD simulation reproduces sign change

also if the Berthelot mixing rule is applied. The possible reason is that the lattice model only depends on the interaction potential and kinetic effects are completely ignored.

1.6 Outline of the thesis

The aim of this thesis is to gain a better understanding of the thermal diffusion behavior in liquid mixtures. Generally, we follow two approaches. First, we study systematically Soret coefficients in simple low molecular weight mixtures, which are accessible by molecular dynamic simulations. Secondly, we perform measurements on colloidal suspensions which can be described by analytical theories. Finally we investigate also micellar systems, which show a rich phase behavior. Therefore the thesis is organized as follows:

In Chapter 1 we present Soret coefficients for a aqueous mixture, which show a sign change of the Soret coefficient with concentration. We investigated two systems, acetone/water and dimethyl-sulfoxide(DMSO)/water. Both systems had been studied by NEMD simulations [85, 62] and a sign change has been predicted for both systems at a water weight fraction around 80%. Our experimental are in good agreement with the simulation results.

In Chapter 2, we discuss the thermal diffusion behavior of a sterically stabilized colloidal dispersion octadecyl coated silica particles ($R_h = 27$ nm) in toluene. We performed temperature and concentration dependent measurements. Additionally we performed dynamic light scattering measurements to characterize the interaction potential between spherical silica particles. The obtained results are compared with the theoretical expression given by Dhont [20, 21]. Our experimental study confirms the theoretical expressions derived for hard spheres.

In the last two chapters we investigate the thermal diffusion behavior of more complex systems, non-ionic surfactants in aqueous solution. First, in Chapter 3, we study the system $C_{10}E_8$(decyl octaethylene glycol ether) in water. $C_{10}E_8$ shows a fairly simple phase behavior and forms mainly elongated micelles in solution. The study shows that the thermal diffusion behavior of this system is independent of the choice of the dye and the collective diffusion coefficient agrees with the results obtained by dynamic light scattering measurements.

In order to investigate the influence of different micelle shapes in the thermal diffusion behavior, we investigate in Chapter 4 the thermal diffusion behavior of $C_{12}E_6$ (hexaethylene

glycol monododecyl ether) in water. $C_{12}E_6$ has a rich phase diagram and forms spherical as well as elongated micelles at ambient temperatures. Surprisingly, we found for this system a second slow mode in the concentration part of the TDFRS diffraction signal. To clarify the origin of this second mode we investigated also , C_6E_4 (tetraethylene glycol monohexyl ether), C_8E_4 (tetraethylene glycol monooctyl ether), $C_{12}E_5$ (pentaethylene glycol monododecyl ether), $C_{16}E_8$ (octaethylene glycol monohexadecyl ether). The origin of the slow mode of the TDFRS signal will be tentatively interpreted in terms of a ternary mixture of neutral micelles, dye-charged micelles, and water.

2 Experimental investigation of the Soret effect in acetone/water and dimethylsulfoxide/water mixture

Abstract

The thermal diffusion behavior of acetone/water and dimethylsulfoxide(DMSO)/water mixtures has been experimentally investigated by a transient holographic grating technique named thermal diffusion forced Rayleigh scattering (TDFRS). For both systems has been a sign change of the Soret coefficient S_{T} with varying water content predicted by simulations [C. Nieto Draghi *et al.*, J.Chem.Phys. **122**, 114503(2005)] . The sign change of S_{T} could be confirmed by the experiment and the agreement between the experimental and simulation data was in the entire concentration range reasonable.

2.1 Introduction

A temperature heterogeneity in a fluid mixture induces a mass flux, which results in a concentration gradient. This effect is known as Ludwig-Soret effect.[55, 101] For a binary mixture in a temperature gradient ∇T, the enrichment of one component ∇c is characterized by the Soret coefficient S_{T}, as

$$S_{\mathrm{T}} = -\frac{1}{c_0(1-c_0)}\frac{\nabla c}{\nabla T}. \tag{2.1}$$

The sign of the Soret coefficient indicates the direction of the thermophoresis.[**?**] Although the Ludwig-Soret effect has been discovered 150 years ago, there is still no microscopic understanding for the effect in fluid mixtures.[114]

In the past, the thermal diffusion behavior of simple fluid mixtures has been studied extensively [116**?** , 26, 52, 27, 19**?** , 7]. Organic liquid mixtures have been used in a benchmark

test, to establish reference data.[74] Recently, a special focus has been on the dependence of S_T on parameters such as mass and moment of inertia.[116, 19**?**] For many associating liquids, where the specific interactions, such as hydrogen bonding or electrostatic interactions, exist, sign changes of S_T with composition have been observed.[52, 78, 116, 106]

Molecular dynamics (MD) simulations have become an important tool in the investigation of thermal diffusion behavior in Lennard-Jones model fluids and small-molecule liquids.[38**?** , 33, 69**?**] Lately, the simulation techniques for non-equilibrium properties have been improved, which have led to a reasonable agreement between simulations and experiments for associating and non-associating liquid mixtures [70, 85**?**]. Simulations and also a two-chamber lattice model calculation have shown that the relation between the cross interactions and the pure interactions influence whether the sign of the Soret coefficient changes with concentration.[85, 56, 121] Lately, Nieto-Draghi *et al.* [62] predicted also a sign change for the associating liquid mixtures acetone/water and water/dimethyl sulfoxide(DMSO), which so far has not been confirmed by experiments.

In the present paper, we investigate the Soret coefficient of acetone and DMSO in water for different concentrations by thermal diffusion forced Rayleigh scattering (TDFRS). The experimental results are compared with the recently published simulation data and the influence of different parameters such as the hydrogen bond capability, mass and moment of inertia are discussed.

2.2 Experiment

2.2.1 Sample preparation

Acetone was purchased from Laborchemie Handels-GmbH (purity$>$ 99.9%) , and DMSO was ordered from Sigma-Aldrich (purity$\geq$99.9%). We used deionized water (Milli-Q). All substances were used without further purification. The mixtures were prepared as follows: First a tiny amount (roughly 10^{-5}wt by weight) of the dye basantol yellow [**?**], was dissolved in the solvents. For each solution the optical density was adjusted to 2-3 cm^{-1} at a wavelength of $\lambda = 488$ nm. Samples for the TDFRS measurements were prepared just before the measurement to avoid evaporation. The solutions were filtered directly by 0.45 μm filter (Spartan) into the sample cells. The temperature was controlled by a circulating water bath

and all measurements were performed at $T = 298 \pm 0.02$ K.

2.2.2 Data analysis and set-up

The thermal diffusion behavior of the solutions was investigated by thermal diffusion forced Rayleigh scattering (TDFRS). A detailed description of the set-up can be found elsewhere[**?**]. In brief, a grating is created by the interference of two laser beams ($\lambda = 488$ nm). A tiny amount of inert dye, which has a strong absorption band at $\lambda = 488$ nm, was added into the solution to convert the optical grating into a temperature grating. Both grating contribute to the refractive index grating, which is read out by the diffraction of a third laser beam ($\lambda = 633$ nm). The heterodyne diffraction signal ζ_{het} is evaluated by the equation,

$$\zeta_{\mathrm{het}}(t) = 1 + \left(\frac{\partial n}{\partial T}\right)^{-1} \left(\frac{\partial n}{\partial c}\right) S_{\mathrm{T}} c\,(1-c)\left(1 - e^{-q^2 D t}\right), \tag{2.2}$$

with the refractive index increment with concentration at constant pressure and temperature $(\partial n/\partial x)$, the derivative of the refractive index with temperature at constant pressure and concentration $(\partial n/\partial T)$ and the collective diffusion coefficient D.

2.2.3 Refractive index increments

The refractive indices of the mixtures were measured with an Abbe refractometer. The refractive index increment $(\partial n/\partial x)$ was determined from the derivative of a fifth order polynomial fit of the refractive index data. We used the molar fraction of water as concentration variable. $(\partial n/\partial T)$ was directly measured by an interferometer. The contrast factors $(\partial n/\partial x)$ and $(\partial n/\partial T)$ are shown in Fig.2.1 and 2.2, respectively. For the acetone/water mixture, the slope of refractive index n changes from positive to negative at $x = 0.4$, while $(\partial n/\partial x)$ of DMSO/water constantly decreases with DMSO concentration. $(\partial n/\partial T)$ value of both solutions decreases with decreasing water content.

2.3 Results and discussion

For both aqueous solutions we performed TDFRS measurements in the entire concentration range. In Fig.2.3 the Soret coefficient S_{T} is shown as function of molar fraction of aceton and

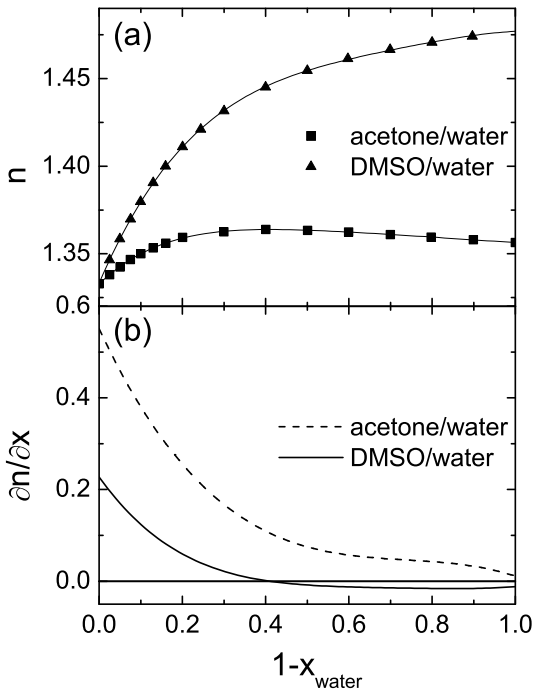

Figure 2.1: Refractive index n (a) and derivative of the refractive index $(\partial n/\partial x)$ (b) on the molar fraction of water for the mixture acetone/water (■, dashed line) and DMSO/water (▲, solid line).

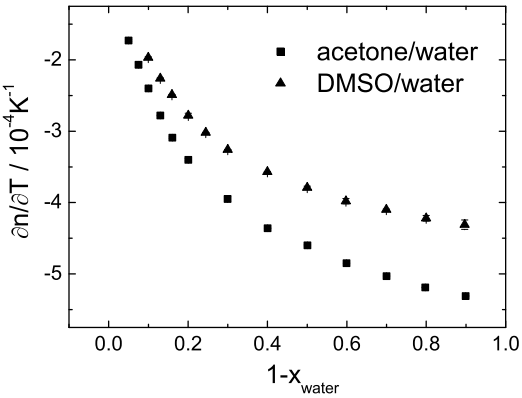

Figure 2.2: The refractive index increment with temperature $(\partial n/\partial T)$ as function of the molar fraction of water for acetone/water (■) and DMSO/water (▲).

DMSO, respectively. In the water rich region the Soret coefficient of acetone S_{T} decreases with increasing acetone concentration and reaches a minimum at a molar fraction of $x = 0.5$. For higher acetone concentrations ($x > 0.5$) S_{T} increases with x_{aceton}. Typically, the error bars do not exceed the symbol size, but for concentrations around $x = 0.5$ the uncertainties became larger due to the low value of the refractive index increment $(\partial n/\partial x)$, which leads to a small amplitude of the concentration part of the TDFRS-signal (cp. Eq. 2.2). The Soret coefficient of DMSO in water decreases with DMSO concentration and reaches almost a plateau or wide minimum for $x > 0.6$. Both systems show a sign change of Soret coefficient with concentration. Similar to other aqueous solutions such as methanol-water [106] and ethanol-water [52, 118, 26, 47], the sign change occurs in the water rich region at approximately $x = 0.11$ for acetone and around $x = 0.2$ for DMSO.

In Fig.2.3, we plot the simulation data obtained by boundary driven reverse non-equilibrium MD by Rousseau *et al.* [85, 62], which are also obtained at ambient temperature and pressure. Also the simulations results show a sign change from positive to negative with decreasing water content. Compared to the experimental results the simulations predict the sign change at

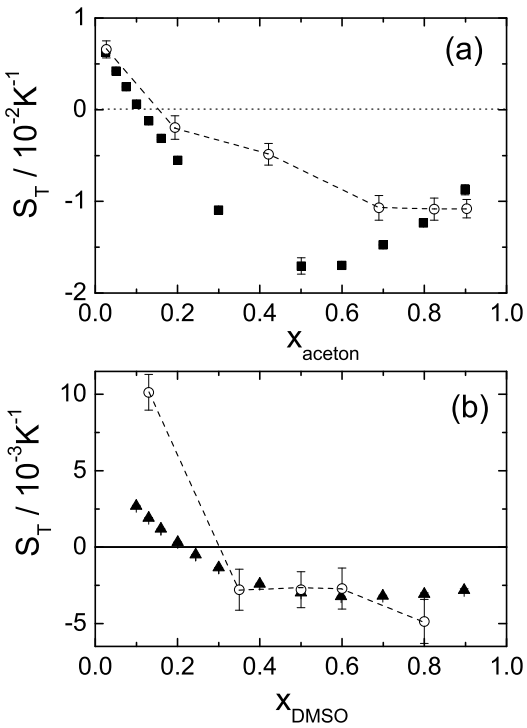

Figure 2.3: Soret coefficient of acetone (a) and DMSO (b) as a function of the molar fraction. ■ and ▲: data from TDFRS measurement. ○: simulation results from [62]

Table 2.1: Some parameter of the solvents: mass (M), absolute mass difference to water (ΔM), radius of gyration (R_g), z-component of the moment of inertia, Hildebrandt parameter (δ), $S_{\mathrm{T}}^{\pm} = S_{\mathrm{T}} = 0$ and the concentration $(1 - x_{\mathrm{water}}^{\mathrm{hyd}})$, where the hydrogen network breaks down.

component	M[?] / a.m.u.	ΔM a.m.u.	R_g[?] / Å	μ[?] / Debye	I_z g·Å^2/Mol	δ[?] MPa$^{1/2}$	$(1 - x_{\mathrm{water}})$ at $S_{\mathrm{T}}^{\pm}$	$(1 - x_{\mathrm{water}}^{hyd})$
water	18.02		0.615	1.85	1.71	47.9		
methanol	32.04	14.02	1.552	1.70	20.7	29.6	0.15	
ethanol	46.07	28.05	2.259	1.69	63.1	26.0	0.14	0.08[14]
acetone	58.08	40.06	2.746	2.88	103.3	20.2	0.11	0.06[?]
DMSO	78.13	60.11	2.840	3.96	120.6	24.5	0.20	0.10[?]

a slightly lower water content. Although in the case of DMSO it is hard to decide, because there are very few simulation data around the sign change concentration. Nevertheless, even taken into account the limited number of points the difference in the sign change concentration is quite small. It is worth to notice that simulation predicts pronounced larger values for the Soret coefficient of acetone than for the other three mixtures, which is also confirmed by the experiment. For acetone/water mixtures (in Fig.2.3a), the simulation data are consistent with experimental data for the high and low water content. The minimum of the Soret coefficient around $x = 0.5$ is not reproduced in the simulations. For the system DMSO/water (in Fig.2.3b), the simulation data agree with our experimental data within the error bars for molar fractions above $x > 0.3$, while the simulation data overshot the experimental data by a factor of four.

Acetone and DMSO show similar molecular structures. While the central atom of acetone is carbon, it is sulphur in the case of DMSO. Compared to acetone DMSO has a larger mass, size, dipole moment and moment of inertia (compare Tab. 3.1). Recently, Köhler and coworkers [116] wrote the Soret coefficient as a sum of three contributions:

$$S_{\mathrm{T}} = a_M \Delta M + b_I \Delta I + S_T^0. \tag{2.3}$$

where $\Delta M = M_1 - M_2$ and $\Delta I = I_1 - I_2$ are the absolute difference in mass and moment of inertia of the two components, respectively. The third contribution, S_T^0, reflects the chemical

differences of the molecules.

It is difficult to apply this equation to associating fluids because they show a rather pronounced concentration dependence in contrast to non-associating liquids.[**?**] Furthermore, the chemical contribution might will be quite different indicated by difference in properties such as the hydrogen-bond capability and dipole moment. The four aqueous systems listed in Table 3.1 show a similar trend. For high water content the water molecules migrates to the warm side, while for lower water content the migration is reversed (cp. Fig. 2.4). This implies that only in the case of high water content the heavier component moves to the cold. With increasing water content the Soret coefficient decays linearly, changes sign between $x_{\text{water}} = 0.1 - 0.2$, and passes through a more or less shallow minimum and reaches a final or plateau value. The first three systems show a linear correlation with the Hildebrandt parameter δ as it also has been observed in simulations for Lennard-Jones fluid[83], but the system DMSO deviates from the other systems. On the other hand the concentration dependence for DMSO is similar to methanol and ethanol, while acetone shows a unusual dependence on the composition with a pronounced minimum.

The two studied systems here belong to the class of associating systems and exhibit non-ideal thermodynamic and dynamic properties due to the existence of strong hydrogen-bond interaction between different components[**?**]. Simulation results [85, 121] and also lattice calculations [56] show that the pronounced concentration dependence of those mixtures are strongly related to the cross interactions. Thus it was found that for a binary mixtures, if the cross interaction of the two components is stronger than the average value of the pure components, the minority component accumulates always on the cold side. As in the case of the mixture PEO/ethanol/water[47] there is a correlation between the concentration, where $S_{\text{T}}^{\pm}$ changes sign and the concentration, where the hydrogen bond network of pure water breaks by the addition of a second component (cp. Table 3.1).[14**?** **?**] This indicates that thermal diffusion is quite sensitive to changes in the fluid structure.

2.4 Conclusion

In this paper, we have presented Soret coefficient for acetone and DMSO in water mixtures. The Soret effect of both systems shows a strong dependence on the composition. Similar

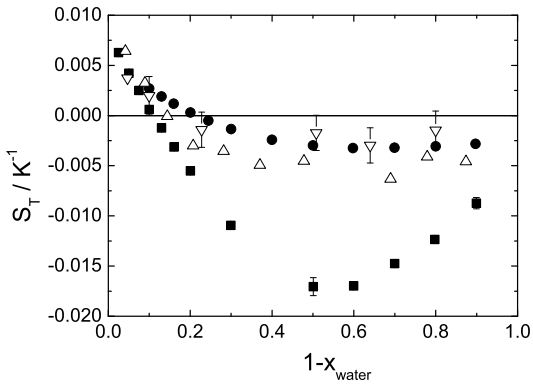

Figure 2.4: Soret coefficient of methanol (△), ethanol (▽), acetone (■) and DMSO (●) in water as function of $1 - x_{\text{water}}$.

to other two associated systems, methanol/water and ethanol/water, we found that Soret coefficient of non-water component of the studied mixtures decreases with decreasing water content and changes sign, when the molar fraction of the non-aqueous component is between 10% and 20%. The data for acetone show the most pronounced minimum, while the other three systems behave very similar. Our experimental data compare well with the previously published simulation data.

3 Thermal diffusion behavior of hard sphere suspensions

Abstract

We studied the thermal diffusion behavior of octadecyl coated silica particles ($R_h = 27$ nm) in toluene between 15.0°C and 50.0°C in a volume fraction range of 1% to 30% by means of thermal diffusion forced Rayleigh scattering. The colloidal particles behave like hard spheres at high temperatures and as sticky spheres at low temperatures. With increasing temperature, the obtained Soret coefficient S_T of the silica particles changed sign from negative to positive, which implies that the colloidal particles move to the warm side at low temperatures, whereas they move to the cold side at high temperatures. Additionally, we observed also a sign change of the Soret coefficient from positive to negative with increasing volume fraction. This is the first colloidal system for which a sign change with temperature and volume fraction has been observed. The concentration dependence of the thermal diffusion coefficient of the colloidal spheres is related to the colloid-colloid interactions, and will be compared with an existing theoretical description for interacting spherical particles. To characterize the particle-particle interaction parameters, we performed static and dynamic light scattering experiments. The temperature dependence of the thermal diffusion coefficient is predominantly determined by single colloidal particle properties, which are related to colloid-solvent molecule interactions.

3.1 Introduction

Colloidal particles are small enough to exhibit thermal motion commonly referred to as Brownion motion. Being just very large molecules in solvent, colloidal particles show many physical phenomena that are also found in ordinary molecular systems. Consequently, colloids have been used frequently to study fundamental questions in physics. Therefore, it is expected that they are also a suitable model system to illuminate the microscopic mechanism underlying the Ludwig-Soret effect, which was discovered already 150 years ago[55, 101]. This effect, also known as thermal diffusion, describes the diffusive mass transport induced by a temperature gradient in a multi-component system. In a binary fluid mixture with non-uniform concentration and temperature, the mass flow J_m of component 1 contains contributions stemming from gradients in concentration *and* in temperature,

$$J_m = -\rho D \nabla w - \rho w(1-w) D_{\mathrm{T}} \nabla T \tag{3.1}$$

Here ρ is the mass density of the homogeneous mixture, D is the translational diffusion coefficient, w is the weight fraction of component 1 and D_{T} is the thermal diffusion coefficient. The Soret coefficient S_{T} is defined as $S_{\mathrm{T}} \equiv D_{\mathrm{T}}/D$, which is proportional to the ratio of the concentration- and temperature-gradient in the stationary state

$$S_T = -\frac{1}{w(1-w)} \frac{|\nabla w|}{|\nabla T|}. \tag{3.2}$$

A number of studies show that interactions play an important role for the thermal diffusion behavior, where long ranged repulsion between charged micelles and colloids have been considered [71, 59, 80].

Conceptually, thermal diffusive behavior of *highly diluted* and *concentrated* solutions can be differentiated. In dilute solutions, where colloid-colloid interactions can be neglected, the thermal diffusion coefficient of the colloids is determined by the nature of the interactions between single colloidal particles and solvent molecules (and possibly other solutes like ions that form a double layer around the colloids). Structural changes of the surrounding solvation layer due to temperature changes and/or changes of the solvent composition may induce a sign change of the thermal diffusive behavior of single colloidal particles. One example is the sign change of Soret coefficient of poly(ethylene oxide) in ethanol/water as function of

the solvent composition[47]. Here, a sign change is observed at a weight fraction of water where hydrogen bonds break by adding ethanol. For concentrated solutions, colloid-colloid interactions affect the thermal diffusive behavior of the colloidal particles. A pronounced concentration dependence of the Soret coefficient has been found in experiments [66, 71] and is predicted by theory [20, 21].

In recent years, modern optical techniques have been developed which allow the investigation of complex fluids with slow dynamics such as polymer solutions and blends, micellar solutions, colloidal dispersions and bio-molecules[80, 93, 16, 42, 23, 24, 82]. The main issues of interest were the derivation of scaling laws and to understand the sign change of the Soret coefficient for macromolecular and colloidal systems on the basis of existing theories for molecular fluids.

In the past few years several theoretical concepts have been proposed to understand single particle and colloid-colloid interaction contributions to the thermophoretic motion of colloidal particles[30, 10, 67, 68, 20, 21]. Bringuier and Bourdon proposed a relation between the Soret coefficient in terms of a mean-field potential energy, which gives in principle access to both the single-particle as well as the colloid-colloid interaction contributions. In rare cases for which the mobility of the particle is known, a comparison with experimental data is possible. While the majority of the theoretical approaches give expressions for the single particle contribution, the work by Dhont gives explicit expressions for the contribution of colloid-colloid interactions to the thermal diffusion coefficient D_{T}. These interaction contributions lead to a concentration dependence of the thermal diffusion coefficient. According to this theory, a sign change of the Soret coefficient as a function of temperature and concentration is possible for appropriate interaction parameters.

This paper is concerned with experiments on thermal diffusion of a colloidal hard-sphere model system. The experimental data will be compared to the above mentioned theoretical predictions for hard spheres. This paper is organized as follows: in Section II, we will summarize the relevant part of theory by Dhont. In Section III we briefly describe the experimental details and summarize the working equations. In Section IV, we will present thermal diffusion forced Rayleigh scattering (TDFRS) and light scattering (DLS and SLS) results. Finally, the results from experiments are compared to theory as far as the interaction contributions are concerned.

3.2 Theory

3.2.1 The interaction potential between colloids

The interaction between silica particles coated with octadecyl chains in various organic solvents has been extensively studied[86**? ?** , 109]. The same type of colloidal particles are used in the present study. At low temperatures, the octadecyl chains grafted to the surface of the colloidal particles give rise to a very short-ranged, attractive interaction potential. The range of the attractive component of the interaction potential is very much smaller as compared to the size of the core of the colloids. At high temperatures, the depth of the attractive potential vanishes, where the colloids interact through a hard-core potential.

The interaction potential at lower temperatures for such ”sticky spheres” can be written as,

$$V(R|T) = \begin{cases} \infty & \text{for } R < 2a \\ \varepsilon(T)\frac{R-2a-\Delta}{\Delta} & \text{for } 2a \leq R \leq 2a+\Delta \\ 0 & \text{for } 2a+\Delta < R \end{cases} \tag{3.3}$$

where a is the radius of the colloidal spheres, R is the distance between the centers-of-mass of the spheres, ε is the depth of the attractive potential and Δ is the range of the attractive potential. The range Δ is approximately equal to the length 0.3 nm of the octadecane molecules. The depth ε of the attraction is in this case related to the quality of the solvent for the octadecyl brush. In particular, the depth of the attraction is temperature dependent, since the quality of the solvent changes with temperature. The temperature dependence of ε can be described by [86]

$$\varepsilon(T) = \begin{cases} L(\frac{\theta}{T}-1)k_BT & \text{for } T < \theta \\ 0 & \text{for } T \geq \theta \end{cases} \tag{3.4}$$

where L is proportional to the overlap volume fraction of two brushes and θ is the θ-temperature of the chain-solvent combination.

According to eq.(3.4) for the depth of the attraction, the potential (3.3) reduces to the hard-sphere potential above the θ-temperature,

$$V(R|T) = \begin{cases} \infty & \text{for } R \leq 2a \\ 0 & \text{for } R > 2a \end{cases} \tag{3.5}$$

The interaction parameters L and θ can be obtained from static and dynamic light scattering. Static light scattering probes the second virial coefficient B_2,

$$B_2 \equiv \int_0^\infty (1-exp(-\frac{V(R|T)}{k_B T}))r^2 dr = 4V_{\mathrm{HS}}[1+\frac{3\Delta}{2a}F_D(\beta\varepsilon)] , \tag{3.6}$$

where

$$F_D(\beta\,\varepsilon) = (1+\beta\varepsilon - exp\{\beta\varepsilon\})/\beta\varepsilon , \tag{3.7}$$

with $\beta = 1/k_B T$ (k_B is Boltzmann's constant). For high temperatures, where $\beta\varepsilon = 0$, this reduces to the well-known hard-sphere result $B_2 = 4V_{\mathrm{HS}}$, where V_{HS} is the volume of a colloidal particle. Dynamic light scattering probes the collective diffusion coefficient which is equal to [21]

$$D = D_0[1+\phi(1.45+4.50\frac{3\Delta}{2a}F_D(\beta\,\varepsilon))] , \tag{3.8}$$

to leading order in concentration. Here, ϕ is the volume fraction and D_0 is the Einstein translational diffusion coefficient of a non-interacting colloidal sphere.

3.2.2 Thermal diffusion of interacting colloids

According to the theory by Dhont[21], the additive contribution to the interacting part of the thermal diffusion coefficient $D_{\mathrm{T,int}}^{\mathrm{theo}}$, which arises from colloid-colloid interactions, consists of two contributions,

$$D_{\mathrm{T,int}}^{\mathrm{theo}} = D_{\mathrm{T}}^{(0)} + D_{\mathrm{T}}^{(i)} , \tag{3.9}$$

where $D_{\mathrm{T}}{}^{(i)}$ accounts for a possible temperature dependence of the colloid-colloid pair-interaction potential, and $D_{\mathrm{T}}{}^{(0)}$ is the remaining contribution. The latter contribution is the only contribution that would remain in case the pair-potential would be temperature independent. It should be mentioned that $D_{\mathrm{T,int}}^{\mathrm{theo}}$ is related to the interaction contribution $D_{\mathrm{T,int}}$ to the thermal diffusion coefficient D_{T} defined in Eq. 3.1, as,

$$D_{\mathrm{T,int}} = V_c^0 D_{\mathrm{T,int}}^{\mathrm{theo}}/[\phi(1-\phi)] . \tag{3.10}$$

This relation is derived in appendix 3.7. By integration of the Smoluchowski equation, it is found that,

$$D_{\mathrm{T}}^{(0)} = D_0\frac{\rho_{\mathrm{N}}}{T}[1+\alpha_T^0\phi + \mathscr{O}(\phi^2)] , \tag{3.11}$$

and,

$$D_{\mathrm{T}}^{(i)} = D_0 \frac{\rho_{\mathrm{N}}}{T} [\alpha_T^i \phi + \mathscr{O}(\phi^2)] \,, \tag{3.12}$$

where ρ_{N} is the number density of colloids, ϕ is the volume fraction of colloids, and α_T^0 and α_T^i are the leading-order virial coefficients for $D_{\mathrm{T}}^{(0)}$ and $D_{\mathrm{T}}^{(i)}$, respectively. The Smoluchowski equation approach leads to explicit expressions for these virial coefficients in terms of the pair-interaction potential for colloid-colloid interactions and hydrodynamic interaction functions.

For the case of a hard sphere, the pair-interaction potential is temperature independent, so that,

$$\alpha_T^i = 0 \,. \tag{3.13}$$

A calculation of α_T^0 for the hard-sphere potential then leads to,

$$D_{\mathrm{T,int}}^{\mathrm{theo}} = D_0 \frac{\rho_{\mathrm{N}}}{T} [1 - 0.35\phi + \mathscr{O}(\phi^2)] \,. \tag{3.14}$$

Hence, from eq. 3.10, to leading order in colloid concentration,

$$D_{\mathrm{T}} = D_{\mathrm{T,int}} + D_{\mathrm{T,sing}} = \frac{D_0}{T} \frac{1-0.35\phi}{1-\phi} + D_{\mathrm{T,sing}} \approx \frac{D_0}{T}(1+0.65\phi) + D_{\mathrm{T,sing}} \,, \tag{3.15}$$

where $D_{\mathrm{T,sing}}$ is the single particle contribution to the thermal diffusion coefficient, that is, the diffusion coefficient that one would measure at infinite dilution where colloid-colloid interactions are absent. The single particle contribution $D_{\mathrm{T,sing}}$ relates to specific interactions of the colloidal interface and solvent, which is generally temperature dependent. From the well-known leading order concentration dependence of the translational diffusion coefficient $D = D_0(1+1.45\phi)$ [4], the Soret coefficient for hard-spheres is thus found to be equal to,

$$S_{\mathrm{T}} = \frac{D_{\mathrm{T}}}{D} = \frac{1}{T} \frac{1-0.35\phi}{(1-\phi)(1+1.45\phi)} + \frac{D_{\mathrm{T,sing}}}{D_0(1+1.45\phi)} \approx \frac{1}{T}(1-0.80\phi) + S_{\mathrm{T,sing}}(1-1.45\phi) \,, \tag{3.16}$$

where $S_{\mathrm{T,sing}}$ is the single-particle contribution to the Soret coefficient.

3.3 Experiment

3.3.1 Synthesis

Silica-core particles were synthesized by the hydrolysis and condensation of tetraethylorthosilicate(TEOS) following Stöber[103]. These particles were rendered organophilic by a grafting procedure with octadecyl alcohol according to van Helden[**?**]. The dispersion was purified from the excess octadecyl alcohol by vacuum distillation followed by repeated cycles of centrifugation and re-dispersion, first in chloroform and cyclohexane and then in toluene to prepare the final stock solution with a volume fraction of 10.75%. The concentration of these solutions was determined by drying a small volume of dispersion to constant weight at 50°C, from which the volume fraction of the dispersions was obtained using the density of the particles. The density of the particles was determined from the density of a dispersion with a concentration of 0.186 g cm^{-3}. This was done by weighting 1 cm^3 of the dispersion as well as the solvent toluene. Assuming additivity of volumes of solvent and particles, which is a good assumption for these colloidal dispersions, a density of the particles of ρ=1.73 g cm^{-3} was obtained.

Elemental analysis was performed by the Central Division of Analytical Chemistry (ZCH) of the Forschungszentrum Jülich on a LECO CHNS-932 analyzer. The sample was dried for overnight at 50 °C under vacuum. An average carbon content of 11 wt% was obtained, which is attributed to 13 wt% alkyl chains. However the amount of alkyl chains on the surface might be lower than this value, because of trapping of alkyl chains within the core of the particle [**?**].

3.3.2 Sample preparation

For TDFRS measurements, the colloidal samples were prepared as follows. For samples with a volume fraction below 10 %, a certain amount of the stock dispersion was diluted by adding toluene, while for the higher concentrated samples, part of the stock dispersion was concentrated by carefully evaporating the toluene under a nitrogen flow. Thirteen different concentrations of colloidal dispersions were prepared. The colloid content varies between 1 % and 30 % in volume. Each solution was filtrated directly into an optical quartz cell with 0.2 mm path length (Hellma) through a 5 μm PTFE membrane filter. The colloidal samples for

the TDFRS measurements were always prepared one day before the measurement to deposit the possible dust in the solution.

The thermal diffusive behaviour of octadecane/toluene mixtures was also studied. The octadecane (Aldrich, purity≥99.5 %) and toluene (Fluka, purity≥99.0 %) were used without further purification. The process to prepare a sample for TDFRS measurement is the same as that of the colloidal dispersion.

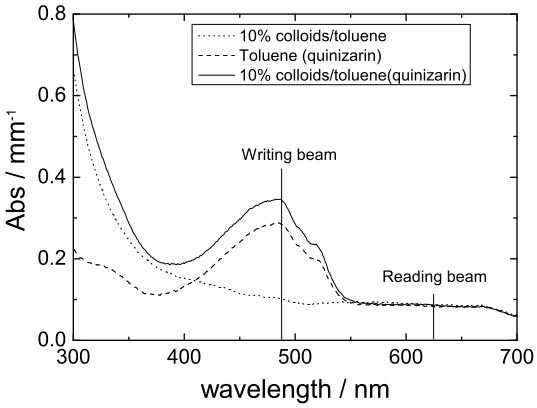

Figure 3.1: Absorption spectra of colloidal suspensions in toluene. Solid line: 10 % colloids in toluene with quinizarin. Dashed line: Toluene with quinizarin. Dotted line: 10 % colloids in toluene without quinizarin. The concentrations of quinizarin in these samples is the same.

A trace amount of quinizarin (Aldrich purity 96 %, less than 10^{-4} by weight fraction) is added and used to create a temperature grating by absorption from an optical grating. Absorption spectra were measured with a Carry 50 spectrometer and a rectangular quartz cuvette with a path length of 1 mm (Hellma). Fig.3.1 shows the absorption curves. Comparing the absorption curves with colloids (solid line) and without colloids (dashed line), one finds no shift of the absorption band to other wavelengths. We can therefore assume that the dye is homogenously distributed in the dispersion and does not adsorb at the colloidal surfaces as in the case of boehmite[16]. The additional apparent absorption at low wavelengths is due to

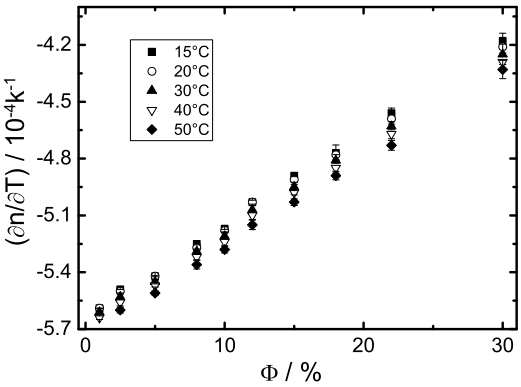

Figure 3.2: Concentration and temperature dependencies of $\partial n/\partial T$ of suspensions with toluene as the solvent.

the light scattering of the colloidal particles, which is shown by the spectrum of the colloidal suspension without dye (dotted line). The contribution of the scattered light to the total absorption is around 15% at the wavelength of 488 nm, but it does not influence the prerequisite of the TDFRS experiments (strong absorption at 488 nm, negligible absorption at 632.8 nm).

3.3.3 Thermal diffusion forced Rayleigh scattering (TDFRS)

The experimental setup of TDFRS has been described in detail elsewhere [114, 66]. In brief, an interference grating was written by an argon-ion laser operating at the wavelength of λ=488 nm. The grating was read out by a He-Ne laser at λ=632.8 nm. The intensity of the diffracted beam was measured with a photomultiplier. The TDFRS measurements were carried out in a temperature range from 15.0 to 50.0 °C. The temperature of the sample cell was thermostatically controlled by circulating water bath with an uncertainty of 0.02 °C.

To calculate the Soret coefficient S_{T} and the thermal diffusion coefficient D_{T} from TDFRS data, the refractive index increments $\partial n/\partial T$ and $\partial n/\partial w$ of the colloidal dispersion are required. These increments are measured separately by using a Michelson interferometer at a wavelength of 632.8 nm[50]. Fig.5.2 shows the increment $\partial n/\partial T$, measured at different tem-

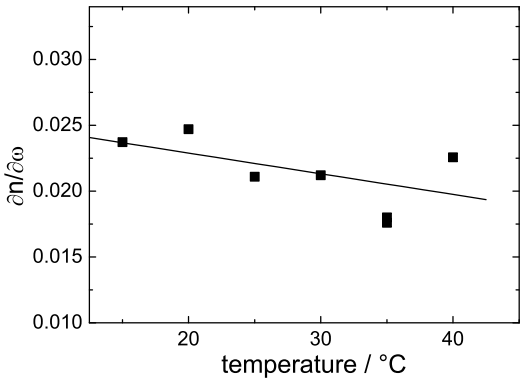

Figure 3.3: Temperature dependencies of $\partial n/\partial w$ for suspensions with toluene as the solvent. The solid line shows a linear fit of the data.

peratures as a function of the colloid concentration of the dispersion. As can be seen, $\partial n/\partial T$ varies linearly with concentration within the investigated range. In Fig.3.3, the increment $\partial n/\partial w$ decreases slightly with increasing temperature.

The refractive index increments were also determined for the octadecane/toluene mixture with a weight fraction 5 % octadecane. $\partial n/\partial T$ was found to be equal to $-5.51 \cdot 10^{-4}$, $-5.52 \cdot 10^{-4}$, $-5.54 \cdot 10^{-4}$, $-5.57 \cdot 10^{-4}$ and $-5.59 \cdot 10^{-4}$ K^{-1} for 15, 20, 30, 40 and 50 °C, respectively, and $\partial n/\partial w$ is equal to -0.076.

In the TDFRS experiment, the heterodyne signal intensity of the read out laser is proportional to the amplitude of the refractive index gradient $\Delta n\,(T,w)$ as [50],

$$\Delta n\,(T,w) = \left(\frac{\partial n}{\partial T}\right)\Delta T + \left(\frac{\partial n}{\partial w}\right)\Delta w\,. \tag{3.17}$$

The normalized total intensity $\zeta_{\mathrm{het}}\,(t)$ to the thermal signal is related to the Soret coefficient as,

$$\zeta_{\mathrm{het}}\,(t) = 1 + \left(\frac{\partial n}{\partial T}\right)^{-1}\left(\frac{\partial n}{\partial w}\right) S_{\mathrm{T}} w\,(1-w)\left(1 - e^{-q^2 D t}\right)\,. \tag{3.18}$$

The Soret coefficient S_{T} in eq.3.18 is defined as the Soret coefficient of component 1. A positive sign of S_{T} implies that component 1 moves to the cold side.

3.3.4 Dynamic light scattering (DLS)

Dynamic light scattering (DLS) was carried out in the angular range $30^\circ < \theta < 135^\circ$ with a Kr-ion laser (wavelength $\lambda = 647.1$ nm). An ALV-5000E correlator was used to measure the auto correlation function. The samples for the DLS experiment were prepared and cleaned in the same way as those for the TDFRS measurements and filtered directly into a cylindrical cell with an inner diameter of 8.5 mm. The sample cell was placed in a thermostated bath with a temperature uncertainty of 0.1 °C. Before data acquisition we stabilized the sample cell for at least 30 minutes.

The measured auto correlation function of the scattered light intensity $g^{(2)}(q,t)$ is related to the normalized field correlation function $g^{(1)}(q,t)$ through the Siegert relation,

$$g^{(2)}(q,t) = B\left(1+\beta[g^{(1)}(q,t)]^2\right) , \tag{3.19}$$

where B and β are the baseline and a constant related to the coherence of detection, respectively. Measured correlation functions were fitted to a second cumulant approximation,

$$\ln g^{(1)}(t) = -\bar{\Gamma}t + \frac{\mu_2}{2!}t^2 , \tag{3.20}$$

where $\bar{\Gamma}$ is the decay rate and μ_2 is the second cumulant. The second cumulant accounts for the polydispersity of the colloids : $\mu_2/\bar{\Gamma}^2$ equals the relative standard deviation of the size of the colloids. If the fluctuation of the scattering light intensity is due to the translational diffusion motion of colloids, the decay rate is related to the mass diffusion coefficient D as,

$$D = \lim_{q\to 0} \bar{\Gamma}/q^2 . \tag{3.21}$$

For the small colloidal spheres studied in the present paper, the asymptotic value for the collective diffusion coefficient for small wave vectors q is attained for all scattering angles. For the sticky-sphere potential in Eq.3.3, the mass diffusion coefficient D is related to the interaction parameters as given by Eq.3.8. This allows to determine interaction parameters by dynamic light scattering.

For very small colloid concentrations, D is equal to the Stokes-Einstein diffusion coefficient $D_0 = k_\mathrm{B}T/6\pi\eta_0 R_\mathrm{h}$ (with η_0 the shear viscosity of the solvent and R_h the hydrodynamic radius of a colloidal sphere), which allows for the characterization of the (average) colloid-particle size.

3.3.5 Static light scattering (SLS)

Static light scattering (SLS) was carried out in the angular range $30^\circ < \theta < 150^\circ$ with a Helium-Neon laser (632.8 nm, $P = 20$ mW). The cylindrical quartz cells had a diameter of 2 cm. The temperature stability and filtering procedure was the same as in the DLS experiment. Data were corrected for solvent background and converted into Rayleigh ratios as follows,

$$\Delta R_\theta = \frac{I_{\text{solution}} - I_{\text{tol}}}{I_{\text{tol}}} \left(\frac{n_{\text{solv}}}{n_{\text{tol}}} \right)^2 R_{\text{tol}} \tag{3.22}$$

where I_{solution} and I_{tol} denote the scattered intensities corresponding to solution and toluene reference, respectively. n_{solv} and n_{tol} denote the refractive index of solvent and toluene. The Rayleigh ratio of toluene was taken to be $R_{\text{tol}} = 1.3526 \times 10^{-5}$ cm^{-1}. We investigated six concentrations between $c = 0.58$ and 4.29 g/L. Scattering data were analyzed using the linear approximation by a Zimm plot,

$$\frac{Kc}{\Delta R_\theta} = \frac{1}{M_{\text{w}}} \left(1 + \frac{q^2 {R_{\text{g}}}^2}{3} \right) + 2A_2 c \ , \tag{3.23}$$

where $K = 2\pi^2 n^2 (\partial n/\partial c)^2/\lambda_0^4 N_{\text{A}}$ and c is the colloid concentration in g/L. R_{g} the radius of gyration. A_2 is the second virial coefficient, which relates to the leading virial coefficient B_2 for the osmotic pressure as,

$$B_2 = A_2 M_{\text{W}}^2 / N_{\text{A}} \ , \tag{3.24}$$

where M_{W} is the mass and N_{A} is Avogadro's constant.

3.4 Results

3.4.1 Characterization and phase behaviour of the colloidal dispersion

Fig.3.4a shows the TEM image of the investigated colloidal particles. It is obvious that the particles are not perfectly spherical. The size distribution of the radius is displayed in Fig.3.4b. This distribution renders and number-average radius of $< R_{\text{TEM}} >$=14.3±5.8 nm.

Additionally we performed DLS measurements to characterize the colloidal dispersions in the same temperature range as for the TDFRS measurements. The volume fraction of the

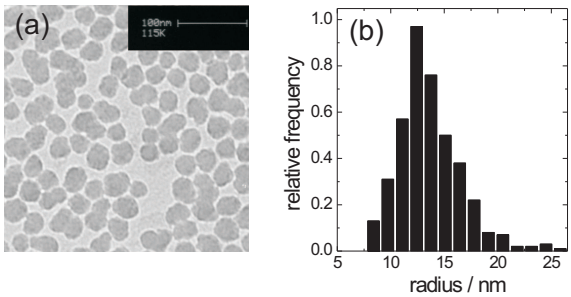

Figure 3.4: (a) TEM image of the colloidal particles. (b) size distribution of the colloidal particles

Table 3.1: Temperature dependence of characteristic parameters for colloid/toluene dispersions. The parameters were obtained by DLS using a volume fraction of colloids around 0.25%.

T (°C)	$< D_0 >$ / by extrapolation ($10^{-7} cm^2 s^{-1}$)	$< R_\mathrm{h} >$ (nm)	$\mu_2/\overline{\Gamma}^2$	R_N (nm)
15.0	1.30 / 1.38	26.5	0.12	15.0
20.0	1.39 / 1.49	26.5	0.11	15.7
30.0	1.61 / 1.70	26.7	0.13	14.5
40.0	1.85 / 1.85	26.5	0.13	14.3
50.0	2.05 / 2.20	27.4	0.15	13.6

colloids for DLS measurements is 0.25 %, at which concentration colloid-colloid interactions can be neglected. By analyzing DLS data, colloidal parameters, such as the self diffusion coefficient (D_0), hydrodynamic radius (R_h) and the polydispersity index ($\mu_2/\overline{\Gamma}^2$) were obtained, which are shown in Tab.3.1. The diffusion coefficient D_0 increases with increasing temperature, which is due to the decrease of the viscosity. The average hydrodynamic radius $< R_h >$ is found to be temperature independent $< R_\mathrm{h} >= 26.5 \pm 0.4$nm. This result deviates significantly from $< R_\mathrm{TEM} >$. The difference can be understood by the different statistical weights

in obtaining averages from the two methods. For DLS, the contribution to the measured scattered intensity of each colloidal particle proportional to its volume squared. Hence, for a polydisperse system the large colloidal particles will contribute significantly more to the detected scattered intensity. The radius obtained from TEM pictures, however, is a number-averaged value. One can calculate the number-averaged radius R_N from the DLS result[105] by

$$R_N = < R_h > /(1+\mu_2/\overline{\Gamma}^2)^5 \tag{3.25}$$

The calculated R_N in Tab.3.1 shows good agreement with the TEM result.

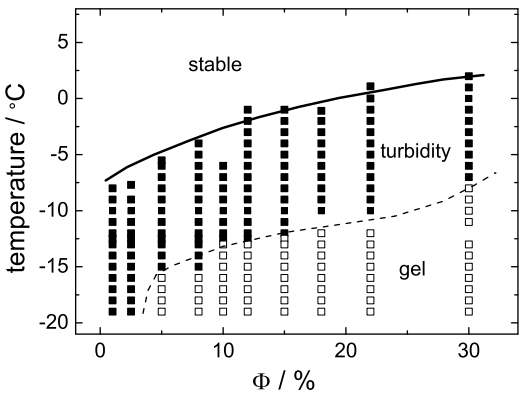

Figure 3.5: Experimental phase diagram. ■, turbidity. □, gel. Lines are drawn to guide the eye.

The phase diagram was measured experimentally by slowly cooling down dispersions with varying concentration. The boundary between stable and turbid phases was measured by observing the sharp decrease of the intensity of a through-going beam, and the gel line was obtained by observing the sample by eye. The obtained phase diagram is shown in Fig.3.5. In the high temperature regime the dispersion is stable. With decreasing temperatures, the attractive force between the particles increases, and the dispersion becomes turbid. Further cooling down leads to a gel phase for volume fractions above 5 % within the investigated

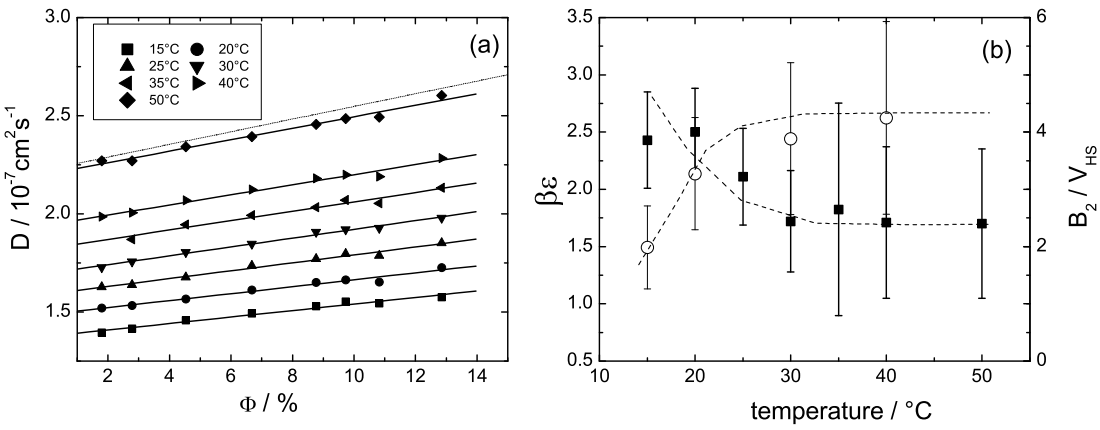

Figure 3.6: (a) Translational diffusion coefficient in dependence of concentration at various temperatures. The solid lines are linear fits to the data. The dotted line is the theoretical concentration dependence of hard spheres: $D = D_0(1 + 1.45\phi)$[4]. (b) Dependence of $\beta\varepsilon$ (■) and B_2 (◯) on the temperature. The dashed lines are guides to the eye.

temperature range. Thermal diffusion experiments are always done at the temperature range at least 15-20 °C higher than the unstable region.

In order to characterize the attractive potential between the colloids, DLS and SLS measurement were performed. DLS measurements were performed for the colloidal dispersion in a concentration range ϕ=1.8-13 % and a temperature range 15-50 °C. As displayed in Fig.3.6(a), the translational diffusion coefficient increases linearly for all temperatures with increasing volume fraction. With a particle radius of $a = 27$ nm (which is the radius relevant for scattering experiments) and a width of the interaction potential $\triangle$=0.3 nm (which is the thickness of grafted octadecyl layer onto the surfaces of the colloids) [86, 109] we determined the attractive potential parameter $\beta\varepsilon$ by fitting the data according to Eq.3.8 for DLS. As can be seen from Fig.3.6b, $\beta\varepsilon$ decreases with decreasing temperature. As expected, the depth of the attractive interaction increases on approach of the gas-liquid phase transition line from

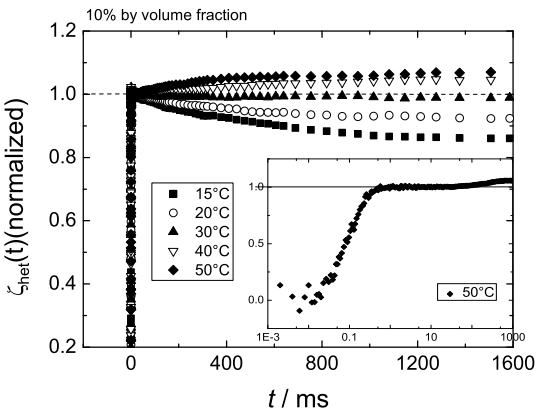

Figure 3.7: Typical normalized TDFRS signals of colloidal suspensions with a volume fraction of 10 % at different temperatures. The inset give the signal for the measurement at 50 °C as a function of time on a log scale.

the stable region in the phase diagram. With increasing temperature, the attractive potential vanishes, which makes it more difficult to determine $\beta\varepsilon$ from dynamic light scattering and leads to large error bars.

Additionally, we performed SLS measurements in order to determine the second virial coefficient. The data were analyzed using the linear approximation by Zimm (Eq.3.23). The so determined A_2 parameter was converted to B_2 according to Eq.3.24. The ratio B_2/V_{HS} increases with temperature and reaches the plateau value of 4 for hard spheres at temperatures above about 30 °C (see Fig.3.6(b)).

The light scattering experiments thus show that attractions can be neglected at temperatures above 30 – 50 °C.

3.4.2 Thermal diffusion measurements

TDFRS measurements were performed in the concentration range between 1 % and 30 % for different temperatures between 15 °C and 50 °C. Typical normalized heterodyne TDFRS signals $\zeta_{\mathbf{het}}(t)$ are displayed as function of time in Fig.3.7. The volume fraction of the colloidal

dispersion is ϕ =10 %. The inset shows the signal measured at 50 °C with a logarithmic time scale. The rapid increase of $\zeta_{\text{het}}(t)$ is due to the establishment of the temperature gradient, and the following slower variation reflects the formation of a concentration gradient due to thermal diffusion. The signal $\zeta_{\text{het}}(t)$ has been normalized to the thermal plateau. As can be seen, the concentration part of the signal decays at lower temperatures and increases at higher temperatures. Since $(\partial n/\partial w) > 0$, this implies that the colloids move at low temperatures to the warm and at high temperatures to the cold side.

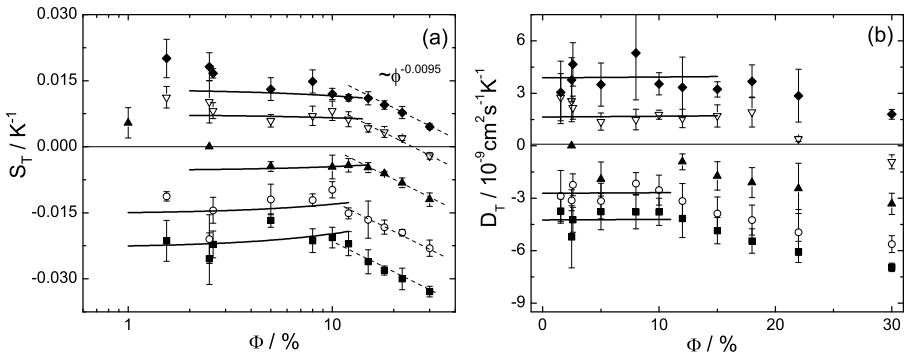

Figure 3.8: Concentration dependence of (a) the Soret coefficient and (b) the thermal diffusion coefficient D_{T}. The temperatures are 15°C(■), 20°C(◯), 30°C(▲), 40°C(▽) and 50°C(♦). The solid lines represent the fit of data according to Eq.3.16 and Eq.3.15, respectively.

Fig.3.8 presents the Soret coefficient and the thermal diffusion coefficient as a function of the volume fraction at various temperatures. Both S_{T} and D_{T} show a weak concentration dependence in the low concentration regime, while a pronounced decrease is observed in the high concentration regime. As can be seen there is a sign change with increasing concentrations at $T = 30$ °C and $T = 40$ °C. The errors displayed in Fig.3.8(a) correspond to one standard deviation. High uncertainties occur for low concentrations, where the amplitude of the concentration part of the signal is rather small.

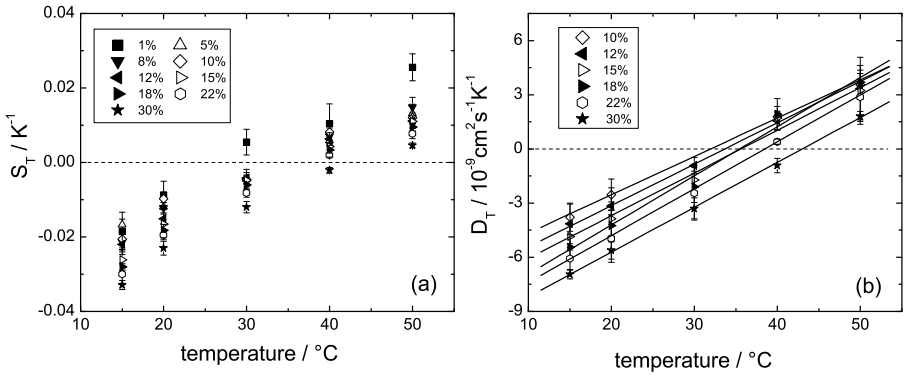

Figure 3.9: Dependence of (a) the Soret coefficient and (b) the thermal diffusion coefficient as a function of temperature at various volume fractions.

The Soret coefficient S_T and the thermal diffusion coefficient D_T versus temperature are plotted in Fig.3.9 for various concentrations. Both coefficients increase with increasing temperatures, and the strong temperature dependence eventually leads to a sign change from negative to positive between 30 °C and 45 °C. The sign change temperature $T^{\pm}$ increases with increasing volume fraction (see Fig.3.10), which might be an indication for a stronger interaction between the colloids. Sign change of the thermal diffusion coefficient with varying temperature has also been found for several other systems. For example, PEO in the mixture of water and ethanol [47], PNiPAM/ethanol solution [44], SDS , and several biomacromolecule solutions [42]. In all aqueous systems the Soret coefficient increases with temperature, while for the system PNiPAM/ethanol S_T decreases with increasing temperature.

3.4.3 Thermal diffusion of free octadecane in toluene

The surfaces of our colloidal particles are grafted with octadecyl chains. The interface between the colloidal material, the octadecyl brush, and pure solvent is probably the dominant

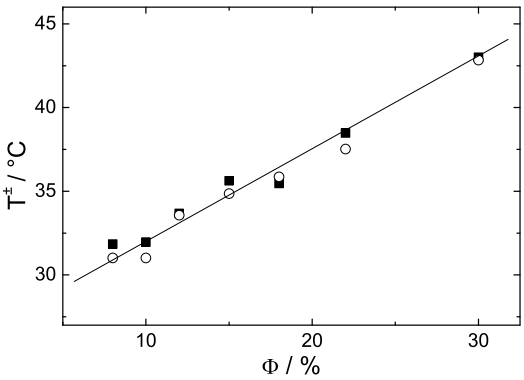

Figure 3.10: The temperature $T^{\pm}$ at which the sign change of the thermal diffusion coefficient occurs as a function of volume fraction. ■: from polynomial fit of S_{T} in terms of volume fraction. ◯: from linear fit of D_{T} in terms of volume fraction.

factor for thermal diffusion of single colloidal particles [98, 99]. In order to get a better insight in the single particle diffusive behavior of the colloids, one might learn from the thermal diffusive behavior of free octadecyl chains dissolved in toluene, which is the solvent used for the colloids. The octadecane concentration is 5 wt%.

As can be seen from Fig.3.11, the Soret coefficient and thermal diffusion coefficient are negative within the entire temperature range under consideration. Free octadecyl chains therefore tend to migrate to the warm side. For our colloids, however, colloidal particles migrate for higher temperatures to the cold side. It thus seems that the confinement of the octadecyl chains due to grafting has an appreciable effect and/or there are other reasons for a single colloidal particle, independent of the grafted brush, to migrate to the cold side at high temperatures.

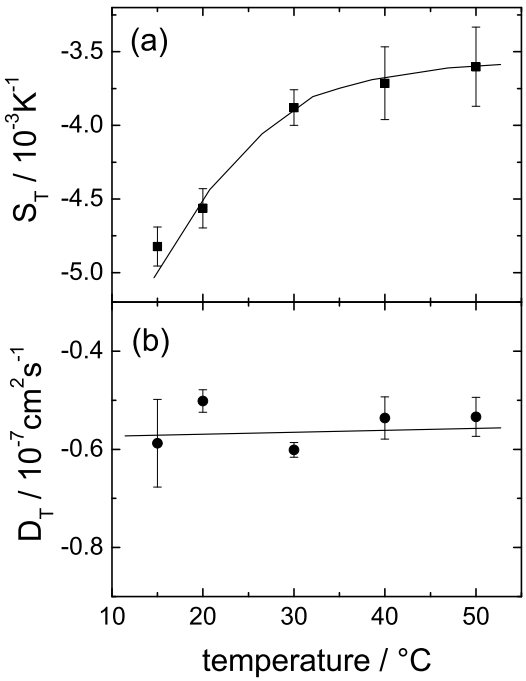

Figure 3.11: Dependence of S_T (a) and D_T (b) of octadecane in toluene versus temperature. The solid lines are guides to the eye.

3.5 Discussion

As we have mentioned in Sec.3.2, the expressions for the Soret coefficient and thermal diffusion coefficient given in Dhont's theory only account for the contributions due to colloid-colloid interactions. To compare the experimental data with theory, the single particle contribution $S_{T,sing}$ and $D_{T,sing}$ should be added to these expressions. Since we do not have an analytical expression to calculate the single particle contribution, a comparison with theory can only be based on the concentration dependence at a fixed temperature.

In Fig.3.8, one can observe a strong concentration dependence for S_T and D_T. This con-

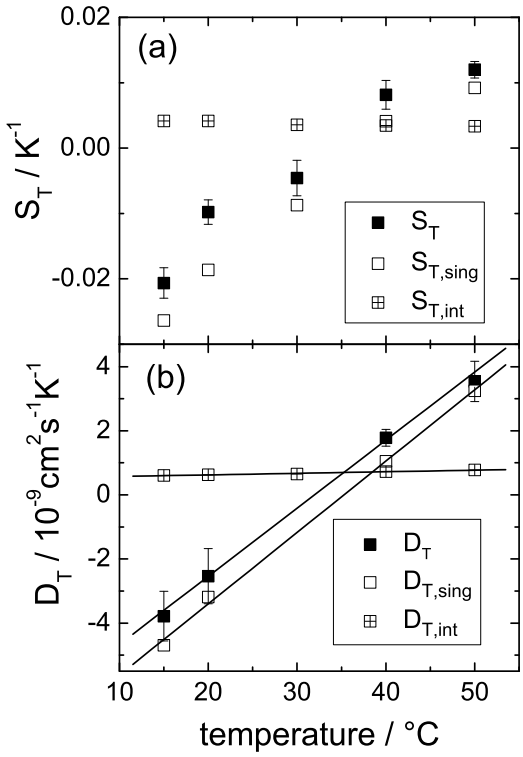

Figure 3.12: (a) The experimental Soret coefficient (■) and its single (□) and interaction contribution (⊞) as function of temperature. (b) Shows the corresponding plot for the thermal diffusion coefficient. The volume fraction of the colloidal dispersion is $\phi = 10$ %. The solid lines are linear fits to the data.

centration dependence is related to colloid-colloid interactions. The interaction parameters are independently determined by static and dynamic light scattering experiments. In the investigated temperature range, even at the low temperatures the attractive contributions are still quite weak. As a result, the colloids can be regarded as hard spheres. The solid lines in Fig.3.8 show the fits of our experimental data to the theoretical expressions Eq.3.16 and Eq.3.15, respectively. Fitting was performed in the low concentration range ($\phi < 12$ %). As can be seen, the theory is confirmed within experimental error. It should be mentioned that the slope of D_{T} and S_{T} as a function of concentration is rather small, which is, however, in accordance with theory. The slope is so small, that more accurate measurements would be needed to quantitatively confirm the theory. It seems not feasible to do accurate experiments to an extent that the theoretically predicted slope can be verified quantitatively. It would be worthwhile to perform experiments close to the phase transition line, where attractions become important. The concentration dependence for such sticky spheres is expected to be more pronounced as compared to hard spheres.

In the high concentration regime, for all temperatures, both D_{T} and S_{T} of the colloids decrease markedly with increasing concentration. The decrease of D_{T} and S_{T} at high concentrations was also observed by Rauch *et al*.[81, 82] and Zhang *et al*. [119] for the Polystryrene/toluene solution. In Rauch's work, the decay of D_{T} with concentration was interpreted by the increase of the local viscosity, which is due to the approaching of the glass transition. In our case the drop of S_{T} and D_{T} might have a similar reason, because at the higher concentrations we are closer to the gelation boundary. In Fig.3.8(a), we observe for concentrated dispersions ($\phi > 15$ %) that S_{T} follows a scaling law $S_{\mathrm{T}} \propto \phi^{-0.0095} \propto c^{-0.0095}$ for all temperatures. Compared to the scaling law $S_{\mathrm{T}} \propto C^{-1.0}$ for polystryrene/toluene, the exponent is two orders of magnitudes smaller.

The single particle contributions $S_{\mathrm{T,sing}}$ and $D_{\mathrm{T,sing}}$ as obtained from the fit are plotted in Fig.3.12. From this figure one can see that the single particle contribution to D_{T} and S_{T} increases with temperature and changes sign from negative to positive. The single particle contribution is probably mainly determined by the interface interaction between the colloid and solvent[98, 1]. It seems therefore appropriate to compare the thermal diffusion behavior of the surface material, octadecane, in toluene. Comparing the Soret coefficient S_{T} of octadecane (see Fig.3.11(a)) with $S_{\mathrm{T,sing}}$, we find that both parameters increase with temperature,

however in the studied temperature range S_T of octadecane is negative and does not change sign.

Fig.3.9 shows that the thermal diffusion behavior of the studied colloidal system has a strong dependence on the temperature. At low temperatures the colloids move to the warm side, while at high temperature the colloids prefer the cold side. Increasing the temperature improves the solvent quality, while at low temperatures we are closer to poor solvent conditions. Also for polymers it was observed by experiment[36, 17], simulations[121] and by lattice model calculations[56], that under poor solvent conditions the solutes tend to accumulate in the warm region. Both S_T and D_T increase with the temperature. The linear temperature dependence of D_T that is found seems to be quite universal for many systems and was interpreted by a semi-empirical expression $D_T = A(T - T^{\pm})$, where $T^{\pm}$ is the sign-change temperature and A is a system-dependent amplitude[42]. Sometimes the temperature dependence of D_T is related to the thermal expansion coefficient of solvent[42**?**], but there is no quantitative theory to predict the amplitude.

Since the thermal diffusion behavior of the colloidal system consist of a single and a colloid-colloid interaction part, and both contributions depend on the temperature, it is worth to investigate the two effects separately. While the colloid-colloid interaction part of S_T and D_T displayed in Fig.3.12 is almost temperature independent, the single parts show a pronounced increase with temperature. Therefore, we conclude that the temperature dependence is mainly caused by the single particle contribution.

For all investigated concentrations we observed a sign change with temperature. Although a sign change with temperature and concentration has also been predicted by the theory of Dhont[21], the physical origin might be different in our case. As we have seen, our system is close to a hard sphere system, so that the observed sign change with temperature is not caused by a temperature dependence of the interaction potential between the colloidal particles, but is probably a single particle contribution. This hypothesis is supported by our study of octadecane in toluene, which shows also a pronounced temperature dependence (see Fig.3.11), although we could not observe a sign change in the investigated temperature range. Therefore, we conclude that sign change of S_T and D_T of the studied colloidal system with temperatures is not caused by varying attraction between the particles but due to changes of the colloidal interface structure.

3.6 Conclusion

The thermal diffusion behavior of alkyl coated spherical colloidal particles dispersed in toluene was investigated by thermal diffusion forced Rayleigh scattering (TDFRS). The thermal diffusion behavior of this colloidal system presents a pronounced dependence on both concentration and temperature. Negative thermal diffusion coefficient were observed in the low temperatures regime, which means the colloidal particles tend to concentrate on the warm side, while a positive thermal diffusion coefficient was found in the high temperature region, which corresponds to the migration of the colloids to the cold side. The sign change of the thermal diffusion behavior with increasing temperature was observed for every studied concentration. For 30 °C and 40 °C we also observed a sign change with increasing volume fraction. To our best knowledge, this is the first time that a sign change of the thermal diffusion coefficient for spherical colloids has been observed not only in dependence of concentration but also in dependence of temperature.

According to the light scattering measurement and the phase diagram, we know that the attractive potential increases with decreasing temperature. However in the studied temperature range, the colloids exhibit predominantly hard sphere behavior. Due to experimental limitations like the occurence of condensation, lower temperatures can not be reached and therefore the range of strong attractions is unaccessible. Strongly attractive colloids will be studied in the future with a similar system but with different coating density, rendering the phase transition line at higher temperatures.

The experimental results were compared to theory, where the single particle contribution is treated as a fitting parameter. For the first time the theory by Dhont has been tested. In the intermediate concentration range we found a weak concentration dependence of the thermal diffusion coefficient, in accordance with theory. The effects of temperature are dominated by the single particle contribution, for which there is not a suitable theory available yet.

Single particle thermal diffusion was studied by investigating the thermal diffusion of the coating material in toluene. It turns out that octadecane tends to migrate to the warm side and shows a negative Soret coefficient. The combination of the positive colloid-colloid interaction contribution and the negative single particle contribution may explain the sign change of the thermal diffusion of the colloids with increasing temperature.

3.7 Appendix: Conversion of D_T^{theo} to D_T

The experimentally determined D_T need to be converted for comparison with the theory by Dhont [21]. Dhont defines D_T^{theo} by the following flux equation,

$$\frac{\partial}{\partial t}\rho_N = D\nabla^2\rho_N + D_T^{theo}\nabla^2 T \ , \tag{3.26}$$

where ρ_N=N/V is the number density of the colloids. N and V are total number of colloids and the volume respectively.

Experimentally, the fitting function for the TDFRS heterodyne signal is derived from,

$$\frac{\partial w}{\partial t} = D\nabla^2 w + w(1-w)D_T\nabla^2 T \ , \tag{3.27}$$

which is equal to,

$$\frac{\partial \phi}{\partial t} = D\nabla^2 \phi + \phi(1-\phi)D_T\nabla^2 T \ , \tag{3.28}$$

where the w and ϕ are weight fraction and volume fraction respectively. The volume fraction can be obtained by,

$$\phi = V_c^0 \cdot \frac{N}{V} \ , \tag{3.29}$$

where the V_c^0 is the geometric volume of a single colloidal particle. The mass conservation equation Eq.3.26 can thus be written as,

$$V_c^0 \cdot \frac{\partial \rho_N}{\partial t} = V_c^0 D\nabla^2\rho_N + V_c^0 D_T^{theo}\nabla^2 T \ , \tag{3.30}$$

that is,

$$\frac{\partial \phi}{\partial t} = D\nabla^2\phi + V_c^0 D_T^{theo}\nabla^2 T \ . \tag{3.31}$$

Comparison of Eq.3.31 and Eq.3.28 yields,

$$D_T = \frac{V_c^0 D_T^{theo}}{\phi(1-\phi)} \ . \tag{3.32}$$

Actually, D_T^{theo} contains two contributions

$$D_T^{theo} = D_{T,int}^{theo} + D_{T,sing}^{theo}, \tag{3.33}$$

where $D^{\text{theo}}_{\text{T,int}}$ originates from colloid-colloid interactions and $D^{\text{theo}}_{\text{T,sing}}$ is the single particle contribution. Theory predicts that for hard spheres,

$$D^{\text{theo}}_{\text{T,int}} = D_0 \frac{\rho_{\text{N}}}{T}(1-0.35\phi)\ , \tag{3.34}$$

to leading order in volume fraction. If we replace the $D^{\text{theo}}_{\text{T}}$ in Eq.3.32 by Eq.3.33 and Eq.3.34, we obtain,

$$D_{\text{T}} = \frac{D_0 \rho_{\text{N}} V_c^0}{\phi(1-\phi)T}(1-0.35\phi) + D_{\text{T,sing}} = \frac{D_0(1-0.35\phi)}{T(1-\phi)} + D_{\text{T,sing}}\ . \tag{3.35}$$

Hence,

$$D_{\text{T}} \ = \ \frac{D_0}{T}(1+0.65\phi) + D_{\text{T,sing}}\ , \tag{3.36}$$

again to leading order in volume fraction.

4 Soret effect in a nonionic surfactant system with a simple phase behavior

Abstract

We studied the thermal diffusion behavior of $C_{10}E_8$ (decyl octaethylene glycol ether) in water by means of thermal diffusion forced Rayleigh scattering (TDFRS). We determined the two diffusion coefficients D_T, D and the Soret coefficient S_T in a concentration range from $w = 5$ %wt to 25 %wt in a temperature range from $T = 20$ °C to 40 °C. The obtained Soret coefficients S_T were positive for all temperatures and concentrations. Additionally, we also performed dynamic light scattering experiments in the same temperature range in order to compare the measured diffusion constants and characterize the system. Special attention was paid to the tiny amount of inert dye which needs to be added for absorption and thermalization of the light energy. The influence of an organic dye and an organic coloured salt on the experimentally determined transport properties has been studied. The results show that all coefficients are independent of the choice of the dye for this particular surfactant system.

4.1 Introduction

Surfactants are widely used as emulsifying agents and detergents and have been investigated thoroughly [**? ?**]. Those systems often exhibit interesting physicochemical properties. Especially nonionic surfactants of the general type C_mE_n, where m indicates the number C-atoms in the hydrocarbon chain, and n represents the number of ethylene oxide units $(\text{-}OCH_2CH_2)_n$-OH, have been studied intensively [58**? ?**]. Due to alteration of m and n, head-group

interactions and micelles size can be changed systematically. The delicate balance of alkyl-chain/water repulsion and repulsion between adjacent headgroups within the micelle, together with surface curvature and limitations due to alkyl chain packing lead to specific characteristics of C_mE_n as structural changes of the micelles, phase separation, critical phenomenon, and so on [58**?**]. Furthermore, the addition of electrolytes and nonelectrolytes have a large effect on the phase behavior of nonionic surfactants because of their effect on the water structure and their hydrophilicity.

So far many properties of the nonionic surfactant systems have been investigated but there is limited knowledge on the thermal diffusion behavior for nonionic micellar solutions. Thermal diffusion describes the thermal diffusion current in the presence of a temperature gradient. In an binary fluid mixture with non-uniform concentration and temperature, the mass flow J_m of one component contains both contributions stemming from the concentration and from the temperature gradient [18]:

$$J_\mathrm{m} = -\rho D \nabla w - \rho w (1-w) D_\mathrm{T} \nabla T. \tag{4.1}$$

D denotes the collective diffusion coefficient, D_T the thermal diffusion coefficient, ρ the mass density, and w the concentration in weight fractions. In a stationary state where the diffusion flow J_m vanishes the Soret coefficient S_T is given by

$$S_\mathrm{T} \equiv \frac{D_\mathrm{T}}{D} = -\frac{1}{w(1-w)} \frac{\nabla w}{\nabla T}. \tag{4.2}$$

In recent years, considerable experimental effort has been devoted to the thermal diffusion of complex molecular systems, such as micellar phases of soluted surfactants, colloidal suspensions, and polymer solutions [72, 53, 6**?** , 81]. The Soret coefficient has been measured as a function of various parameters, such as charge, temperature and concentration of the diffusing particles, and the salt content [72]. For aqueous systems it turned out that hydrogen bonds can change the thermal diffusion behavior significantly by reversing the sign [**?**]. All experiments show that specific interactions and surface effects have a strong impact on thermodiffusive behavior. Also, the formation of micelles is dominated by interfacial effects. Therefore, it is expected that the shape of the micelles has an influence on the thermal diffusion behavior.

In the past, mainly ionic surfactant systems have been investigated [**?** **?**]. Recently, strong interaction effects for the Soret coefficient of an ionic micellar system have been observed,

where the salt concentration dependence of the Soret coefficient for the micellar system is reversed going from very dilute to higher surfactant concentrations [72]. There is, however, very little knowledge about the thermal diffusion behavior of nonionic surfactants except for some preliminary studies on C_8E_4 in a thermal diffusion cell in the group of Piazza [**?**]. Due to the fact that the surfactant has a lower density than water and moves to the cold side, the measurements were complicated by convection.

Convection problems can be effectively avoided by the so called Thermal Diffusion Forced Rayleigh Scattering (TDFRS) method. In the experiment rather small temperature differences of several μK are sufficient to obtain a reliable measurement signal. A drawback of the method might be the fact that a tiny amount of dye is needed to convert the electric field energy by absorption into thermal energy. The chosen dye should show a strong optical absorption at the writing wavelength, but only a weak absorption at the readout wavelength of the otherwise transparent liquids. Ideally, the dye is inert, which means that the dye should not show any photobleaching and does not contribute to the diffraction signal. For organic mixtures it has been shown that the addition of an organic dye leads only to a very weak contribution, which does not influence the mean values but leads to slightly asymmetric error bars [115]. In the case of aqueous systems it is much harder to find an inert dye. Typically, the water soluble dyes change their properties and are dependent of pH, ionic strength and other parameters. For the investigation of the surfactant system we used two different dyes: basantol yellow [**?**], a tri-valent metal organic salt which is directly soluble in water, and alizarin, an organic dye which becomes soluble only in the presence of the surfactant. Both organic compounds probably change the balance of the hydrogen bond formation and it is expected that the phase behavior of the micelles is influenced. Especially for electrolytes there are numerous studies for surfactant systems [**? ? ? ? ? ? ?**]. Depending on the nature of the anion the two-phase boundary either shifts to lower or higher temperatures [**?**]. Due to the fact that the added dye is a tri-valent salt we expect a change of the phase behavior by addition of the dye. In order to study the influence of the dye we performed all measurements with both dyes.

In this paper we describe thermal diffusion measurements of the surfactant $C_{10}E_8$ in water in a concentration range from $w = 5 - 25$ %wt at 20,30 and 40 °C. Additionally, we also performed dynamic light scattering measurements to characterize the system.

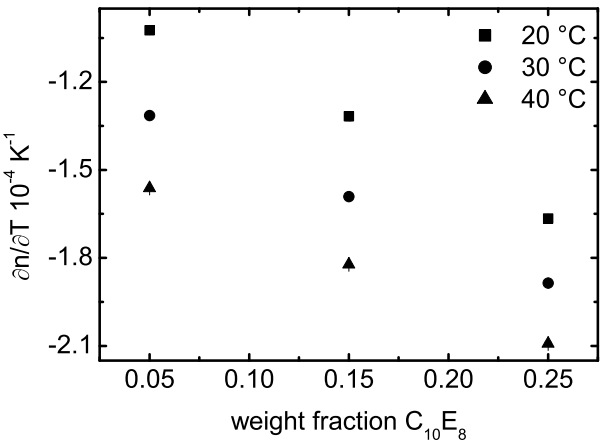

Figure 4.1: $(\partial n/\partial T)_{w,p}$ of $C_{10}E_8$ in water as a function of the surfactant weight fraction at 20° (■), 30° (●) and 40° (▲). The samples contained the same small amount of basantol yellow [**?**] as used in the TDFRS experiment.

4.2 Experiment and data analysis

4.2.1 Sample Preparation and contrast factors

$C_{10}E_8$ ([$CH_3(CH_2)_9$-$(OCH_2CH_2)_8OH$], decyl octaethylene glycol ether; purity $\geq$ 98%; M.W. = 510.72) was purchased from Fluka BioChemika, Japan. The surfactant was used without further purification. The alizarin was purchased from Riedel-deHaën and basantol yellow we obtained from BASF.

In order to prepare the samples for the TDFRS experiment a small amount of dye needs to be added to the samples. The dye has an absorption band at the wavelength of the writing beam, $\lambda_w = 488$ nm and is transparent at the read-out wavelength, $\lambda_r = 633$ nm. The absorption coefficient at λ_w was adjusted to a value $\alpha = 1.5 - 3$ cm^{-1}. This low absorption leads to a weight fraction of less than 10^{-5} basantol yellow. The weight fraction of the alizarin is of the same order of magnitude.

If we used basantol yellow as the dye, we first prepared an aqueous solution with the desired absorption using deionized water (Milli-Q). Then the surfactant was added and stirred at least for 4 hours at room temperature. In the case of the organic dye alizarin, we added the dye and the surfactant at the same time. The mixture was then also stirred at least for 4 hours at room temperature to mix all components thoroughly. After preparation the solutions were filtrated by a 0.45 μm filter (Spartan) directly in the sample cells. The sample cells for the TDFRS experiment were Quartz cells (Hellma) with a layer thickness of 0.2 mm. For the light scattering experiment we used cylindrical glass cells with an inner diameter of 8.5 mm. The optical path length of the cells for the $(\partial n/\partial T)_{w,p}$ experiment was 10 mm.

The temperature derivative of the refractive index $(\partial n/\partial T)_{w,p}$ was determined at $\lambda_r =$ 632.8 nm, using a scanning Michelson interferometer [5]. Figure 5.2 shows $(\partial n/\partial T)_{w,p}$ of $C_{10}E_8$ in water as a function of the weight fraction. The refractive index increments $(\partial n/\partial w)_{p,T}$ were determined with an Abbe refractometer at three different temperatures T =20, 30 and 40°C to $(\partial n/\partial w)_{p,T}$=0.134, 0.132 and 0.130, respectively.

4.2.2 TDFRS and DLS

The TDFRS experiment operates as follows: A grating, created by the interference of two laser beams ($\lambda_w = 488$ nm), is written into a sample. A small amount of dye, dissolved in the

sample, converts the intensity grating into a temperature grating (thermal grating), which in turn causes a concentration grating by the effect of thermal diffusion. Both gratings contribute to a combined refractive index grating, that is read out under Bragg condition by another laser of different wavelength ($\lambda_r = 632.8$ nm). Analyzing the time dependent diffraction efficiency the transport coefficients (mutual diffusion coefficient D, thermal diffusion coefficient D_{T} and Soret coefficient S_{T}) can be obtained, requiring neither external calibration nor absolute intensity measurement. Other characteristic features of TDFRS experiments are the elimination of convection due to the low temperature modulation of several μK, and the short equilibration times of the order of milliseconds, as well as the simultaneous yielding of the transport coefficients in one single measurement. A more detailed description of the set-up can be found elsewhere [**? ?**]

The dynamic light scattering (DLS) measurements were carried out in the angular range $20^\circ < \theta < 120^\circ$. A Kr-ions laser was used as the light source (wave length $\lambda = 647.1$ nm). An ALV-5000E correlator was used to measure the correlation function of scattered light. The cylindrical sample cell was placed in a temperature controlled bath with a temperature stability of $\delta T = \pm 0.1^\circ$C, the temperature of which was controlled with an uncertainty of 0.1 °C. The sample solutions were kept at measured temperature for at least 30 minutes to ensure equilibrium before starting data acquisition.

4.2.3 Data analysis

The normalized heterodyne diffraction intensity of the TDFRS experiment for a binary mixture is given by:

$$\zeta_{\mathrm{het}}(t) = 1 + \left(\frac{\partial n}{\partial T}\right)_{w,p}^{-1} \left(\frac{\partial n}{\partial w}\right)_{p,T} S_{\mathrm{T}} w(1-w)\left(1 - e^{-q^2 D t}\right) \tag{4.3}$$

The quantities $(\partial n/\partial T)_{w,p}$ and $(\partial n/\partial w)_{p,T}$ do not follow from the TDFRS experiment and have to be determined separately.

4.3 Results and Discussion

Figure 5.8 shows the phase diagram for decyl octaethylene glycol ether($C_{10}E_8$) in water [**?**], which shows in the displayed temperature range no two-phase region. In the literature it is re-

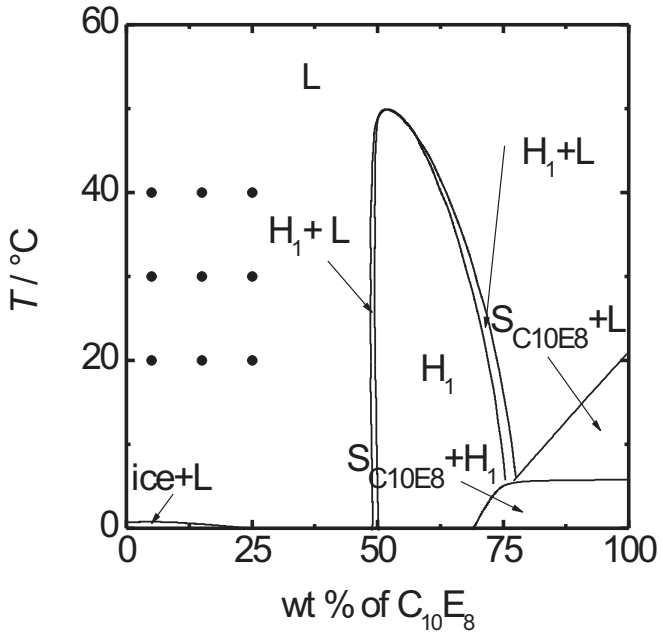

Figure 4.2: Schematic phase diagram of $C_{10}E_8$ [**?**] in water. The different regions are abbreviated in the following way: micellar solution (L), hexagonal (H_1) and the solid of pure $C_{10}E_8$ (S_{C10E8}). The solid circles represent the concentrations and temperatures where TDFRS measurements have been performed.

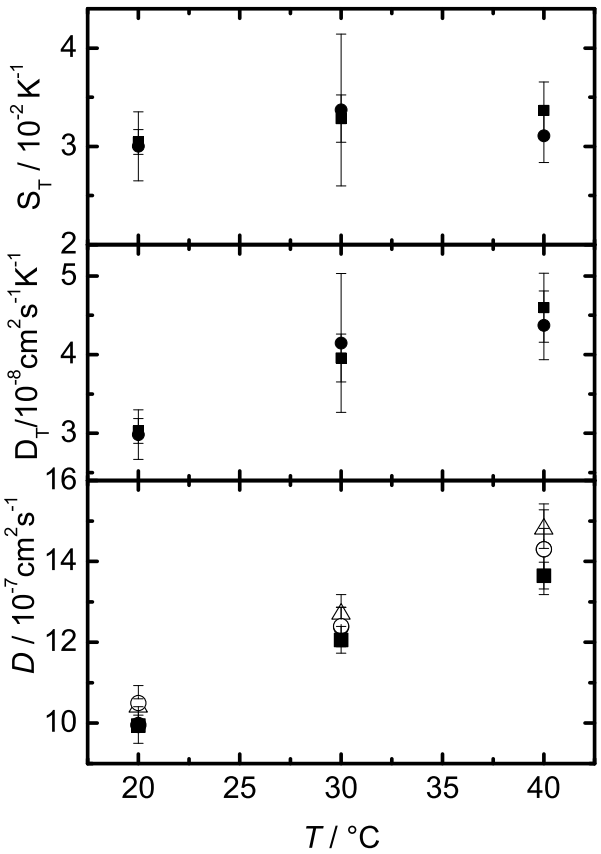

Figure 4.3: Soret coefficient, thermal diffusion coefficient and diffusion coefficient of $C_{10}E_8$ ($w = 0.15$) in water at different temperatures containing basantol yellow (●) and alizarin (■). For comparison the diffusion coefficients were also determined by DLS measurement without dye (△) and with basantol yellow (○).

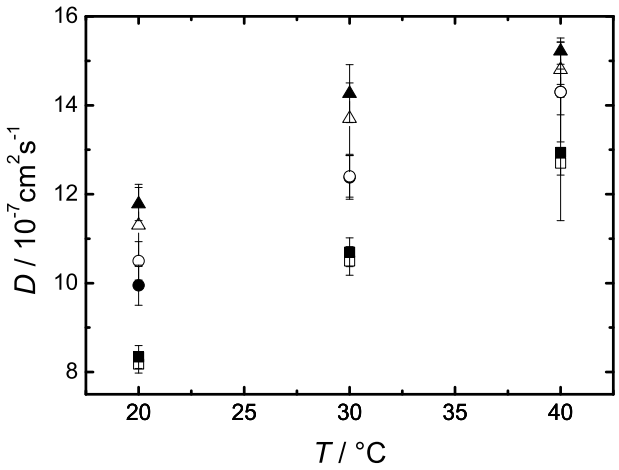

Figure 4.4: Diffusion coefficient of $C_{10}E_8$ in water for different surfactant concentrations ($w = 0.05$ (■), $w = 0.15$ (●), $w = 0.25$ (▲)) in dependence of temperature. The open symbols refer to DLS experiment while the solid symbols refer to the TDFRS measurements. In both experiments the solutions contained basantol yellow.

ported that there is a critical temperature around 85 °C, but no critical concentration is given [**? ?**]. TDFRS experiments were carried out in the micellar solution phase which are indicated by solid circles in the phase diagram. In the investigated temperature and concentration range $C_{10}E_8$ in water forms probably only spherical micelles, but it might be expected that at higher concentrations close to the hexagonal phase also cylindrical micelles are formed. 4. The experimental temperature and concentration range is far from the critical temperature so that the diffusion of the micelles is still not dominated by the critical slowing down.

One crucial aspect is the addition of the dye. It needs to be scrutinized that the dye does not change the phase behavior of the surfactant system. As already mentioned in Section 4.1, especially due to the addition of an electrolyte as in the case of basantol yellow, the phase behavior of the surfactant system can be changed significantly [**?**]. Another complication might come from the hydrophobic/hydrophilic hybrid nature of basantol yellow which might act as a cosurfactant. Therefore, we made also measurements with alizarin as organic dye and compared the results obtained for the diffusion coefficient by the TDFRS experiment with DLS measurements, which were also performed without dye. The results for a surfactant concentration of $w = 0.15$ are displayed in Fig. 4.3. The Soret coefficients show a very weak temperature dependence, while the thermal diffusion and diffusion coefficient increase with temperature. The obtained results are independent of the chosen dye. The diffusion coefficients agree with the diffusion coefficients which were obtained from DLS experiment with and without dye. These results indicate that the added dyes do not have any significant influence on the diffusion of micelles, which implies the size and the structure of micelles are not modified by the addition of dyes in the experimental condition. This is also confirmed in Fig. 4.4, which shows the diffusion coefficients for $C_{10}E_8$ for different concentrations ($w = 0.05, 0.15, 0.25$) in dependence of temperature measured by DLS and TDFRS. The solutions for the DLS measurements contained the same amount basantol yellow as the TDFRS sample. The diffusion constants increase with temperature and the values obtained with the different methods agree within the error bars. The error bars refer to one standard deviation. Nevertheless, the diffusion coefficients determined by DLS seem to be systematically lower than the values obtained by TDFRS. This is probably caused by the different weighting of the two methods. The TDFRS signal is weighted by the mass, M, of the micelle, while the DLS correlation function is weighted by the square of the mass, M^2, of the micelle.

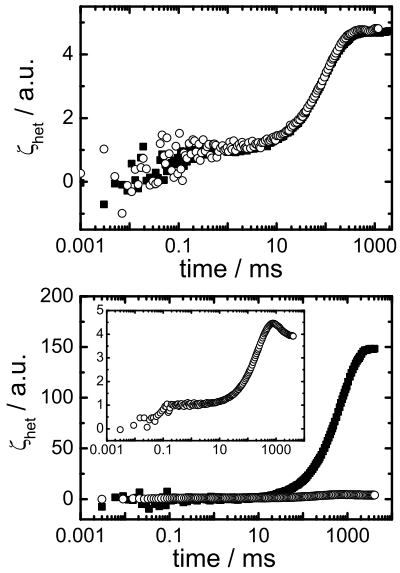

Figure 4.5: Normalized heterodyne signal ζ_{het} measured for $C_{10}E_8$ ($w = 0.15, T = 20$ °C; top figure) and $C_{12}E_6$ ($w = 0.05, T = 30$ °C; bottom figure) in water. The solutions contained either basantol yellow (○) or alizarin (■) as dye. In the lower figure the inset shows the enlarged diffraction signal ζ_{het} for the aqueous $C_{12}E_6$ with basantol yellow.

The Soret coefficient of $C_{10}E_8$ is S_T=0.032 $\pm$ 0.005 which is obtained from averaging over all data points shown in Fig. 4.3. The positive sign of S_T corresponds to that the concentration gradient is established with the migration of micelles towards the cold side of the fluid. Here we use the sign notation for S_T as follows: In a binary mixture of A and B, S_T of A is positive if A moves to the cold side. Therefore, the sign does not depend on the density of two components. In the case of the SDS (sodium dodecyl sulfate) micelles, the sign of S_T is also positive [72]. The value of S_T of $C_{10}E_8$ has the same order of magnitude with SDS micelles, although we can not directly compare the magnitudes because of a huge contribution of electrostatic forces on thermal diffusion behavior for SDS systems. So far, there are no data for the Soret coefficient of nonionic micelle systems for comparison. It is desired, for example, to study other nonionic surfactants in the same family as C_mE_n. Indeed, ongoing research shows interesting features in regard to the choice of dye and to the dependencies of temperature and surfactant concentration. For instance, $C_{12}E_6$ in the micellar phase show a dramatic changes in their thermal diffusion behavior. The use of dye, alizarin, induces ca. 30-folds intensity of TDFRS signal in comparison with the dye basantol yellow (Fig. 4.5). Furthermore, $C_{12}E_6$ solution with basantol yellow showed a two-mode behavior. At the present stage, we do not discuss this point. But it needs to be pointed out that $C_{10}E_8$ is a well characterized system which forms only spherical micelles while other surfactants often show a transition to more elongated micelles. It suggests that a modification of interactions at the interface leads to a structural change of micelles which may have a relation with the thermal diffusion behavior to a great extent. To clarify these system dependence behaviors we will report the experimental results for several nonionic surfactant systems in the future.

4.4 Conclusions

The presently investigated surfactant $C_{10}E_8$ in water which shows the same behavior on thermal diffusion independently of the nature of the added dye by means of TDFRS and DLS experiments. On going research shows that this is not a general feature. Another nonionic surfactant $C_{12}E_6$ shows a drastic change in thermal diffusion behavior with the choice of the dye. To clarify under which circumstances the behavior remains stable or is changed will be object of future research.

5 Soret effect in a nonionic surfactant system with a complex phase behavior

Abstract

We studied the thermal diffusion behavior of $C_{12}E_6$ (hexaethylene glycol monododecyl ether) in water by means of thermal diffusion forced Rayleigh scattering (TDFRS) and determined Soret coefficients, thermal diffusion coefficients and diffusion constants at different temperatures and concentrations. At low surfactant concentrations the measured Soret coefficient is positive which implies that surfactant micelles move towards the cold region in a temperature gradient. For $C_{12}E_6$/water at a high surfactant concentration of $w_1 = 90$ wt% and a temperature of $T = 25°$C, however, a negative Soret coefficient S_T was observed. Since the concentration part of the TDFRS diffraction signal for binary systems is expected to consist of a single mode, we were surprised to find a second, slow mode for $C_{12}E_6$/water system in a certain temperature and concentration range. To clarify the origin of this second mode we investigated also , C_6E_4 (tetraethylene glycol monohexyl ether), C_8E_4 (tetraethylene glycol monooctyl ether), $C_{12}E_5$ (pentaethylene glycol monododecyl ether), $C_{16}E_8$ (octaethylene glycol monohexadecyl ether) and compared the results with the previous results for $C_{10}E_8$ (octaethylene glycol monodecyl ether). Except for C_6E_4 and $C_{10}E_8$ a second slow mode was observed in all systems usually for state points close to the phase boundary. The diffusion coefficient and Soret coefficient derived from the fast mode can be identified as the typical mutual diffusion and Soret coefficients of the micellar solutions and compare well with the independently determined diffusion coefficients in a dynamic light scattering experiment. Experiments with added salt show that the slow mode is suppressed by the addition of $w_{NaCl} = 0.02$ mol/L sodium chloride. This suggests that the slow mode is related to the small amount of absorbing ionic dye, less than 10^{-5} by weight, which is added in TDFRS experiments to create a temperature grating. The origin of the slow mode of the TDFRS signal will be tentatively interpreted in terms of a ternary mixture of neutral micelles, dye-charged micelles, and water.

5.1 Introduction

Surfactants in solution are used extensively in the production of food, pharmaceuticals, cosmetics, detergents, textiles, and paints, and are also important in enhanced oil recovery. Surfactant systems often exhibit interesting physicochemical properties due to the difference in chemical composition of the head and tail groups of the surfactant molecules. In the past three decades nonionic surfactants of the general type C_mE_n, where m indicates the number of C-atoms in the alkyl chain (the tail), and n represents the number of ethylene oxide units $(-OCH_2CH_2)_n$-OH in the head group, have been studied intensively [58]. In aqueous solutions, these surfactants form a variety of structures including spherical or elongated micelles, lamellae, and inverted micelles. The boundaries between different phases as well as the structure of the micelles in the micellar phase are determined by the hydrophilic/hydrophobic balance of C_mE_n in water, which depends on temperature and concentration [**?** 58].

Diffusion in a multi component fluid may be driven by composition, temperature, or pressure gradients. For mixtures subject to a temperature gradient at constant pressure, thermal diffusion, also known as Ludwig-Soret effect, leads to the formation of a concentration gradient. In the case of a binary mixture the flux, $\mathbf{J}_1$, of one of the components in response to the temperature, T, and concentration, w_1, gradients may be written as [107]

$$\mathbf{J}_1 = -D\left(\rho\nabla w_1 + \rho w_1\left(1-w_1\right)S_\mathrm{T}\nabla T\right), \tag{5.1}$$

where D is the translational mass diffusion coefficient, S_T the Soret coefficient, and ρ the total mass density. The thermal diffusion coefficient D_T is related to the Soret and diffusion coefficients through $D_\mathrm{T} = DS_\mathrm{T}$. In the steady state of the system, where the flux $\mathbf{J}_1$ vanishes, the Soret coefficient describes the ratio of concentration and temperature differences along the direction of the gradient. We use the sign convention that the Soret coefficient is positive if the first named component is enriched in the colder region [51]. Thermal diffusion has important applications, for example, in the separation of solutes. The effect is related to chemical and physical properties such as the mass of the molecules, the structure of the solutes, and chemical interactions. However, the microscopic mechanism of the effect is not yet completely understood, especially for complex systems .

In recent years, considerable experimental effort has been devoted to the thermodiffusion of complex molecular systems, such as micellar phases of soluted surfactants, colloidal sus-

pensions, and polymer solutions [72, 53, 6**?** , 81, 119**?**]. Experiments [**?** 72] and theoretical calculations [**?** 30] on the thermal diffusion behavior of micellar systems have mostly been carried out for ionic surfactant systems. Experiments yielded positive Soret coefficients of the micelles for all systems studied. Piazza and Guarino also investigated how the addition of salt changes the Soret effect and found that, in the dilute regime, the Soret coefficient decreased with increasing salt content [72], while the opposite is true for higher surfactant concentrations. They interpreted their findings in terms of the Debye screening length using an interfacial tension mechanism proposed by Ruckenstein [87].

Recently, we studied the thermal diffusion behavior of the non-ionic surfactant $C_{10}E_8$ in water in a thermal diffusion forced Rayleigh scattering (TDFRS) experiment [66]. The obtained Soret coefficients S_T were positive for all temperatures and concentrations and the diffusion coefficients determined by TDFRS agreed with those obtained by dynamic light scattering (DLS). In the concentration and temperature range investigated in that work, $C_{10}E_8$/water forms primarily elongated spherical micelles [**?**] and undergoes no structural transitions. In the present work we focus on the system $C_{12}E_6$/water, which exhibits rich phase behavior and the coexistence of spherical and elongated micelles in a certain temperature and concentration range [**?** **?**]. We studied systematically the dependence of the transport coefficients on temperature, surfactant concentration, and salt concentration. Surprisingly, we found for this surfactant system a second mode in the TDFRS experiment in a certain temperature and concentration range. Since such a two-mode behavior has not been observed in micellar solutions before, we investigated several other surfactant systems in order to clarify the origin of the second mode. Surprisingly, we found for this and several other systems a second mode in the TDFRS experiment, which has not been observed before.

The paper is organized as follows: in the next section, Sec. 5.2, we present the working equations that are used to analyze the TDFRS experiments and explain an iterative procedure to correct for inadequacies of the electronic instrumentations. In the experimental section (Sec. 5.3) we describe briefly the sample preparation, the experimental apparatus and the determination of refractive index increments, which are necessary for the evaluation of the diffraction data. We discuss also the choice of dye, which is necessary to create a temperature gradient. In Sec. 5.4 we present thermal diffusion results for the $C_{12}E_6$/water system for a range of temperatures and concentrations. For a very high surfactant concentration,

where the surfactant forms inverted micelles in water, we observe a negative Soret coefficient for the surfactant, which is uncommon for micellar solutions. For lower surfactant concentrations, the Soret coefficients of $C_{12}E_6$/water are positive. For a certain temperature and concentration range, we observed an unusual second mode in the TDFRS signal. Results of our investigation of several other surfactant systems (C_6E_4, C_8E_4, $C_{12}E_5$, and $C_{16}E_8$), also presented in Sec. 5.4, allow us to relate the appearance of the mode to the distance from the boundary to the two-phase region. Furthermore, experiments on $C_{12}E_6$ with added salt show that the origin of the second, slow mode is ionic in nature. In Sec. 5.5 we summarize our results and present a tentative interpretation of the origin of the slow mode.

5.2 Working equations

5.2.1 TDFRS

The diffraction efficiency of the optical grating created in a TDFRS experiment changes with time, t; a thermal grating is formed first and induces at later times a concentration grating. When the total intensity of the diffracted beam, $\zeta_{\text{het}}(t)$, is normalized to the thermal signal the Soret coefficient, S_{T}, and the diffusion coefficient, D, may be determined from the amplitude and the time constant of $\zeta_{\text{het}}(t)$, respectively,

$$\zeta_{\text{het}}(t) = 1 + \left(\frac{\partial n}{\partial T}\right)_{w,p}^{-1} \left(\frac{\partial n}{\partial w_1}\right)_{T,p} S_{\text{T}} w_1 (1 - w_1) \left(1 - e^{-q^2 D t}\right). \tag{5.2}$$

The partial derivatives in Eq. (5.2) represent the increments of the refractive index, n, with temperature, T, and mass fraction, w_1 at constant pressure, p, and are measured separately. The scattering vector, q, is also determined independently.

Equation (5.2) describes a TDFRS signal with a single mode decay. In some of the experiments on micellar solutions a second, slower mode was also observed. The two-mode TDFRS signals were well described by the following expression for the normalized heterodyne intensity

$$\begin{aligned}\zeta_{\text{het}}(t) = 1 &+ \left(\frac{\partial n}{\partial T}\right)_{w_1,p}^{-1} \left(\frac{\partial n}{\partial w_1}\right)_{T,p} w_1 (1 - w_1) \\ &\left(S_{\text{T}f} \times \left(1 - e^{-q^2 D_f t}\right) + S_{\text{T}s} \times \left(1 - e^{-q^2 D_s t}\right)\right),\end{aligned} \tag{5.3}$$

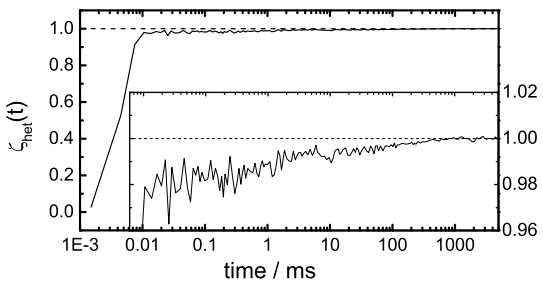

Figure 5.1: Measured excitation function in comparison with an ideal excitation function. The inset shows an enlargement of the plateau.

where the subscripts f and s stand for fast and slow mode, respectively, and where the decay times and the amplitudes of the two modes have been expressed in terms of two diffusion coefficients, D_f and D_s, and two amplitude coefficients, $S_{\mathrm{T}f}$ and $S_{\mathrm{T}s}$, respectively. Our results presented in Section 5.4 show that the fast-mode observed in solutions with two-mode decay is very similar to the single mode observed in solutions with one-mode decay. This suggests that the coefficients D_f and $S_{\mathrm{T}f}$ may be identified with the typical mutual diffusion and Soret coefficients of the micellar solutions.

The theory for TDFRS experiments assumes a step function for the excitation of the thermal grating. In actual experiments, this ideal excitation function is often not realized due to the limited rising time of the optical grating. Wittko and Köhler [115] developed a method that takes this non-ideality into account: In the course of an experiment, one measures both the TDFRS signal and the rise of the intensity in one of the fringes of the optical grating (see Sec. 5.3.4). This rise in the intensity represents the actual excitation function of the thermal grating. The measured TDFRS signal and the measured excitation function are then deconvoluted in an iterative process to yield the ”ideal” TDFRS signal. We extended the approach of Wittko and Köhler [115] to the case of a two-mode decay and included error estimates and the corresponding weights in the fits to the measured signals. Fig. 5.1 displays a typical excitation in comparison with the ideal step excitation function. The rising time for the optical grating to reach 98% of the final intensity value is on the order of 20 μs and

is followed by a slower increase of the intensity. The final value of the intensity is reached after 0.5 s. Since the characteristics of the excitation function may change with time, it is necessary to measure the excitation function frequently between measurements.

5.2.2 DLS

The auto correlation function of the scattered light intensity $g^{(2)}(q,t)$ is related to the normalized field correlation function $g^{(1)}(q,t)$ by

$$g^{(2)}(q,t) = B\left(1+\beta \mid g^{(1)}(q,t) \mid^2\right) \tag{5.4}$$

where B and β are the base line and a constant related to the coherence of detection, respectively [**?**]. Measured correlation functions were analyzed by the cumulant method to obtain an average decay rate $\bar{\Gamma}$,

$$\ln \mid g^{(1)}(t) \mid = -\bar{\Gamma}t + \frac{\mu_2}{2!}t^2 - \frac{\mu_3}{3!}t^3 + \ldots \tag{5.5}$$

where μ_i is the i-th cumulant and $\mu_2/\bar{\Gamma}^2$ gives the normalized dispersion of the distribution. When the fluctuation of the scattered light intensity is due to the translational diffusive motion of the solute molecules, the decay rate $\bar{\Gamma}$ is related to the translational diffusion coefficient through $D = \bar{\Gamma}/q^2$.

5.3 Experiment

5.3.1 Sample Preparation.

$C_{12}E_6$ (hexaethylene glycol monododecyl ether ; purity $\geq$ 98%) was ordered from Nikkol Chemicals, Tokyo. C_6E_4 (tetraethylene glycol monohexyl ether; purity = 98.3%) was purchased from Bachem AG, Switzerland. $C_{12}E_5$ (pentaethylene glycol monododecyl ether ; purity $\geq$ 98%), C_8E_4 (tetraethylene glycol monooctyl ether ; purity $\geq$ 98%) and $C_{16}E_8$ (octaethylene glycol monohexadecylether; purity $\geq$98%) were purchased from Fluka Bio-Chemika, Japan. All surfactants were used without further purification.

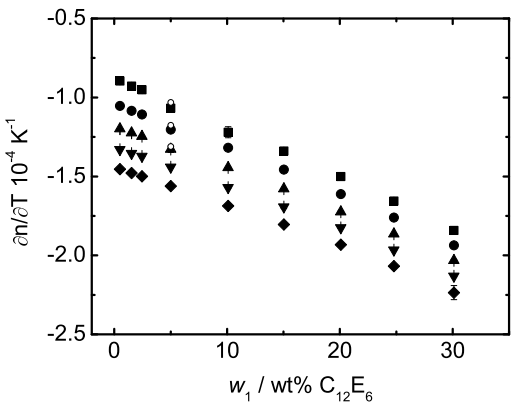

Figure 5.2: $(\partial n/\partial T)_{w,p}$ of $C_{12}E_6$ in water as a function of the surfactant concentration at 20°C (■), 25°C (●), 30°C (▲), 35°C (▼), 40°C (♦). The samples contained the same small amount of basantol yellow typically used in the TDFRS experiment. The open symbols refer to a measurement $C_{12}E_6$ ($w_1 = 0.05$) without dye. The error bars correspond to one standard deviation of the mean for repeated measurements. They barely exceed the symbol size.

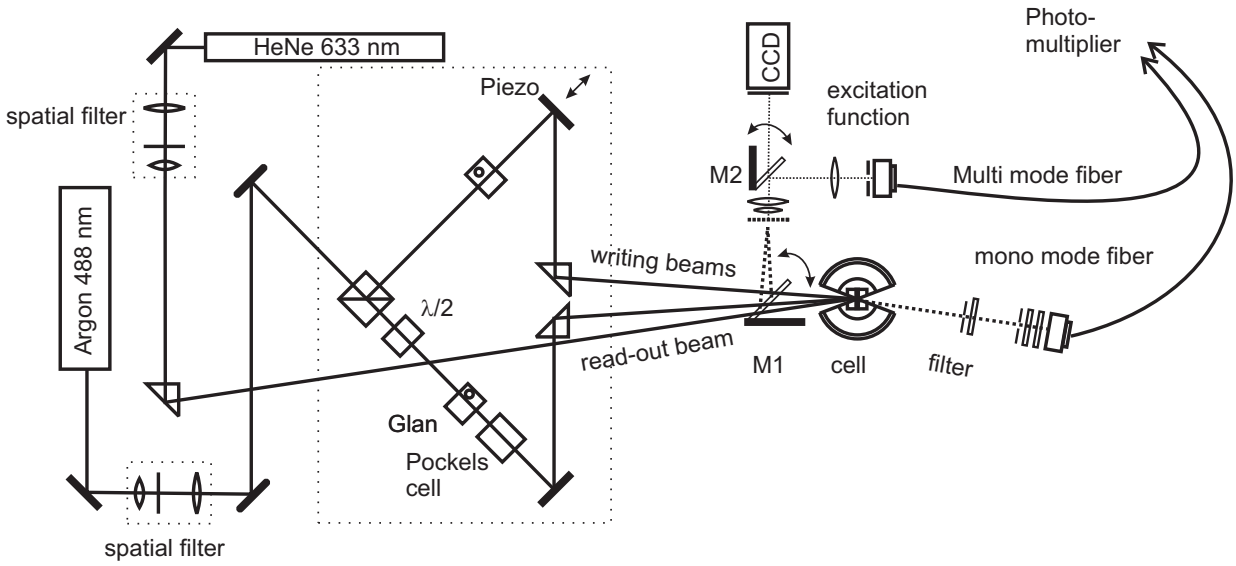

Figure 5.3: Schematic drawing of the TDFRS set-up. The two flip mirrors, M1 and M2, and the multimode fiber serve to measure the excitation function of the optical grating.

In order to prepare the samples for the TDFRS experiment a small amount of dye needs to be added to the samples. In the experiments we used basantol yellow, [**?**] a trivalent salt (Cobalt complex) which was provided by BASF. Basantol yellow is delivered as an aqueous solution, which contains also small amount of 2-(2-butoxyethoxy-)ethanol and 2,2'-dihydroxydipropylether. Drying the powder before adding it to the surfactant solution did not lead to a significant difference in the result. The optical density at λ_w was adjusted by addition of 0.001 wt% basantol yellow to $1.5-3$ cm^{-1}.

For the experiments, we first prepared an aqueous dye solution with the desired absorption using deionized water (Milli-Q). Then the surfactant was added and stirred for 4 hours at room temperature. For most of this work, we used solutions with less than 30 wt% surfactant (see Fig.5.8). However, for the $C_{12}E_6$ surfactant, experiments were also carried out at a high surfactant concentration (90 wt%). After preparation, the solutions were filtered by a 0.45 μm filter (Spartan) directly into the sample cells. For the TDFRS experiment we used Quartz cells (Hellma) with a layer thickness of 0.2 mm. The sample cells were sealed tightly by a Teflon stopper. In the light scattering experiment we used cylindrical glass cells with an inner

diameter of 8.5 mm. The optical path length of the cells used to determine the refractive index increment with temperature $(\partial n/\partial T)_{w,p}$ was 10 mm.

5.3.2 Refractive index increments

The quantities $(\partial n/\partial w_1)_{T,p}$ for the surfactant systems were determined with a single measurement cell by means of a scanning Michelson interferometer operating at a wavelength of 632.8 nm [115]. In this way we obtained $(\partial n/\partial w_1)_{T,p}$=0.130 at T=25°C. Measurements with an Abbé refractometer between 20°C and 40°C confirmed this value and showed that $(\partial n/\partial w_1)_{T,p}$ is constant in the investigated temperature range $(\partial n/\partial w_1)_{T,p}$= 0.131 ± 0.001.

Figure 5.2 shows the refractive index increments with temperature $(\partial n/\partial T)_{w,p}$ of $C_{12}E_6$ in water as a function of surfactant weight fraction at different temperatures. The samples used for the $(\partial n/\partial T)_{w,p}$ measurements came from the same batch as those samples measured in the TDFRS experiment and contained the same small amount of basantol yellow. The difference to a sample without dye is smaller than 1% (see open symbols in Fig. 5.2). For the high surfactant concentration of $w_1 = 90$ wt% we measured $(\partial n/\partial T)_{w,p} = -3.71 \times 10^{-4}$ K^{-1} at 25 °C.

5.3.3 Dynamic light scattering

The dynamic light scattering (DLS) measurements were carried out for angles between 20° and 120°. A Kr-ion laser was used as the light source (wavelength $\lambda = 647.1$ nm). Correlation functions of scattered light were measured by an ALV-5000E correlator. The cylindrical sample cell was placed in a thermostated bath, which was controlled with an uncertainty of 0.1 °C. The sample solutions were kept at the measured temperature for at least 30 minutes to ensure equilibrium conditions before starting data acquisition.

5.3.4 TDFRS

The experimental setup of TDFRS is sketched in Fig. 5.3. The interference grating was written by an argon-ion laser operating at the wavelength of λ=488 nm. The grating was read by a He-Ne laser at λ=632.8 nm. The intensity of the diffracted beam was measured by a photomultiplier. A mirror mounted on a piezo crystal was used for phase shift and

stabilization to obtain the heterodyne signal. The flip mirror $M1$ in front of the cell was used to image the diffraction grating on a CCD camera to determine the grating vector. The typical grating vector in the experiments was around $q = 3100$ cm^{-1} which corresponds to a fringe spacing around $d = 20$ μm. A second flip mirror $M2$ in front of the CCD camera was used to record the excitation function. For the measurement of the excitation function a second fiber (multi mode) was connected to the photomultiplier and the same recording equipment was used as for TDFRS measurements.

The TDFRS measurements were carried out in a temperature range from 20.0 to 40.0 °C. The temperature of the sample cell was thermostatically controlled by circulating water with an uncertainty of 0.02 °C. Deterioration of the sample due to long heating and absorption of carbon dioxide leads to changes in the absorption spectrum. Therefore, we measured the absorption spectrum after each TDFRS experiment and discarded the samples when changes were significant.

5.3.5 Dye influence on the TDFRS signal

In this section we study in more detail the influence of the added dye. Ideally, the dye is inert, which means that there is no photobleaching and no dye contribution to the diffraction signal. For organic mixtures, it has been shown that the addition of an organic dye results in very small dye contributions to the signal (on the order of 0.5%). These contributions do not influence the mean values of the transport coefficients but lead to slightly asymmetric error bars [115]. In the case of aqueous systems it is more difficult to find an inert dye. Typically the spectroscopic properties of dyes depend on pH, ionic strength and other parameters. We investigated roughly 30 different water soluble dyes. Of those, only basantol yellow and alizarin were inert with respect to the TDFRS experiment. Due to the strong pH-dependence of the absorption spectrum of alizarin, and since alizarin is only soluble in the presence of the surfactant, we preferred basantol yellow and employed it throughout the experiments described here. Basantol yellow has already been used successfully in numerous studies on polymer solutions [**?** 46] and with another non-ionic surfactant system.[66] As it turns out, this dye has a physical effect on the micelles of some of our non-ionic surfactant systems. In order to separate these effects from potential spurious dye effects, we estimate in this section contributions of the dye itself to the TDFRS signal. Later, in Sections 5.4 and 5.5,

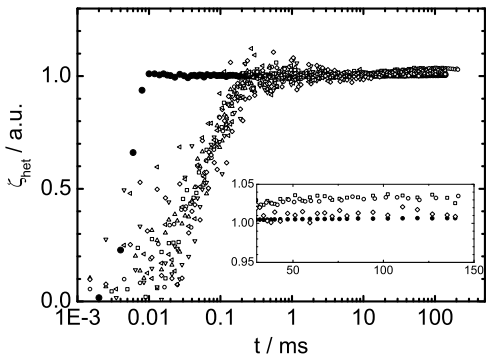

Figure 5.4: Excitation function (●) in comparison with heterodyne signal $\zeta_{\text{het}}^{\text{dye}}$ of an aqueous solution of basantol yellow with various optical densities: 3.9 cm^{-1} (◊), 5 cm^{-1} (▽), 5.5 cm^{-1} (◁), 7 cm^{-1} (△), 10 cm^{-1} (◯, □). The inset shows the concentration signal for the highest and lowest dye concentrations.

we investigate and discuss the effect of the dye on interactions between micelles.

As a first test, we measured the diffraction signal for five aqueous solutions of the dye. For an inert dye, there should be no concentration contribution to the signal but only a thermal contribution, which becomes identical with the excitation function at long times. Figure 5.4 shows a comparison of the excitation function for an aqueous solutions of basantol yellow with various optical densities between 3.9 cm^{-1} and 10 cm^{-1} at a wavelength λ=488 nm. The inset in figure 5.4 shows a clear concentration contribution to the signal for the highest dye concentration. However, at typical dye concentrations, the amplitude of the concentration signal is very low and typically below 1% of the total signal. From the time dependence of the diffraction signal, we can also determine the thermal diffusivity of water. The extrapolated thermal diffusivity $D_{\text{th}} = 1.37 \times 10^{-3}$ cm^{2}s^{-1} for an optical density of 2 cm^{-1} at a temperature of $T = 25°$C compares well with the literature value of $D_{\text{th}} = 1.45 \times 10^{-3}$cm^{2}s^{-1} for water [**?**]. From the concentration contribution to the TDFRS signal in aqueous dye solutions, we estimate that the contribution of the dye to the amplitude of the concentration signal for a measurement of the surfactant in water is typically below 0.5%. Only for very lowest

surfactant concentrations ($w_1 < 5$ wt%) is the contribution of the dye around 5%. Due to the smallness of the dye contribution to the TDFRS signal we neglect it in the following.

We also investigated the distribution of the dye in the micellar solutions. For C_6E_4, C_8E_4, $C_{10}E_8$, $C_{12}E_5$, $C_{12}E_6$, $C_{16}E_8$ we prepared aqueous solutions with surfactant concentrations $w_1 = 2.5\%$ and for C_6E_4 with $w_1 = 5\%$, which are above the critical micelle concentration. All solutions contained a typical amount of basantol yellow and were quenched by 3-5°C into the two-phase region. After the temperature quench we waited until the surfactant-rich und the water-rich phase had formed. In the case of the long-chain surfactant systems, $C_{12}E_5$, $C_{12}E_6$, and $C_{16}E_8$/water, the color of the upper, surfactant rich phase was a deep orange and that of the lower phase was colorless. For the shorter chain surfactants C_6E_4, C_8E_4, and $C_{10}E_8$ the colors of the surfactant-rich and water-rich phase were a deeper and fainter orange, respectively. For $C_{12}E_6$ we also tested the effect of salt on the distribution of the dye and found that even an amount of salt that is sufficient to suppress the second mode (see Sec.5.4.3) does not change the color of the phases. For the C_mE_n systems studied here, the dye distribution between the two phases reflects the surfactant concentration; the dye is enriched in the surfactant rich phase and depleted in the water rich phase. The surfactant concentration in the water rich phase decreases rapidly with increasing chain length of the alkyl chains of the surfactants [**?**]. Since the dye concentration in the water rich phase, as indicated by the color of the phase, also decreases rapidly with alkyl chain length we conclude that the dye molecules are attracted to the surfactant molecules. Nevertheless, the temperature grating in the TDFRS experiment is not expected to be influenced by this attraction since, first of all, all experiments were performed in the homogenous micellar L_1-phase with a homogenous surfactant distribution. Furthermore, we did not observe a shift of the absorption band to longer wavelength as has been observed for colloidal systems, where the dye molecules are preferentially adsorbed on the colloidal surface [16]. This suggests that the constant exchange of surfactant molecules between micelles and solution prevents the formation of stable adsorbates.

As will be discussed in Sec. 5.4.2, we investigated the effect of the dye on the phase transition temperature for the $C_{12}E_6$/water system and found that the dye increases the transition temperature for low surfactant concentrations. Since the change in the phase transition temperature is generally not large and decreases with increasing concentration, we do not expect a strong effect on the measured diffusion and Soret coefficients, except for dilute solutions

very close to the phase boundary.

5.4 Results

In this section we present the TDFRS results for $C_{12}E_6$ in water and compare them with results for other C_mE_n/water systems. We start with a comparison of the measured diffraction signals of $C_{12}E_6$ with those obtained recently for $C_{10}E_8$ [66]. In contrast to the previous measurements we observed a second mode for $C_{12}E_6$ in water. Further analysis of the data shows that the diffusion coefficients determined from the fast mode agree well with the literature. In the following subsection we discuss TDFRS signals for four more non-ionic surfactant systems to establish patterns in the occurrence of the second mode. In the last subsection we discuss the influence of salt on the second mode.

5.4.1 Characteristics of $C_{12}E_6$ in water

Fig. 5.5 displays normalized heterodyne signals for $C_{12}E_6$ and $C_{10}E_8$. For both surfactants, the signals are normalized to the thermal plateau, which is reached at around 500 μs. The difference in the signals is quite striking. While in the case of $C_{10}E_8$ the diffraction intensity increases steadily before reaching its steady state plateau, in the case of $C_{12}E_6$ the diffraction signal passes through a maximum and decays to the final equilibrium value. This two-mode decay of the TDFRS signal is characteristic for $C_{12}E_6$ solutions at higher temperatures and lower surfactant concentrations (see Fig. 5.8) and was not observed for concentrations above $w_1 = 25$ wt% in the investigated temperature range.

As an independent test of our TDFRS results, we performed dynamic light scattering (DLS) experiments on $C_{12}E_6$ in water with and without added dye. We found that the addition of the dye did not lead to significant changes in the measured values for the mass diffusion coefficient D. Figure 5.6 shows DLS and TDFRS results for the diffusion coefficient of $C_{12}E_6$ for different temperatures as a function of concentration. In these experiments, the solutions for the DLS measurements contained the same amount of basantol yellow as the TDFRS samples. In the TDFRS experiments, the diffusion coefficients were derived from the fast mode. The results presented in Fig. 5.6 show that the values obtained by the two different methods agree within experimental error, where the error bars correspond to one standard

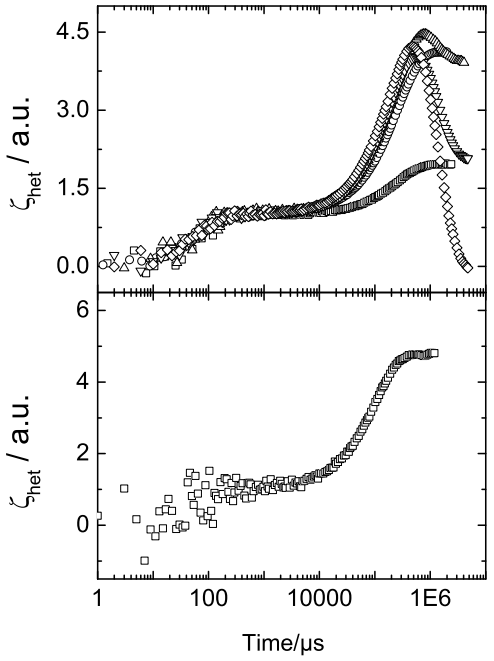

Figure 5.5: Normalized heterodyne signal ζ_{het} measured for $C_{12}E_6$ ($w_1 = 5$ wt%) at different temperatures $T = 20$ °C (□), 25 °C (○), 30 °C (△), 35 °C (▽), and 40 °C (◊) (upper figure) and $C_{10}E_8$ ($w_1 = 15$ wt%, $T = 20$ °C (□)) (lower figure), respectively.

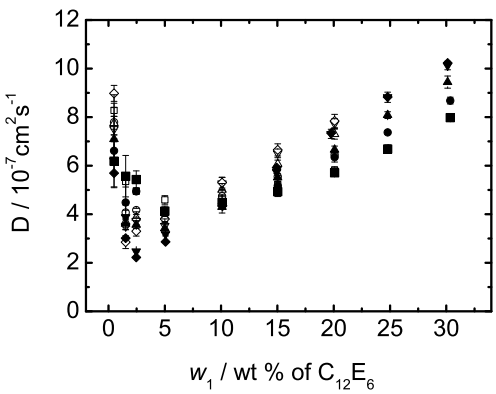

Figure 5.6: Diffusion coefficient of $C_{12}E_6$/water in dependence of surfactant concentrations at different temperatures $T = 20$ °C (■, □), 25 °C (●, ○), 30 °C (▲, △), 35 °C (▼, ▽), and 40 °C (♦, ◊) determined by TDFRS (solid symbols) and DLS (open symbols). In the case of two-mode TDFRS signals, the data presented in this graph were determined from the fast mode. For both TDFRS and DLS measurements the solutions contained basantol yellow.

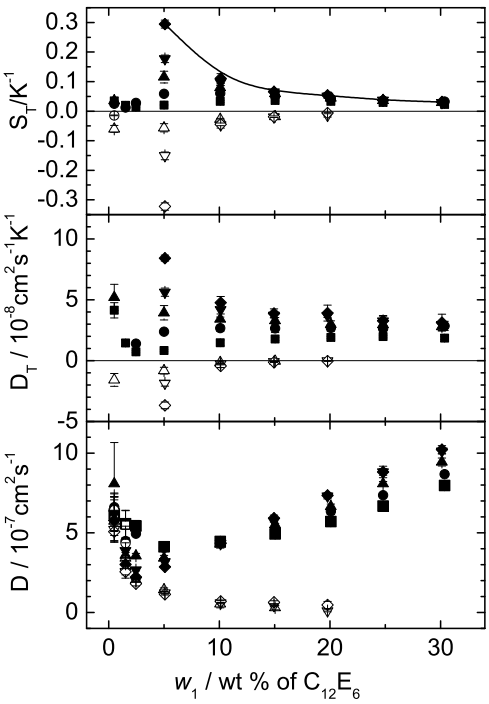

Figure 5.7: Soret coefficient S_T, diffusion coefficient D, and thermal diffusion coefficient D_T of $C_{12}E_6$ in water in dependence of the surfactant concentration w_1 for different temperatures $T = 20$ °C (■, □), 25 °C (●, ○), 30 °C (▲, △), 35 °C (▼, ▽), and 40 °C (♦, ◊). The solid symbols refer to the fast mode and the open symbols to the second mode. The solid line in the top graph is a guide to the eye for the decreasing Soret coefficient with increasing concentration.

deviation.

The diffusion coefficient data in Fig. 5.6 show a pronounced minimum at a weight fraction of about $w = 2.5$ wt%. This is expected for mixtures near a phase boundary [**?**] and agrees with earlier observations on this and related nonionic micellar solutions [**? ? ? ?**]. For small surfactant concentrations, the diffusion coefficients decrease with increasing temperature while the opposite is true for larger surfactant concentrations. In addition to the vicinity of the phase transition, micellar growth [**?**] and the onset of entanglements between micelles [**?**] are believed to contribute to the complicated composition and temperature dependence of the diffusion coefficients in micellar solutions.

Figure 5.7 provides a survey of the measured Soret coefficients S_T, diffusion coefficients D, and thermal diffusion coefficients D_T of $C_{12}E_6$ in water as a function of the surfactant concentration w_1 at different temperatures. The data determined from the single mode in solutions with one-mode decay and from the fast mode in solutions with two-mode decay are represented by filled symbols in Fig. 5.7 and are also presented in Table 5.1. Since their signals show the same characteristics they will be referred to collectively as “fast mode” data. In the concentration range presented in Fig. 5.7, the fast mode Soret coefficients are positive for all temperatures investigated. For concentrations 5 wt% $< w_1 <$30 wt%, the S_T values decrease with increasing surfactant concentration. At its maximum near $w_1 = 5$ wt%, S_T increases strongly with temperature. The temperature dependence becomes less pronounced at higher concentrations and, at a concentration of $w_1 = 30$ wt%, the Soret coefficient is temperature independent within the experimental error. For concentrations smaller than 5 wt%, the fast mode Soret coefficients are quite small and show little dependence on temperature. Unfortunately, the data for very low concentrations are quite noisy due to the small amplitude of the concentration signals so that it is difficult to discern the concentration dependence in this range. Not shown in the figure is our result for a solution at high surfactant concentration, $w_1 = 90$ wt%, where inverted micelles form. For this concentration, the Soret coefficient $S_T = -0.011 \pm 0.001$ is negative, indicating that the inverted micelles move to the warmer regions of the fluid.

The coefficients determined from the slow mode of the TDFRS signal are represented by open symbols in Fig. 5.7. The diffusion coefficients associated with the slow mode decrease monotonically with increasing composition and approach zero as the amplitude of the slow

modes vanishes near 20 wt%. While the values of the slow-mode diffusion coefficients are comparable to those determined from the fast mode for low concentrations, they become markedly smaller for concentrations larger than 2.5 wt%. Just as in the case of the fast mode, the amplitude of the slow mode decreases with decreasing temperature and increasing composition for intermediate compositions. However, the sign of the amplitude is negative indicating that the species responsible for the mode is enriched in the warmer regions of the fluid. In order to interpret the slow mode coefficients, we recall that TDFRS signals with two-mode decays have previously been observed in ternary mixtures of a dilute polymer in mixed solvents [**?**]. For ternary mixtures where cross effects between the two solutes can be neglected, the heterodyne signal intensity may be expressed as [**?**]

$$\zeta_{\text{het}}(t) = 1 + \sum_{i=1,2} \left(\frac{\partial n}{\partial T}\right)^{-1}_{w_1,w_2,p} \left(\frac{\partial n}{\partial w_i}\right)_{T,p,w_{j\neq i}} w_i\,(1-w_i)\,S_{\text{T}i} \times \left(1 - e^{-q^2 D_i t}\right), \quad (5.6)$$

where $i \in \{1,2\}$ denotes the solute species. This expression reduces to Eq. (5.3), when the composition variations of the index of refraction are not sensitive to the solvent species, and when a prefactor $r = w_2(1-w_2)/w_1(1-w_1)$ is included in the definition of the second amplitude coefficient $S_{\text{T}s}$ in Eq. (5.3). Our discussion in Sec. 5.5 suggests that the inclusion of dye molecules in some micelles may be responsible for the slow mode. Such micellar solutions may be considered ternary mixtures of regular micelles, dye-marked micelles, and water. In this case, the index of refraction changes are indeed expected to be insensitive to the micelle species, which justifies treating them as a common prefactor in Eq. (5.3). Since the dye concentration is extremely low and constant, the dye marked micelles are dilute at all surfactant concentrations. This implies that cross-diffusion contributions to the decay times may be neglected and that the diffusion coefficients D_f and D_s may be associated with the mass diffusion of the regular micelles in water and the self-diffusion of the dye-marked micelles in the solution, respectively. While for high surfactant concentrations a cross contribution to the amplitudes cannot be excluded, cross diffusion effects are expected to be negligible for low surfactant concentrations. This implies that the amplitude coefficient $S_{\text{T}s}$ is closely related to the Soret coefficient of the dye-marked micelles. However, since the exact concentration of these micelles is not known, we have absorbed the parameter $r = w_2(1-w_2)/w_1(1-w_1)$ in the value of the amplitude $S_{\text{T}s}$. Thus, the measured values of the Soret coefficients of the slow component differ from the actual values by a concentration

dependent factor and only qualitative conclusions can be drawn about the thermal diffusion behavior of this component.

5.4.2 Characteristics of some additional non-ionic surfactant systems

To gain a better understanding of the second slow process in the diffraction signal of the TDFRS experiment, we investigated other non-ionic surfactants in water. Fig. 5.8 shows the phase diagrams for the six investigated surfactants C_6E_4 [**?**], C_8E_4 [**?**], $C_{10}E_8$ [**?**], $C_{12}E_5$ [58], $C_{12}E_6$ [58**?**] and $C_{16}E_8$ [58] in water. The circles in Fig. 5.8 mark the temperatures and concentrations of our measurements, where open and filled symbols indicate one or two mode behavior, respectively. The shape of the micelles just above the critical micelle concentration is highly dependent on surfactant type and solution conditions (concentration, electrolyte level, temperature). The systems with the smallest surfactant molecules C_6E_4 and C_8E_4 show a rather simple phase diagram with an isotropic micellar phase consisting of spherical micelles and a two-phase region. For $C_{10}E_8$ in the isotropic micellar phase (L_1) the shape of the micelles is somewhat elongated [**?**]. In the case of $C_{12}E_5$, $C_{12}E_6$, and $C_{16}E_8$ in the L_1-phase, the spherical micelles change their structure with increasing concentration to rod-like micelles which entangle at high concentrations [**?**].

There have been numerous studies of the effect of electrolytes on the phase separation in micellar solutions [**? ? ? ? ? ? ?**]. The addition of salts may shift the phase boundary towards lower temperatures, as for example in the case of sodium chloride, or towards higher temperatures, as for example in the case of potassium iodide [**?**]. Since basantol yellow is a trivalent salt, we determined its effect on the phase separation of $C_{12}E_6$/water and found that it shifts the phase boundary by $\Delta T \approx 2.2°$C for a surfactant concentration of $w = 5$ wt%. The addition of 10^{-2} M sodium chloride to the surfactant mixture with dye brings the system back to the original phase separation temperature. The temperature shift induced by basantol yellow is more pronounced at lower surfactant concentrations ($\Delta T \approx 5°$C for $w = 2.5$ wt%) but is still reversed by the addition of the same amount of salt.

The TDFRS results for all investigated non-ionic surfactant systems of the type C_mE_n are summarized in Fig. 5.9, where we present the normalized heterodyne diffraction signals for these systems at a surfactant concentration of $w_1 = 2.5$ wt% for three different temperatures.

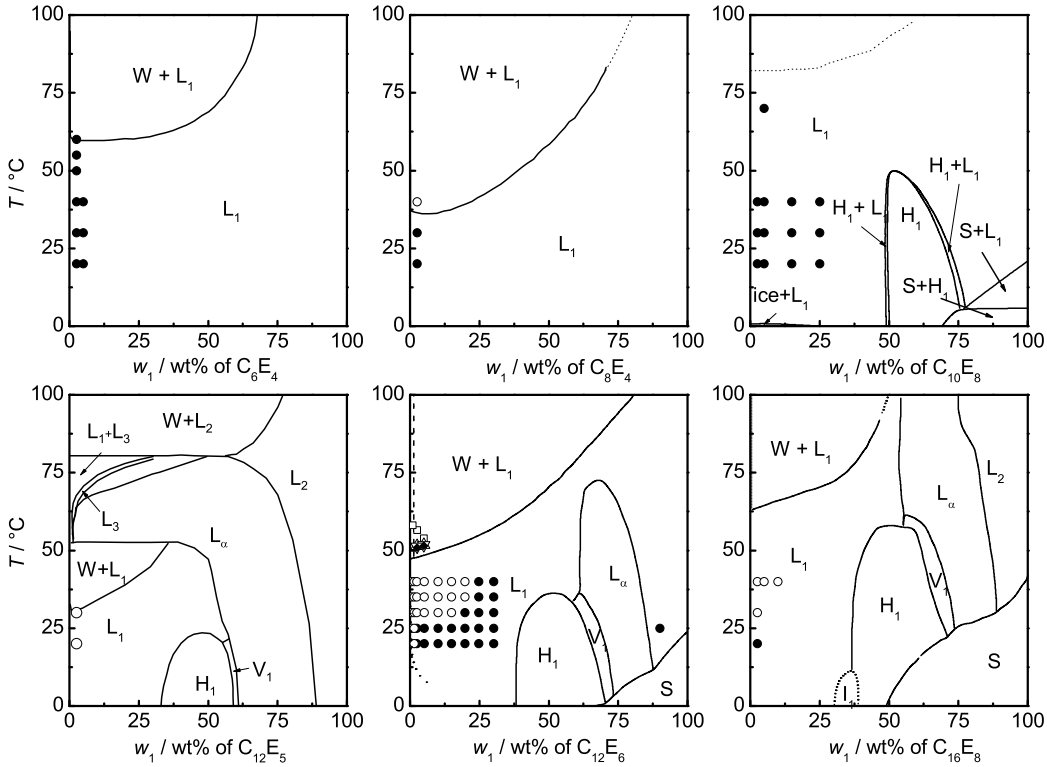

Figure 5.8: Schematic phase diagram for C_6E_4 [**?**], C_8E_4 [**?**], $C_{10}E_8$ [**?**], $C_{12}E_5$ [58], $C_{12}E_6$ [58**?**] and $C_{16}E_8$ [58] in water. The different regions are abbreviated in the following way: water (W), micellar solution (L_1), isotropic solution not fully miscible with water or surfactant (L_2), hexagonal (H_1), lamellar (L_α), bicontinuous cubic (V_1), coexisting phase ($W+L_1$), solid surfactant phase (S) and close packed spherical micelle phase (I_1). The two-phase region for $C_{10}E_8$/water is indicated only by a dotted line, since only the cloud point temperature is available in the literature [**?**]. The dashed line in the phase diagram of $C_{12}E_6$/water refers to the percolation line given by Strey and Pakusch [**?**]. For $C_{12}E_6$/water we determined also the phase separation temperature at two surfactant concentrations (▽), and also for the same solutions containing basantol yellow (□), sodium chloride (◊) and basantol yellow+sodium chloride (△). The open and solid circles mark the concentration and temperature range where TDFRS experiments have been performed. Depending on the system, temperature, and concentration either one-mode (●) or two-mode behavior (○) has been observed.

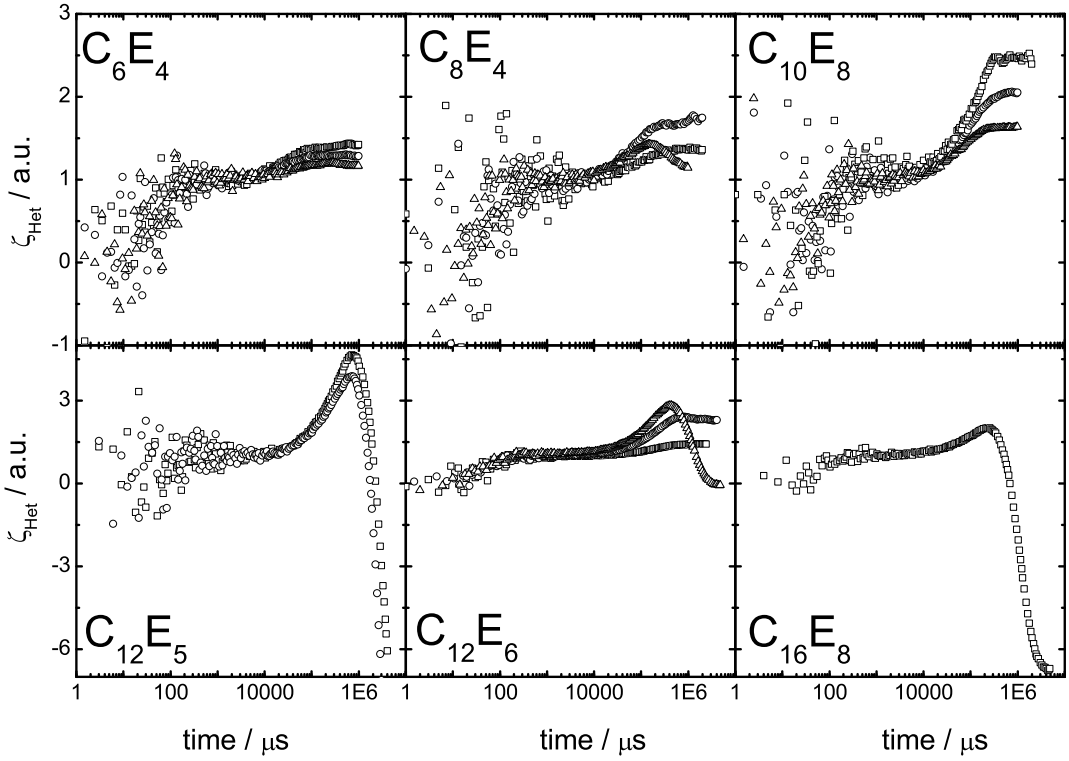

Figure 5.9: Normalized heterodyne signals ζ_{het} measured for C_6E_4, C_8E_4, $C_{12}E_5$, $C_{12}E_6$ and $C_{16}E_8$ in water at different temperatures ($T = 20$ °C (□), 30 °C (○), 40 °C (△)). For all systems, the surfactant concentration was $w_1 = 2.5$ wt%.

Except for C_6E_4 and $C_{10}E_8$ all surfactant systems show typical two-mode behavior: a positive concentration signal at shorter times followed by a slower process with negative amplitude, which is due to an inversion of the grating. The surfactant $C_{12}E_5$ in water shows the most distinct behavior: the second mode is so slow that the system had not reached the steady state after 5 seconds.

5.4.3 Characteristics of the surfactant solutions in the presence of salt

In order to investigate the effect of ion concentration we performed TDFRS experiments on surfactant solutions with added sodium chloride, a simple uncolored salt. Figure 5.10 shows the normalized heterodyne diffraction signal ζ_{het} for $C_{12}E_6$ and $C_{16}E_8$ in water at a surfactant concentration of $w_1 = 2.5$ wt% and a temperature of $T = 40$ °C for several salt concentrations. For both surfactant systems, the second mode becomes weaker and finally disappears with increasing salt concentration. In Fig. 5.11 we present the results for the fast and slow-mode diffusion coefficients of $C_{12}E_6$/water at a surfactant concentration of $w_1 = 2.5$ wt% and a temperature of $T = 40$ °C as a function of salt concentration. The results show that the fast-mode diffusion coefficients are almost independent of the salt content, while those determined from the slow mode decrease with increasing salt concentration until the slow mode disappears for higher salt contents ($w_{\text{NaCl}} > 0.02$ mol/L). The addition of salt decreases the magnitude of both S_{T}'s determined from the fast and slow mode with increasing salt content. Experiments with potassium chloride added to the surfactant solutions yielded results similar to those obtained with added sodium chloride.

5.5 Discussion

We have presented results from experiments on aqueous solutions of six non-ionic surfactants of the type C_mE_n, where m and n indicate the number of repeat units in the alkyl tails and ethylene oxide head groups, respectively. Most of the measurements were performed on solutions with surfactant concentrations of less than 30 wt%. In this concentration range, the surfactants form nearly spherical or elongated micelles depending on the surfactant, the concentration, and the temperature. We also investigated one solution with very high surfactant

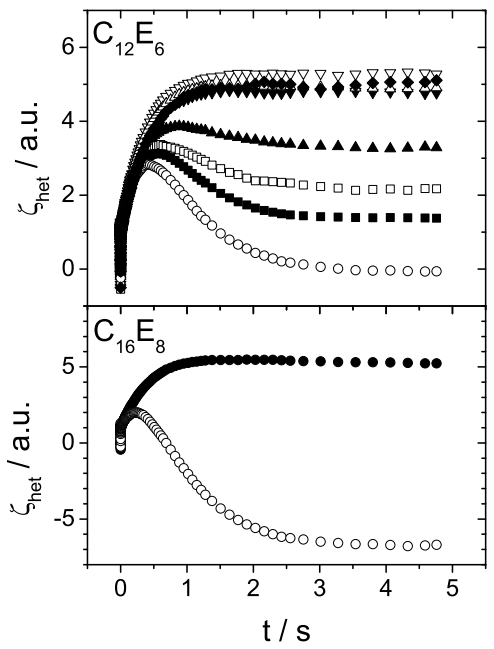

Figure 5.10: Normalized heterodyne signal ζ_{het} measured for $C_{12}E_6$ and $C_{16}E_8$ in water at a temperature of $T = 40$ °C. For both systems, the surfactant concentration was $w_1 = 2.5$ wt% and the solutions contained basantol yellow as dye. $C_{12}E_6$ was studied for different sodium chloride concentrations w_{NaCl} (0.0 mol/L (○), 0.00092 mol/L (■), 0.0018 mol/L (□), 0.0037 mol/L (▲), 0.018 mol/L (△), 0.023 mol/L (▼), 0.037 mol/L (▽), 0.053 mol/L (♦)). $C_{16}E_8$ was studied with (0.149 mol/L (●)) and without salt (○).

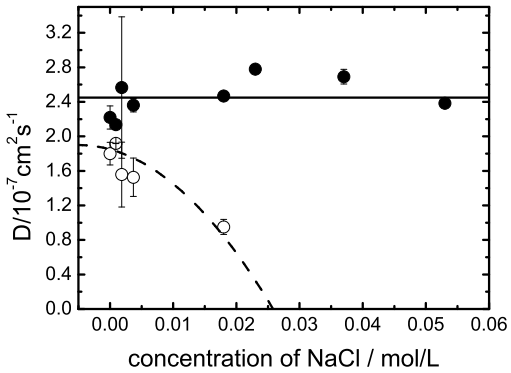

Figure 5.11: Diffusion coefficient, D, derived from the fast (●) and second slow (○) mode for $C_{12}E_6$/water ($w_1 = 2.5$ wt%, $T = 40$ °C) in dependence of sodium chloride concentration. The solid line represents the mean diffusion constant for all salt concentrations. The dashed line is a guide to the eye.

concentration corresponding to inverted micelles.

Thermal diffusion forced Raleigh scattering (TDFRS) and dynamic light scattering (DLS) experiments were carried out to investigate thermal and mass diffusion in the surfactant systems. For typical micellar solutions, one expects the concentration part of the signal in a TDFRS experiment to consist of a single mode with positive amplitude (see bottom panel of Fig. 5.5.). Such single mode signals were indeed observed for part of the micellar solutions investigated in this work. The values of the Soret coefficients determined from these signals are positive and the mass diffusion coefficients agree with those obtained from dynamic light scattering (DLS) within experimental errors. For other solutions, however, we observed a second mode in the TDFRS concentration signal (see top panel of Fig. 5.5). The second mode always had a negative amplitude and a long decay time, corresponding to a negative Soret coefficient and a small mass diffusion coefficient. DLS experiments on the same systems showed no second mode and yielded mass diffusion coefficients that agree well with those obtained from the fast mode of the TDFRS signal.

The TDFRS signals at surfactant concentration $w_1 = 2.5$ wt% presented in Fig. 9 are

representative of the behavior of the different surfactants. For the temperatures and concentrations investigated in this work, only single mode TDFRS signals have been recorded for C_6E_4 and $C_{10}E_8$, only two-mode signals for $C_{12}E_5$, and both one and two mode signals for C_8E_4, $C_{12}E_6$, and $C_{16}E_8$. In general, the thermodynamic states associated with two mode behavior (indicated by open circles in Fig. 5.8) are closer to the miscibility gap than those associated with single-mode behavior (shown as filled circles). This suggests that single-mode signals will be observed in all micellar solutions at sufficiently high concentrations and low temperatures. For the system $C_{10}E_8$/water only single mode behavior has been observed in this work, however, the high phase transition temperature prohibits measurements closer to the phase boundary, where two-mode behavior may be found. For the smallest surfactant, C_6E_4, a careful investigation of states near the phase boundary revealed no two-mode behavior.

Our results presented in Sec. 5.4.1 show that the fast mode observed in solutions with two-mode decay is very similar to the single mode observed in solutions with one-mode decay. The diffusion coefficients extracted from these modes agree within experimental error with our DLS results for the same solutions. Furthermore, the Soret coefficients extracted from the fast and single modes show similar temperature and composition dependence. This confirms that the fast mode coefficients D_f and S_{Tf} introduced in Sec. 5.2 may be identified as the typical mutual diffusion and Soret coefficients of the micellar solutions.

To investigate the temperature and composition dependence of the typical transport coefficients in detail, measurements were performed on the system $C_{12}E_6$/water, for surfactant concentrations between 0.5 wt% and 30 wt% and temperatures between 20 °C and 40 °C. In agreement with literature results, the values of D have a minimum near the critical phase separation concentration of about 2.5 wt% (see Fig. 5.6). The temperature and concentration dependence of the diffusion coefficients is believed to reflect both the distance to the phase boundary and the changes in micellar structure with composition and temperature [**? ? ? ? ?**]. The Soret coefficients S_T and the thermal diffusion coefficients D_T derived from the fast mode and single modes are positive as has been observed before for ionic and non-ionic surfactant solutions. [**?** 72, 66] They have their maximum values and their largest temperature dependence near the concentration, where D is at a minimum (see Fig. 5.7). An increase in the thermal diffusion coefficients with temperature has also been observed in solutions of

poly(ethylene oxide) (PEO) in water [**?**] and may be associated with the approach to the lower critical solution temperature. Just as in the case of PEO in water, the ethylene oxide groups of the surfactants form hydrogen bonds with the water molecules, which leads to a decrease in solubility at higher temperatures. Our results for the solution with high surfactant concentration ($w_1 = 90$ wt%) showed, for the first time, a negative value for the Soret coefficient of a micellar solution. At this high surfactant concentration the micelles in solution are inverted so that the water and ethylene-oxide chains are on the inside of the micelles and the alkyl chains are on the outside. Since the water concentration is low, the hydrogen bond formation between ethylene-oxide chains and water molecules may not be the dominant factor in determining the Soret effect anymore. Furthermore, the difference in surface structure between regular and inverted micelles may contribute to their different thermal diffusion behavior [98].

A second, slow mode has not been observed before in micellar solutions and its origin is not immediately clear. Slow modes have been observed, however, in light scattering experiments on polyelectrolyte solutions at sufficiently high polyelectrolyte and sufficiently low salt concentrations [**? ?**]. In these solutions, the slow moving species has been identified with temporal aggregates of macroions [**? ? ?**]. The origin of the aggregation in polyelectrolyte solutions is attributed to a net attractive interaction between polyions in solutions above a minimum polyion concentrations. For smaller concentrations, on the other hand, the charged chains repel each other which prohibits aggregation [**? ?**]. Two-mode TDFRS signals have previously been observed only in experiments on ternary mixtures consisting of a polymer at low concentration in a mixed solvent [**?**].

As in the case of the polyelectrolytes [**?**], we find that addition of salt decreases the amplitude of the slow mode until it is completely suppressed at sufficiently high salt concentrations (see Fig. 5.10). The only source of free ions in our experiments is the dye basantol yellow, a trivalent salt, that is added in small amounts to the micellar solutions when TDFRS experiments are performed. Temperature quench experiments into the coexistence region of micelle rich and water rich phases show that the dye is enriched in the micelle rich phase and present in the water rich phase only in proportion to the low surfactant concentration. This leads to the conclusion that the dye molecules associate with the surfactant molecules.

Cloud point experiments on the system $C_{12}E_6$/water show that the presence of the dye

increases the phase transition temperature (see Fig. 5.8). This effect is reversed, and the original phase boundary restored, when salt, in an amount sufficient to suppress the slow mode, is added to the dye-containing micellar solutions. The addition of salt by itself has very little effect on the phase boundary. These results show that the dye stabilizes the micelles in solutions and that this stabilizing effect is related to the ionic nature of the dye. Since an increase in the phase transition temperature is associated with a decrease in the attractive interactions between the micelles [**?** **?**], one concludes that the dye molecules introduce a repulsive interaction between the micelles.

The experimental results for the slow mode of the TDFRS signal may tentatively be interpreted in terms of a ternary mixture of neutral micelles, charged micelles and water, if one assumes that at least part of the dye molecules are incorporated into micelles. This is a reasonable assumption, since the dye molecules may act as cosurfactants and nucleate the growth of micelles. In general, one would expect an equilibrium between dye molecules incorporated in micelles and dye molecules in solution, where the activity constant depends on composition, temperature, and type of surfactant. While micelles that contain dye molecule are negatively charged, they will not interact with each other through electrostatic interactions since their separation is much larger than the Debye screening length. Hence, the aggregation mechanism that gives rise to the slow mode in polyelectrolyte solutions does not apply to our micellar solutions. The diffusion coefficients associated with the slow mode decrease monotonically with increasing composition and approach zero as the amplitude of the slow modes vanishes. The temperature and composition dependence of the slow-mode diffusion coefficients is closely correlated with the viscosity [**?**] of the micellar solutions and suggests that the size of the dye-charged micelles does not change much with composition. This size is typically around 5 to 6 nanometers and falls in the range of the size distribution of the regular micelles, which are quite polydisperse. This would explain why a slow mode is not observed in the DLS experiments. The Soret coefficients derived from the slow modes are negative, indicating that the dye-charged micelles are enriched in the warmer regions of the fluid. This is consistent with our finding that the presence of the dye introduces a repulsive interaction between the dye molecules.

While the discussion presented here is tentative, our results suggest that it may be interesting to investigate in a more systematic way nonionic surfactants that are doped with

varying amounts of charge carrying surfactant molecules.

Table 5.1: Soret coefficients, S_{th}, thermal diffusion coefficient, D_T, diffusion coefficient, D for $C_{12}E_6$/water containing basantol yellow as dye. In the presence of a second mode all coefficients were determined from the fast mode.

S_T / K^{-1}															
T/°C	20			25			30			35			40		
w_1															
0.005	0.035	±	0.003	0.025	±	0.001	0.036	±	0.010						
0.015	0.020	±	0.002	0.012	±	0.002									
0.025	0.014	±	0.001	0.028	±	0.002									
0.050	0.021	±	0.002	0.059	±	0.003	0.115	±	0.020	0.177	±	0.013	0.294	±	0.013
0.101	0.033	±	0.003	0.060	±	0.006	0.078	±	0.008	0.097	±	0.010	0.110	±	0.016
0.150	0.036	±	0.002	0.051	±	0.007	0.060	±	0.004	0.065	±	0.003	0.066	±	0.007
0.201	0.034	±	0.002	0.042	±	0.004	0.045	±	0.004	0.051	±	0.002	0.053	±	0.010
0.248	0.030	±	0.002	0.036	±	0.002	0.037	±	0.006	0.037	±	0.005	0.037	±	0.004
0.304	0.023	±	0.001	0.033	±	0.004	0.030	±	0.003	0.029	±	0.002	0.031	±	0.007

D_T / $10^{-7}cm^2s^{-1}K^{-1}$															
T/°C	20			25			30			35			40		
w_1															
0.005	0.414	±	0.063	9.562	±	5.081	0.520	±	0.107						
0.015	0.145	±	0.020	2.641	±	1.355									
0.025	0.074	±	0.008	0.140	±	0.008									
0.050	0.084	±	0.009	0.238	±	0.012	0.393	±	0.059	0.562	±	0.034	0.842	±	0.023
0.101	0.148	±	0.022	0.267	±	0.025	0.341	±	0.017	0.419	±	0.036	0.476	±	0.050
0.150	0.178	±	0.011	0.265	±	0.034	0.329	±	0.025	0.373	±	0.016	0.388	±	0.037
0.201	0.192	±	0.009	0.268	±	0.026	0.299	±	0.028	0.369	±	0.015	0.391	±	0.066
0.248	0.198	±	0.011	0.264	±	0.016	0.296	±	0.048	0.325	±	0.045	0.328	±	0.038
0.304	0.185	±	0.011	0.286	±	0.038	0.281	±	0.034	0.294	±	0.026	0.313	±	0.069

D / $10^{-7}cm^2s^{-1}$															
T/°C	20			25			30			35			40		
w_1															
0.005	6.18	±	1.09	6.62	±	0.88	8.08	±	2.59	6.20	±	1.07	5.78	±	0.64
0.015	5.57	±	0.85	4.49	±	0.94	3.60	±	0.16	3.88	±	0.51	3.02	±	0.24
0.025	5.43	±	0.35	4.94	±	0.13	3.56	±	0.15	2.67	±	0.06	2.22	±	0.13
0.050	4.12	±	0.21	4.06	±	0.07	3.42	±	0.16	3.18	±	0.07	2.87	±	0.10
0.101	4.45	±	0.28	4.43	±	0.14	4.30	±	0.25	4.34	±	0.10	4.35	±	0.23
0.150	4.93	±	0.20	5.17	±	0.16	5.51	±	0.08	5.73	±	0.06	5.92	±	0.20
0.201	5.71	±	0.13	6.35	±	0.20	6.66	±	0.14	7.31	±	0.19	7.34	±	0.14
0.248	6.69	±	0.16	7.37	±	0.08	8.08	±	0.14	8.82	±	0.21	8.83	±	0.36
0.304	7.98	±	0.08	8.68	±	0.14	9.44	±	0.25	10.12	±	0.18	10.23	±	0.25

ACKNOWLEDGEMENT

If you are really involved in your studies and enjoy it, you will definitely not realized the time passed by so fast. Here, to take this chance, I have some words for my experience of the past three years spent in the Forschungszentrum Jülich, and in Jülich.

First of all, I would like to show my sincere appreciations for my promoters Dr. Simone Wiegand and Prof. Jan K. G. Dhont, who offer me the opportunity to pursue my Ph.D. study in the group of Soft Matter. Dear Simone and Jan, thank you so much for your selfless guidance and educating for the past three years. Without your efforts my dream will not come into truth. I also owe special thanks to Dr. Remco Tuinier and Peter Lang for their always being available for the discussions.

I want to express my regards to these people in our group, who support me from the aspects of both experiments and theory. Dear Hartmut, thanks a lot for your unlimited patience to explain me the principles of all kinds instrument and paid so much contribution for maintaining them. I am very honor to be your roommate. Dear Pavel, thank you for your help and cooperation for these measurements. I would like to thank my collages and friends, Johan Buitenhuis, Pavelik Lettinga, Gerhard Meier, Gerhard Nägele, Sylvia Waal, Peter Holmqvist, Kyongok Kang, Mathieu McPhie, Marie Göcking, Hans Hoffmann, Dieter Triefenbach, Christoph Gögelein, Dzina Kleshchanok and Zhenkun Zhang. I will keep it in my mind for all these days we spent together in the group.

To live in Jülich give me the chance to make new friends, with whom my life is beautiful and not lonely any more. They are: Niu Aizhen, Han Bo, Lou Shengrong, Chen Qi, Wu YanHong, Chen Hanyuan, Luo Bing and Deng Dewei. The precious friendship will be in my heart for ever.

Finally, I want to thank my parents and Yang Yuan for their encouragement and understanding.

CURRICULUM VITAE

Hui Ning was born on 28th, 1978 in Zhuozhou, Hebei province, P. R. China. In 1996, he entered the College of Chemistry, Nankai University (Tianjin, China). Four years later, he obtained his Bachelor's degree in chemistry. In 2000, he started his Master study with Prof. Ju Zou on the subject of *Mechanism of the Thermoreversible Gelation of Ionic Polysaccharide*, and three year later he was granted Master degree in polymer chemistry and physics. Later as R&D staff, he worked in Nankai Hecheng Company in 2003. At the beginning of 2004, he joined the soft matter group in IFF, Forschungszentrum Jülich, Germany. There, he started his Ph.D studied under the supervision of Dr. Simone Wiegand and Prof. Jan K. G. Dhont. His Ph.D work focuse on the *Thermal diffusion behavior of complex fluid mixtures*.

LIST OF PUBLICATION

• Wiegand, S. and **Ning, H.** and Kita, R.: Universal concentration dependence of the Soret coefficient in aqueous systems, *J. Non-Equil. Thermody.*, submitted

• **Ning, H.** and Wiegand, S.: Experimental investigation of the Soret effect in acetone/water and dimethylsulfoxide/water mixture, *J. Chem. Phys.*, submitted

• **Ning, H.**; Buitenhuis, J.; Dhont, J.K.G. and Wiegand, S.: Thermally induced sign change of Soret coefficient for a solution of silica particles in toluene, *J. Chem. Phys.*, submitted

• **Ning, H.**; Buitenhuis, J.; and Wiegand, S.: Thermal diffusion behavior of interacting colloids, *Pro 7th international meeting on thermodiffusion San Sebastian*, 389-398, 2006

• Wiegand, S. and **Ning, H.**: To the warm or to the cold? Thermal diffusion in aqueous system, *Pro 7th international meeting on thermodiffusion San Sebastian*, 23-32, 2006

• **Ning, H.**; Kita, R.; Kriegs, H.; Luettmer-Strathmann, J. and Wiegand, S.: Thermal diffusion behavior of nonionic surfactants in water, *J. Phys. Chem. B.*, **110**, 10746-10756, 2006

• **Ning, H.**; Kita, R. and Wiegand, S.: Soret effect in a nonionic surfactant system, *Progr. Colloid Polym. Sci.*, **113**, 111-115, 2006

• Du, D.X.; Zuo, J.; Chen. Y. and **Ning, H.**: Disccusion on the problem of the viscosity measurement of extremely dilute polymer solution, *Ion exchange and Adsorption*, **3**, 214-221, 2003

• Du, D.X.; Zuo, J.; Chen, J. and **Ning, H.**: A study of viscosity behavior of PS/Toluene solution in dilute and extremely dilute concentration region, *Chinese Journal of Reactive Polymers*, **12(1)**, 32-40, 2003

• Meng, F.L.; Luo, L.; **Ning, H.** and Zuo, J.: Advance in the reasearch of κ-carrageenan, *Chemistry*, **5**, 49-56, 2003

• Zuo, J.; Huang, J.F.; An, Y.L. and **Ning, H.**: Diffuison of linear of polystyrene chains in ethyl methacrylate gels, *Polymer physics 2000 Huang shan in China*, 96-97, 2000

• Zuo, J.; **Ning, H.**; An, Y.L. and Huang, J.F.: Effect of pH on dynamic behavior of polyacrylic acid gels, *Polymer physics 2000 Huang shan in China*, 214-215, 2000

Bibliography

[1] S. Alves, G. Demouchy, A. Bee, D. Talbot, A. Bourdon, and A. M. F. Neto. Investigation of the sign of the soret coefficient in different ionic and surfacted magnetic colloids using forced rayleigh scattering and single-beam z-scan techniques. *Phil. Mag.*, 83(17-18):2059–2066, 2003.

[2] I.A. Ananieva, M. Minarik, R. Boutin, O.A. Shpigun, and J. Janca. Characterization of chromatographic silica beads by micro-thermal field-flow fractionation. *J. Loq. Chromatogr. R. T.*, 27(15):2313–2327, 2004.

[3] M. Antonietti, A. Breil, and C. Tank. Chromatographic characterization of complex polymer systems with thermal field-flow fractionation. *Acta Polym. Sin.*, 46(3):254–260, 1995.

[4] G.K. Batchelor. Brownian diffusion of particles with hydrodynamic interaction. *J. Fluid Mech.*, 74:1–29, 1976.

[5] A. Becker, W. Khler, and B. Mller. A scanning michelson interferometer for the measurement of the concentration and temperature derivative of the refractive- index of liquids. *Berichte Der Bunsen-Gesellschaft-Physical Chemistry Chemical Physics*, 99(4):600–608, 1995.

[6] E. Blums, S. Odenbach, A. Mezulis, and M. Maiorov. Soret coefficient of nanoparticles in ferrofluids in the presence of a magnetic field. *Phys. Fluids*, 10(9):2155–2163, 1998.

[7] M. M. Bou-Ali, O. Ecenarro, J. A. Madariaga, C. M. Santamaria, and J. J. Valencia. Measurement of negative soret coefficients in a vertical fluid layer with an adverse density gradient. *Phys. Rev. E*, 62(1):1420–1423, 2000.

[8] D. Braun and A. Libchaber. Trapping of dns by thermophoretic depletion and convection. *Phys. Rev. Lett.*, 89(18):188103–1–188103–4, 2002.

[9] H. Brenner. nonisothermal brownian motion:thermophoresis as the macroscopic manifestation of thermally biased molecular motion. *Phys. Rev. E*, 72:061201–1–16, 2005.

[10] E. Bringuier and A. Bourdon. Colloid transport in nonuniform temperature. *Phys. Rev. E*, 67(1):011404, 2003.

[11] J. Chan, J. J. Popov, S. Kolisnek-Kehl, and D. G. Leaist. Soret coefficients for aqueous polyethylene glycol solutions and some tests of the segmental model of polymer thermal diffusion. *J. Solution Chem.*, 32(3):197–214, 2003.

[12] K. Clusius and G Dickel. *Naturwissenschaften*, 26:546, 1938.

[13] K. Clusius and G Dickel. Zur trennung der chlorisotope. *Naturwissenschaften*, 27:148–149, 1939.

[14] A. Coccia, P. L. Indovina, F. Podo, and V. Viti. Pmr studies on structures of water-ethyl alcohol mixtures. *Chemical Physics*, 7(1):30–40, 1975.

[15] P. Costeseque, D. Fargue, and P. Jamet. Thermodiffusion in porous media and its consequences. In W. Khler and S. Wiegand, editors, *Thermal nonequilibrium phenomena in fluid mixtures*, Lecture Notes Physics, pages 389–427. Springer, Berlin, 2000.

[16] B. J. de Gans, R. Kita, B. Muller, and S. Wiegand. Negative thermodiffusion of polymers and colloids in solvent mixtures. *J. Chem. Phys.*, 118(17):8073–8081, 2003.

[17] B-J de Gans, R. Kita, S. Wiegand, and J. Luettmer Strathmann. Unusual thermal diffusion in polymer solutions. *Phys. Rev. Lett.*, 91:245501, 2003.

[18] S.R. de Groot and P. Mazur. *Non-equilibrium Thermodynamics*. DOver, New York, 1984.

[19] C. Debuschewitz and W. Köhler. Molecular origin of thermal diffusion in benzene plus cyclohexane mixtures. *Phys. Rev. Lett.*, 87(5):055901, 2001.

[20] J. K. G. Dhont. Thermodiffusion of interacting colloids. i. a statistical thermodynamics approach. *J. Chem. Phys.*, 120(3):1632–1641, 2004.

[21] J. K. G. Dhont. Thermodiffusion of interacting colloids. ii. a microscopic approach. *J. Chem. Phys.*, 120(3):1642–1653, 2004.

[22] J. K. G. Dhont, S. Wiegand, S. Duhr, and D. Braun. Thermodiffuison of charged colloids: single-partilce diffusion. page in preparation, 2006.

[23] S. Duhr, S. Arduini, and D. Brauna. Thermophoresis of dna determined by microuidic uorescence. *Eur. Phys. J. E*, 15:277–286, 2004.

[24] S. Duhr and D. Brauna. Thermophoretic depletion follows boltzmann distribution. *Phys. Rev. Lett.*, 96:168301(1–4), 2005.

[25] S. Duhr and D. Brauna. Two-dimensional colloidal crystals formed by thermophoresis and convection. *Appl. Phys. Lett.*, 86:131921(1–3), 2005.

[26] J. F. Dutrieux, J. K. Platten, G. Chavepeyer, and M. M. Bou-Ali. On the measurement of positive soret coefficients. *J. Phys. Chem. B*, 106(23):6104–6114, 2002.

[27] O. Ecenarro, J. A. Madariaga, J. Navarro, C. M. Santamaria, J. A. Carrion, and J. M. Saviron. Fickian and thermal-diffusion coefficients from liquid thermogravitational columns. *Journal of Physics-Condensed Matter*, 2(9):2289–2296, 1990.

[28] A. H. Emery and H. G. Drickamer. Thermal diffusion in polymer solutions. *J. Chem. Phys.*, 23(12):2252–2257, 1955.

[29] W. Enge and Köhler. Thermal diffusion in a critical polymer blend. *Phys. Chem. Chem. Phys.*, 6:2373–2378, 2004.

[30] S. Fayolle, T. Bickel, S. Le Boiteux, and A. Würger. Thermaldiffusion of charged micelles. *Phys. Rev. Lett.*, 95(20):208301–1–208304–4, 2005.

[31] M. Franko and C. D. Tran. Temperature effect on photothermal lens phenomena in water: Photothermal defocusing and focusing. *Chem. Phys. Lett.*, 158(1,2):31–36, 1989.

[32] G. Galliero, B. Duguay, J. P. Caltagirone, and F. Montel. On thermal diffusion in binary and ternary lennard-jones mixtures by non-equilibrium molecular dynamics. *Phil. Mag.*, 83(17-18):2097–2108, 2003.

[33] G. Galliero, B. Duguay, J. P. Caltagirone, and F. Montel. Thermal diffusion sensitivity to the molecular parameters of a binary equimolar mixture, a non-equilibrium molecular dynamics approach. *Fluid Phase Equilibr.*, 208(1-2):171–188, 2003.

[34] J. C. Giddings, K. D. Caldwell, and M. N. Myers. Thermal-diffusion of polystyrene in 8 solvents by an improved thermal field-flow fractionation methodology. *Macromolecules*, 9(1):106–112, 1976.

[35] M. Giglio and A. Vendramini. Thermal-diffusion measurements near a consolute critical-point. *Phys. Rev. Lett.*, 34(10):561–564, 1975.

[36] M. Giglio and A. Vendramini. Soret-type motion of macromolecules in solution. *Phys. Rev. Lett.*, 38(1):26–30, 1977.

[37] K.E. Grew and T.L. Ibbs. *Thermal Diffusion in Gases*. University Press, Cambridge, 1952.

[38] B. Hafskjold. Computer Simulations of Thermal Diffusion in Binary Fluid Mixtures. In W. Köhler and S. Wiegand, editors, *Thermal nonequilibrium phenomena in fluid mixtures*, Lecture Notes in Physics, pages 3–23, Heidelberg, 2002. Springer.

[39] B. Hafskjold, T. Ikeshoji, and S. K. Ratkje. On the molecular mechanism of thermal-diffusion in liquids. *Mol. Phys.*, 80(6):1389–1412, 1993.

[40] J. M. Haile. *MOlecular Dynamics Simulation.Elemetary Methods*. John Wiley & Sons, Chichester, 1992.

[41] K. B. Haugen and A. Firoozabadi. On measurement of molecular and thermal diffuison coefficient in multicomponent mixtures. *J. Phy. Chem. B*, 110:17678–17682, 2006.

[42] S. Iacopini, R. Rusconi, and R. Piazza. The ”macromolecular tourist”: Universal temperature dependence of thermal diffusion in aqueous colloidal suspensions. *Eur. Phys. J. E*, 19:59–67, 2006.

[43] J. Janca. Characterization of chromatographic silica beads by micro-thermal field-flow fractionation. *J. Liq. Chromatogr. R. T.*, 26(6):849–869, 2003.

[44] R. Kita, G. Kircher, and S. Wiegand. Thermally induced sign change of soret coefficient for dilute and semidilute solutions of poly. n-isopropylacrylamide in ethanol. *J. Chem. Phys.*, 121(18):9140–9145, 2004.

[45] R. Kita, P. Polyakov, and S. Wiegand. Ludwig-soret effect of poly(n-isopropylacrylamide): Temperature dependence study in monohydric alcohols. *Macromolecules*, page submitted, 2006.

[46] R. Kita and S. Wiegand. Soret coefficient of poly(n-isopropylacrylamide)/water in the vicinity of coil-globule transition temperature. *Macromolecules*, 38:4554–4556, 2005.

[47] R. Kita, S. Wiegand, and J. Luettmer Strathmann. Sign change of the soret coefficient of poly(ethylene oxide) in water/ethanol mixtures observed by tdfrs. *J. Chem. Phys.*, 121(8):3874–3885, 2004.

[48] W. Köhler. Thermodiffusion in polymer-solutions as observed by forced rayleigh-scattering. *J. Chem. Phys.*, 98(1):660–668, 1993.

[49] W. Köhler and B. Muller. Soret and mass diffusion-coefficients of toluene n-hexane mixtures. *J. Chem. Phys.*, 103(10):4367–4370, 1995.

[50] W. Köhler and R. Schäfer. Polymer analysis by thermal-diffusion forced rayleigh scattering. In M. Schmidt, editor, *New Developments in Polymer Analytics Ii*, volume 151 of *Advances in Polymer Science*, pages 1–59. Springer, Berlin, 2000.

[51] W. Köhler and S. Wiegand, editors. *Thermal nonequilibrium phenomena in fluid mixtures*, volume LNP584 of *Lecture Note in Physics*. Springer, Berlin, 1 edition, 2002.

[52] P. Kolodner, H. Williams, and C. Moe. Optical measurement of the soret coefficient of ethanol water solutions. *J. Chem. Phys.*, 88(10):6512–6524, 1988.

[53] J. Lenglet. *Phys. Rev. E*, 65:031408, 2002.

[54] W. B. Li, J. V. Sengers, R. W. Gammon, and P. N. Segre. Measurement of transport-properties of liquids with equilibrium and nonequilibrium rayleigh-scattering. *Int. J. Thermophys.*, 16(1):23–31, 1995.

[55] C. Ludwig. Diffusion zwischen ungleich erwrmten orten gleich zusammengesetzter lsungen. *Sitz. ber. Akad. Wiss. Wien Math.-naturw. Kl*, 20:539, 1856.

[56] J. Luettmer-Strathmann. Lattice model for thermodiffusion in polymer solutions. *Int. J. Thermophys.*, 26:1693–1707, 2005.

[57] G. Meyerhoff and K. Nachtigall. Diffusion, thermodiffusion, and thermal diffusion of polystyrene in solution. *J. Polym. Sci.*, 57(165):227, 1962.

[58] J. W. Mitchell, J. E. Riley, and B. S. Carpenter. Microscale homogeneity and compositional profiling of borosilicate glass materials. *Mikrochimica Acta*, 3(3-4):253–261, 1983.

[59] K.I. Morozov. Thermodiffusion in magnetic colloids. *J. Magn. Magn. Mater.*, 201:248–251, 1999.

[60] K.I. Morozov. On the theory of the soret effect in colloids. In W. Köhler and S. Wiegand, editors, *Thermal Nonequilibrium Phenomena in Fluid Mixtures*, volume LNP 584 of *Lecture notes in Physics*, pages 38–60. Springer, Berlin, 2002.

[61] K. Nachtigall and G. Meyerhoff. Die messung der diffusionskoeffizienten von hochpolymeren in losung mit einer konvektionsfreien thermodiffusionszelle. *Makromolekulare Chemie*, 33(1):85–88, 1959.

[62] C. Nieto-Draghi, J. B. Avalos, and B. Rousseau. Computing the soret coefficient in aqueous mixtures using boundary driven nonequilibrium molecular dynamics. *J. Chem. Phys.*, 122:114503, 2005.

[63] Carlos Nieto-Draghi. *Transport and structural properties of aqueous solutions of organic solvents*. PhD thesis, Universitat Rovira i Virgili, 2003.

[64] Ning and S. Wiegand. Experimental investigation of the soret effect in acetone/water and water/dimethylsulfoxide mixtures. *J. Chem. Phys.*, submitted, 2006.

[65] H. Ning, J. Buitenhuis, J. K. Dhont, and S. Wiegand. Thermal diffusion behavior of hard sphere suspensions. *J. Chem. Phys.*, in preparation, 2006.

[66] H. Ning, R. Kita, H. Kriegs, J. Luettmer-Strathmann, and S. Wiegand. Thermal diffusion behavior of nonionic surfactants in water. *J. Phys. Chem. B.*, 110:10746–10756, 2006.

[67] A Parola and R. Piazza. Particle thermophoresis in liquids. *Eur. Phys. J. E.*, 15:255–263, 2004.

[68] A Parola and R. Piazza. A microscopic approach to thermophoresis in colloidal suspensions. *J. Phys.: Condens. Matter*, 17:S3639–S3643, 2005.

[69] A. Perronace, G. Ciccotti, F. Leroy, A. H. Fuchs, and B. Rousseau. Soret coefficient for liquid argon-krypton mixtures via equilibrium and nonequilibrium molecular dynamics: A comparison with experiments. *Physi. Rev. E*, 66(3):art. no.–031201, 2002.

[70] A. Perronace, C. Leppla, F. Leroy, B. Rousseau, and S. Wiegand. Soret and mass diffusion measurements and molecular dynamics simulations of n-pentane-n-decane mixtures. *J. Chem. Phys.*, 116(9):3718–3729, 2002.

[71] R. Piazza. Thermal diffusion in ionic micellar solutions. *Phil. Mag.*, 83(17-18):2067–2085, 2003.

[72] R. Piazza and A. Guarino. Soret effect in interacting micellar solutions. *Phys. Rev. Lett.*, 88(20):208302, 2002.

[73] R. Piazza, S. Iacopini, and B. Triulzi. Thermophoresis as a probe of particle-solvent interactions: The case of protein solutions. *Phys. Chem. Chem. Phys.*, 6:1616–1622, 2004.

[74] J. K. Platten, M. M. Bou-Ali, P. Costeseque, J. F. Dutrieux, W. Kohler, C. Leppla, S. Wiegand, and G. Wittko. Benchmark values for the soret, thermal diffusion and diffusion coefficients of three binary organic liquid mixtures. *Phil. Mag.*, 83(17-18):1965–1971, 2003.

[75] J. K. Platten, M. M. Bou-Ali, and J. F. Dutrieux. Precise determination of the soret, thermodiffusion and isothermal diffusion coefficients of binary mixtures of dodecane, isobutylbenzene and 1,2,3,4-tetrahydronaphthalene (contribution of the university of mons to the benchmark test). *Phil. Mag.*, 83(17-18):2001–2010, 2003.

[76] D. W. Pohl, S. E. Schwarz, and V. Irniger. Forced rayleigh-scattering. *Phys. Rev. Lett.*, 31(1):32–35, 1973.

[77] P. Polyakov, S. Wiegand, and J. Luettmer-Strathmann. Study of the thermal diffusion behavior of binary mixtures of benzene with alkanes by thermal diffusion forced rayleigh scattering method and a lattice model. *J. Phys. Chem. B*, submitted, 2006.

[78] I. Prigogine, L. Debrouckere, and R. Amand. Recherches sur la thermodiffusion en phase liquide .2. *Physica*, 16(11-1):851–860, 1950.

[79] S. A. Putnam and D. G. Cahill. Micron-scale apparatus for measurements of thermodiffusion in liquids. *Rev. Sci. Instrum.*, 75(7):2368–2372, 2004.

[80] S. A. Putnam and D. G. Cahill. Transport of nanoscale latex spheres in a temperature gradient. *Langmuir*, 21(12):5317–5323, 2005.

[81] J. Rauch and W. Köhler. Diffusion and thermal diffusion of semidilute to concentrated solutions of polystyrene in toluene in the vicinity of the glass transition. *Phys. Rev. Let.*, 88(18):art. no.–185901, 2002.

[82] J. Rauch and W. Köhler. On the molar mass dependence of the thermal diffusion coefficient of polymer solutions. *Macromolecules*, 38:3571–3573, 2005.

[83] D. Reith and F. Mller-Plathe. On the nature of thermal diffusion in binary lennard-jones liquids. *J. .Chem. Phys.*, 112(5):2436–2443, 2000.

[84] P. Rossmanith and W. Kohler. Polymer polydispersity analysis by thermal diffusion forced rayleigh scattering. *Macromolecules*, 29(9):3203–3211, 1996.

[85] B. Rousseau, C. Nieto-Draghi, and J. Bonet Avalos. The role of molecular interaction in the change of sign of the soret coefficient. *Europhys. lett.*, 67(6):976–982, 2004.

[86] P. W. Rouw, A. Virj, and C. G. de Kruif. Adhexive hard-sphere colloidal dispersions.iii. stickiness in n-dodecane and benzene. *Progr. Colloid Polym. Sci.*, 76:1–15, 1988.

[87] E. Ruckenstein. Can phoretic motions be treated as interfacial-tension gradient driven phenomena. *J. Colloid Interf. Sci.*, 83(1):77–81, 1981.

[88] R. Rusconi, L. Isa, and R. Piazza. Thermal-lensing measurement of particle thermophoresis in aqueous dispersions. *J. Opt. Soc. Am. B*, 21(3):605–616, 2004.

[89] M. E. Schimpf and J. C. Giddings. Characterization of thermal-diffusion in polymer-solutions by thermal field-flow fractionation - effects of molecular-weight and branching. *Macromolecules*, 20(7):1561–1563, 1987.

[90] M. E. Schimpf and J. C. Giddings. Characterization of thermal-diffusion in polymer-solutions by thermal field-flow fractionation - dependence on polymer and solvent parameters. *J. Polym. Sci. Pol. Phys.*, 27(6):1317–1332, 1989.

[91] M. E. Schimpf and J. C. Giddings. *J. Polym. Sci. Pol. Phys.*, 28(6):2673, 1990.

[92] M. E. Schimpf and S. Semenov. Polymer thermophoresis in solvents and solvent mixtures. *Phil. Mag.*, 83(17-18):2185–2198, 2003.

[93] M. E. Schimpf and S. N. Semenov. Mechanism of polymer thermophoresis in non-aqueous solvents. *J. Phys. Chem. B*, 104(42):9935–9942, 2000.

[94] M. E. Schimpf and S. N. Semenov. Latex particle thermophoresis in polar solvents. *J. Phys. Chem. B*, 105(12):2285–2290, 2001.

[95] S. Semenov and M. E. Schimpf. Thermophoresis of dissolved molecules and polymers:consideration of the temperature-induced macroscopic pressure gradient. *Phys. Rev. E*, 69:011201, 2004.

[96] S. Semenov and M. E. Schimpf. Molecular thermodiffusion (thermophoresis) in liquid mixtures. *Phys. Rev. E*, 72:041202, 2005.

[97] Semenov-2003. Mechanism of particle thermophoresis in pure solvents. *Phil. Mag.*, 83(17-18):2199–2208, 2003.

[98] P. M. Shiundu and J. C. Giddings. Influence of bulk and surface-composition on the retention of colloidal particles in thermal field-flow fractionation. *J. Chromatogr. A*, 715(1):117–126, 1995.

[99] P. M. Shiundu, P. S. Williams, and J. C. Giddings. Magnitude and direction of thermal diffusion of colloidal particles measured by thermal field-flow fractionation. *J. Chromatogr. A*, 715(1):117–126, 1995.

[100] J. M. Simon, D. K. Dysthe, A. H. Fuchs, and B. Rousseau. Thermal diffusion in alkane binary mixtures - a molecular dynamics approach. *Fluid Phase Equilibr.*, 151:151–159, 1998.

[101] C. Soret. Sur l'état d'équilibre que prend au point de vue de sa concentration une dissolution saaline primitivement homogène dont deux parties sont portées a des températures différentes. *Arch. Geneve*, 3:48, 1879.

[102] C. Soret. Sur l'état d'équilibre que prend au point de vue de sa concentration une dissolution saaline primitivement homogène dont deux parties sont portées a des températures différentes. *Ann. Chim. Phys.*, 22:293–297, 1881.

[103] W. Stöber, A. Fink, and E. Bohn. Bohn, controlled growth of monodisperse silica spheres in micron size range. *J. Colloid Interf. Sci.*, (26):62–69, 1968.

[104] G. Thomaes. Thermal diffusion near the critical solution point. *J. Chem. Phys.*, 25(1):32–33, 1956.

[105] John C. Thomas. The determination of log normal particle size distributions by dynamic light scattering. *J. Colloid Interf. Sci.*, 117(1):187–192, 1987.

[106] L. J. Tichacek, W. S. Kmak, and H. G. Drickamer. Thermal diffusion in liquids - the effect of non-ideality and association. *J. Phys. Chem.*, 60(5):660–665, 1956.

[107] H.J.V. Tyrell. *Diffusion and Heat Flow in Liquids*. Butterworth, London, 1961.

[108] N.G. van Kampen. Diffusion in inhomogeneous media. *J. Phys. Chem. Solids*, 49(6):673–677, 1988.

[109] H. Verduin and J.K.G. Dhont. Phase diagram of a model adhesive hard-sphere dispersion. *J. Colloid Interf. Sci.*, 172:425–437, 1995.

[110] T. Voelker, E. Blums, and S. Odenbach. Thermodiffusive processes in ferrofluids. *Magnetohydrodynamics*, 37(3):274–278, 2001.

[111] T. Voelker, E. Blums, and S. Odenbach. Determination of the soret coefficient of magnetic particles in a ferrofluid from the steady and unsteady part of the separation curve. *Int. J. Heat Fluid Fl.*, 47:4315–4325, 2004.

[112] A. Voit. *Untersuchung von Transportprozessen in binren Flssigkeiten mit Hilfe thermischer Linsen.* Diplom, University Bayreuth, 2003.

[113] F. C. Whitmore. Experimental study of thermal diffusion in dilute solutions of high polymers. *J. Appl. Phys.*, 31(11):1858–1864, 1960.

[114] S. Wiegand. Thermal diffusion in liquid mixtures and polymer solutions. *J.Phys.:Condens. Matter*, 16:R357–R379, 2004.

[115] G. Wittko and W. Kohler. Precise determination of the soret, thermal diffusion and mass diffusion coefficients of binary mixtures of dodecane, isobutylbenzene and 1,2,3,4-tetrahydronaphthalene by a holographic grating technique. *Phil. Mag.*, 83(17-18):1973–1987, 2003.

[116] G. Wittko and W. Kohler. universal isotope effect in thermal diffuison of mixtures containing cyclohexane and cyclohexane-d_{12}. *J. Chem. Phys.*, 123:014506–, 2005.

[117] A. Würger. Heat capacity-driven inverse soret effect. *Europhys. Lett.*, 74(4):658–664, 2006.

[118] K. J. Zhang, M. E. Briggs, R. W. Gammon, and J. V. Sengers. Optical measurement of the soret coefficient and the diffusion coefficient of liquid mixtures. *J. Chem. Phys.*, 104(17):6881–6892, 1996.

[119] K. J. Zhang, M. E. Briggs, R. W. Gammon, J. V. Sengers, and J. F. Douglas. Thermal and mass diffusion in a semidilute good solvent-polymer solution. *J. Chem. Phys.*, 111(5):2270–2282, 1999.

[120] M. Zhang and F. Müller-Plathe. Reverse nonequilibrium molecular-dynamics calculation of the soret coefficient in liquid benzene/cyclohexane mixtures. *J. Chem. Phys.*, 123:124502, 2005.

[121] M. M. Zhang and F. Müller-Plathe. The soret effect in dilute polymer solutions: influence of chain length, chain stiffness and solvent quality. *J. Chem. Phys.*, 2006. accepted.